Development of Flexible-Based Electrode Arrays as a Neural Interface

by

Theodore Bo-Yi Ng

A thesis submitted in partial fulfillment of the requirements for the degree of

Master of Science

in

Chemical Engineering

Department of Chemical and Materials Engineering
University of Alberta

Abstract

Flexible electrode arrays are a crucial technology for neural interfaces. In this thesis, the continued development of a flexible based electrode array is discussed. Two types of strain relief are introduced into the leads to allow the base to deform like the spinal cord in a repeatable manner. The resulting sandwich and embedded lead configurations were characterized using a tensile tester. In addition, the base material was characterized after exposure to physiological solutions and a sterilization protocol. Results show that the sandwich lead configuration had properties that were better matched to those of the spinal cord tissue. Parametric finite element modelling was also performed to identify the effect of the base modulus after varying several properties associated with the base. The results of the modelling would help in the long term manufacturing of these flexible based electrode arrays.

Acknowledgements

A postgraduate degree is not accomplished without the love, guidance and support of many people. Firstly, I want to thank both my supervisors: Dr. Anastasia Elias and Dr. Walied Moussa. Without their guidance, passion to research and support, I would not be able to achieve what I have and grow as a researcher. A special thank you to Dr. Vivian Mushahwar for her support throughout this process.

In addition, I would like to thank the members of my lab group, Andrea Jeffrey, Ben Nearingburg, Anthony Zeberoff, Xi Haung, Preetam Anbukarasu, Sangita Sridar, Sam Maloney, for helping me throughout this journey. I would also like to say a special thanks to Kenton Hamaluik, Selma Elmallah, Kian Parseyan and Amirali Toosi for helping me out with various specific parts of modelling and experimental work. I would also like to acknowledge my friends, Allen Reule, David Dinh and Kyle Massey for their continued support throughout these two years.

Finally, I want to thank my Mom, Dad and brother, Jonhansel, for their continued guidance and support throughout my Master's degree. It would not have been possible without your love.

A special acknowledgement is made to Alberta Innovates Health Solutions and Project SMART for the funding through these couple years.

Table of Contents

List of Tables

List of Figures

Chapter 1: Introduction

In this chapter, the objectives of the work will be discussed. Furthermore, motivations for work will be outlined. An approach for the research will be presented followed by the outline of the thesis and chapters.

1.1 Objective

The flexible based electrode array (FBEA) is a group of penetrating electrodes on a mechanically compliant polymer base that can deform with the cord. It was designed to improve targeting of specific motor neuron pools for ISMS. The objective of this work is to develop a strain relief mechanism for the flexible based electrode array (FBEA), in order to improve the current design and make the entire array more mechanically compliant with the spinal cord. Current designs of the FBEA involve a base that is too stiff for implantation into spinal cord. The new configuration of the FBEA leads should have material properties that closely resemble the spinal cord and also enable effective lead density scale-up. The goal is to develop a base that is not only mechanically compliant, but also where the mechanical and material properties of the base changes very little when exposed to sterilization and physiological environments over a period of time.

1.2 Motivation

Neural interfaces are devices that are engineered and designed to exchange information electrically with the nervous system [1]. In this work, the focus is on spinal cord neural implants. Spinal cord injury (SCI) is any injury that is caused by trauma that disrupts the signal from various parts of the body to the brain or vice versa. In 2010, there were an estimated 3000 cases of spinal cord injury in Canada alone according to the Rick Hansen Institute with the total number of Canadians impacted by SCI rising to 86,000 cases [2]. Apart from severely reducing the quality of life for people with SCI, it also costs the Canadian medical system close to $3 billion annually [3]. With new cases being reported every year, the estimated cost is expected to rise each coming year.

One method being widely investigated to restore function, coordination and control to the lower extremities is known as Intraspinal Microstimulation (ISMS). ISMS is based on implanting small, hair-like electrodes into the lower regions of the spinal cord regions of the spinal cord to allow for transmission of signals that will imitate brain signals. Previous work has validated ISMS as an appropriate method to restore function to lower extremities. [4, 5].

Initial ISMS experiments involved single wires being implanted one at a time. The main disadvantage of this method was that it was difficult to implant several electrodes at once and locating and targeting specific motor neuron pools was

difficult. The McCreery array [5] and the Utah array [6] were developed as a possible neural interface solution in the brain. However, these arrays are not mechanically compliant with the spinal cord which can cause significant damage to surrounding tissue. In order for the implant to be considered mechanically compliant, the device must be able to deform with the spinal cord, which has been shown to be able to have an axial strain of up to 12% during daily movement [7]. The flexible based electrode array (FBEA) [8] was developed to improve mechanical compatibility with the spinal cord while also improving targeting of motor neuron pools and improve implantation. While the base is flexible, lead wires add significant stiffness to the whole array, which reduces the overall mechanical compatibility of the implant. Also, the lead wires could also be pulled out during array deformation. Lead wires are essential as they provide a pathway for the electrical current from the stimulation source to motor neuron pools. Figure 1.1 shows a stress-strain curve for the polymer base material PDMS and PDMS with one straight Pt/Ir microwire.

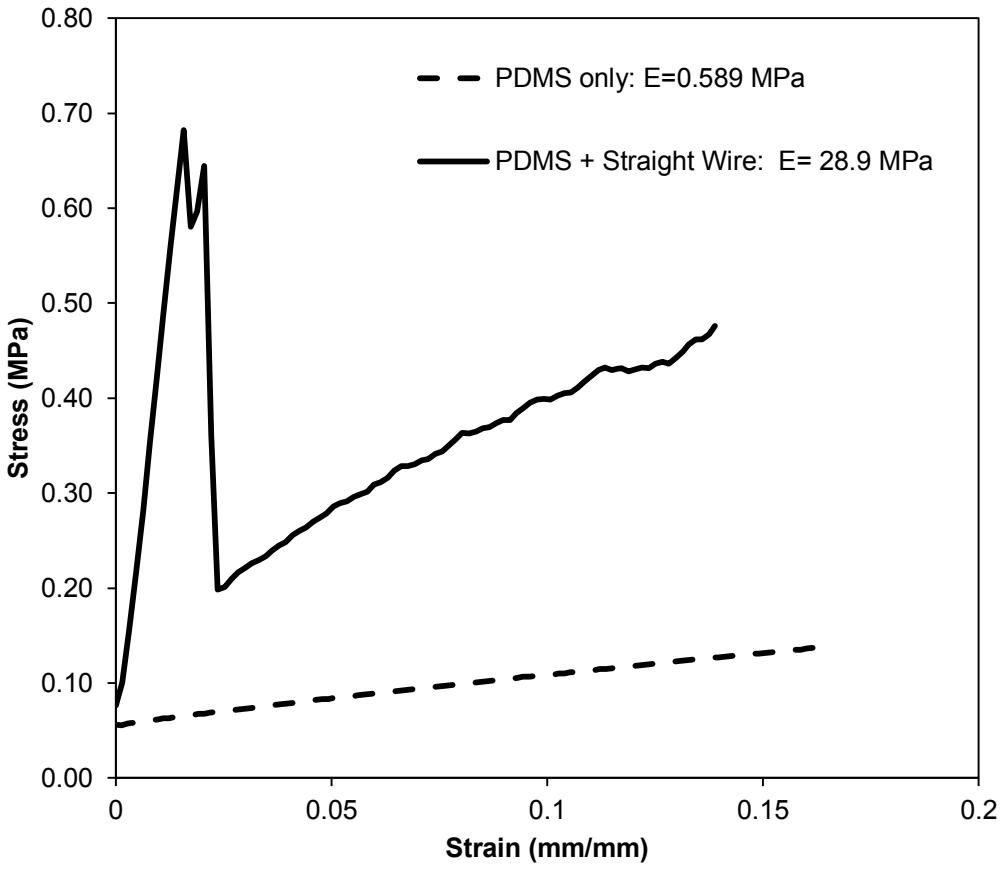

Figure 1.1. Stress-strain curve illustrating the importance of strain relief on the samples.

As seen in the figure, it can be seen that the base material, PDMS, has a low modulus and the addition of a straight wire actually increases the modulus drastically. In addition, the straight wire is unable to withstand recorded physiological strains of 12%. It can be seen that the straight lead wire also breaks

at roughly 2% strain. Based on this data, it is important for a strain relief system to be designed to reduce the modulus mismatch between the polymer and a polymer sample with some wires. Also, it is important for the strain relief mechanism to be able to allow the leads to deform 12% without breaking. This, in turn, will improve the mechanical compatibility of the overall array.

1.3 Research Approach

Two different types of lead configurations were fabricated and characterized: embedded leads and sandwich leads. The embedded leads configuration was fabricated where the polymer was cured around the microwire leads. The second configuration was the sandwich array, which was fabricated where two thin slices of polymer formed a layer above and below the microwire leads. In both lead configurations, strain relief was incorporated in the microwire leads in the form of a sinusoidal wave. For embedded leads, an experimental design was implemented. Two different wire diameters, strain relief amplitudes and number of wires were tested. Using elastic modulus and peak tensile stress, the optimum variables was determined and compared to the electrode array design requirements. Once the optimal wire diameter, and strain relief amplitude were determined according to the design requirements for the electrode array, it was used to further develop the second electrode lead configuration, the sandwich

array. Three different sandwich samples were created: single wires, three wires that all overlap each other and three wires that are equally spaced out. In addition, blank samples (samples without any microwires) were used as a control. Comparing the elastic modulus and tensile stress at 15% strain, the optimum configuration was determined and implemented into the flexible based array.

In addition to developing strain relief for the FBEA, another aspect was to test the material properties of the base after exposure to both physiological conditions and sterilization cycles. After exposure to environments, tensile tests were conducted and the elastic modulus was compared with samples that had not been treated.

Finally, a finite element model (FEM) was created to numerically model the forces used to stretch the base up to 12% of its original length. Models were created to account for changes in strain relief amplitudes, wire diameters, and number of microwires in the samples. In addition, both lead configurations were modeled. In order to model the complex behaviour between base polymer (PDMS) and the microwires, contact elements were used. Modulus values were calculated using far-field stresses and strains. Five different studies were conducted: effect of amplitude, number of microwires in base and strain relief configuration on modulus, effect on wire diameter on sandwich array modulus, load step study to investigate strain at which delamination occurred between base material (PDMS) and wire insulation material (polyimide) in embedded base,

effect of increasing base width on the modulus of a base with fixed strain relief amplitude and spacing between wires, and effect of decreasing wire spacing on the modulus of the base with fixed geometry.

1.4 Outline

This thesis will be divided into five chapters.

The main focus of the second chapter is a literature study of neural interfaces and the challenges associated with their development. Neural engineering and interfaces will be introduced and challenges, such as biocompatibility and mechanical stability will be discussed. One crucial technology associated with neural interfaces is the electrodes and this will also be discussed in this chapter along with ongoing mechanical challenges for implementing this technology. Invasive neural interfaces will be introduced and the challenges presented. The FBEA will be introduced in this section. Current array design and drawbacks will be discussed.

The third chapter will set-up the experiments performed. In the first part of this chapter, the materials of construction for the base will be discussed, followed by parameters of tensile testing applied through the experiments. The remaining part of the chapter will be divided into two sections: embedded and sandwich leads.

Each section will have individual subsections describing the fabrication of each set of samples and the experimental design or plan. Results will then be presented and discussed. A comparison between the embedded arrays and the sandwich will be presented. Finally, a look at how physiological conditions and sterilization procedures influence the base material will also be discussed.

The fourth chapter will introduce a finite element model (FEM) created to model the behaviour of the leads inside the base. Element types, model geometry and boundary conditions will be discussed to set-up the model. Next, a mesh dependency test based on element size will be performed and studied. Five different studies will be discussed. The first will involve varying amplitude of strain relief, number of microwires in base and strain relief configuration (embedded or sandwich) to investigate its effect on modulus. Next, the effect of wire diameter on a sandwich array modulus will be discussed. Third, a load step study to investigate strain at which delamination occurred between base material (PDMS) and wire insulation material (polyimide) in the embedded base will be performed. Fourth, the effect of increasing base width on the modulus of a base with fixed strain relief amplitude and spacing between wires will be discussed. Lastly, the effect of decreasing wire spacing on the modulus of a base with fixed geometry will be investigated.

Finally, the fifth chapter will highlight the major conclusions of the present study.

A list of future work will also be presented.

1.5 References

[1] W.M. Grill, "Neural Interfaces" American Scientist: the Magazine of Sigma XI, the Scientific Research Society, vol. 98, no. 1, pp.48-57, 2010

[2] "Spinal Cord injuries cost health care $3 billion annually | The Star." [Online]. Available: http://www.thestar.com/life/health_wellness/2012/01/27/spinal_cord_injuries_cost_health_care_3_billion_annually.html. [Accessed: 28-August-2013]

[3] V.K. Noonan, M. Fingas, A. Farry, D. Baxter, A. Singh, M.G. Fehlings, and M.F. Dvorak, "Incidence and Prevalence of Spinal Cord Injury in Canada: A National Perspective," Neuro-epidemiology, vol. 38, pp. 219-226, Apr. 2012

[4] V. K. Mushahwar and K. W. Horch, "Proposed specifications for a lumbar spinal cord electrode array for control of lower extremities in paraplegia," IEEE Transactions on Rehabilitation Engineering: A Publication of the IEEE Engineering in Medicine and Biology Society, vol. 5, no. 3, pp. 237-243, Sep. 1997.

[5] D. McCreery, V. Pikov, A. Lossinsky, L. Bullara, and W. Agnew, "Arrays for chronic functional microstimulation of the lumbosacral spinal cord," IEEE Transactions on Neural Systems and Rehabilitation Engineering: A Publication of the IEEE Engineering in Medicine and Biology Society, vol. 12, no. 2, pp. 195-207, Jun. 2004.

[6] S.F. Giszter, "Spinal Cord Injury: Present and Future Therapeutic Devices and Prostheses" The American Society for Experimental NeuroTherapeutics. Inc., vol. 5, pp.147-162, Jan. 2008

[7] S. S. Margulies, D. F. Meaney, L. B. Bilston, L. E. Thibault, N. G. Campeau, and S. J. Riederer, "In Vivo Motion of the Human Cervical Spinal Cord in Extension and Flexion," in Proceedings of the 1992 International IRCOBI Conference on the Biomechanics of impacts, VERONA, ITALY, 1992.

[8] I. Khaled, S. Elmallah, C. Cheng, W. Moussa, V.K. Mushahwar, and A.L. Elias, “A Flexible Base Electrode Array for Intraspinal Microstimulation” IEEE Transactions in Biomedical Engineering, vol. 60, no. 10, pp. 2904-2913, Oct. 2013

Chapter 2: Literature Review

In this chapter, a comprehensive literature review of neural engineering and some of its interfaces will be presented. The end of the chapter will reiterate the main objectives and a brief approach to the experimental and modelling work presented in the following chapters.

2.1 Neural Engineering and Interfaces

The nervous system is a series of neurons that act as a communication highway for the body. These nerves carry sensory signals from the body to the brain and also transmit motor signals or messages from the brain to specific organs or muscles in the body. Like every part of the human body, the nervous system can be damaged by disease or injury. In fact, 10% of Canadians are affected by or live with some form of neural injury or disorder [1]. In order to help improve the quality of life for individuals with neurological diseases, a variety of neural interfaces have been developed. Neural interfaces are a category of technologies that link the nervous system (neurons, brain cells, spinal cord tissue, etc.) to the outside world. Neural interfaces can provide two functions: recording or stimulation. In stimulation, the interface acts as a bridge for electrical current to be transferred to targeted neurons for translation into muscles. Functional electrical stimulation (FES), which is used to activate muscles, allows the restoration of a variety of functions [2]. These functions include picking up

objects, standing, walking, and controlling bladder and bowel movements and even breathing [2]. In recording, the interfaces act as a receiver to pick up electrical signals from the nerves in order to transmit them externally for further processing. Recording is useful in applications such as robotic limb control, where the application of recording can help with the control of a robotic prosthesis [3].

Neural interfaces are a large family of devices which connects the technological world with the neurons within the body. Neural interfaces are comprised of many components that include electrodes, leads, control unit, a stimulator and/or recorder as well as a device that is used to communicate with the outside world. They are described and characterized based on several characteristics: anatomical positioning of the electrode (i.e. extraneural, cortical, etc.), purpose (recording, stimulation, etc.), material, selectivity (type and size of nerves or other cells, and neural activity direction), number of contacts with the nervous system and its level of integration within the nervous system (wireless communication, with or without integrated electronics). Another important consideration for neural interfaces is the manufacturing, packaging and interconnections of these devices, which will not be looked at in too much detail here.

One important part of neural interfaces is the electrodes. The electrode acts as the bridge between the device and the tissue. The electrode is the closest point of

contact between the technological world and our human bodies. Electrodes can be organised into different configurations. These include large pads that sit on the surface of the skin, single wires inserted into the muscle or neural tissue, single electrodes with multiple stimulation and/or recording sites, and even the contoured and straight electrodes in a spiral shaped array that is designed to operate within a cochlear implant. Many applications require interfacing with numerous regions at once. This can be achieved using multiple electrodes arranged in an array, rather than through a single electrode [4-6]. This is especially prevalent in the brain because information processing and storage is distributed [7,8]. Also, recording from a neuronal network using an array of electrodes is more beneficial than recording from a single neuron using a single electrode [7,8].

The first neural prosthesis or interfaces were used to for movement control over 50 years ago [9]. The first brain-to-machine interfaces were developed in the early 1960's and implanted in human volunteers in 1968 [10,11]. With the advent of micro- and nanofabrication technologies in the 1970's, it became possible to manufacture microelectrodes for implantation into neurological tissue. Two categories of neural interfaces were developed over the course of the last 50 years: external (or surface) interfaces and implantable (or invasive) neural interfaces. Surface neural interfaces are non-invasive and involve the electrode being placed on the skin closest to the targeted muscle or organ. Applications for

non-invasive surface electrodes include transcranial magnetic stimulation and electrode applications found in artificial external defibrillators. Transcranial magnetic stimulation involves the use of magnetic fields to stimulate neurons within the brain [12]. In this case, the electrode is found in an electromagnetic coil that is placed on the forehead and scalp. With defibrillators, the electrode is located in the pad that is placed on the skin around your heart [13]. The pad provides electrical current that targets nerves electrically, around the heart. The main advantage of using non-invasive surface electrodes is the ability to apply these electrodes without surgery. Surgery can cause significant discomfort to the patient and long recovery time. These electrodes can be worn under clothing and easily replaced or serviced. The use of surface or external neural interfaces is not very practical for people who needed restoration of sensory or motor functions. This is due to insufficient selectivity and ability to target specific neurons. Therefore, implantable neural interfaces are important for systems associated with sensory and motor rehabilitation. Due to the complicated insertion procedure, these devices must remain functional for a long time to be clinically useful [14]. An advantage of invasive neural interfaces includes the ability to target specific pools of neurons. A major disadvantage of invasive neural interfaces is the actual high risk nature of surgery for implanting these devices, especially within the central nervous system [14]. A long recovery period after surgery is also a

disadvantage [14]. In addition, the biocompatibility of these devices limits their long-term performance [15].

2.2 Foreign Body Response

Many studies have been done to suggest that one of the major challenges to having a stable and consistent implant for use in the central nervous system is the foreign body response. In order to design electrodes that minimize the effect of the foreign body response, the biological mechanisms of the response must be identified and understood.

The foreign body response is the response of the body to an invasive object [15,16]. The human foreign body response can be divided into five separate processes: initial trauma due to implantation, protein adsorption, acute inflammation, chronic inflammation and glial scaring or cellular encapsulation of the implant [17-19].

Implant trauma is the first step in the foreign body response. When a neural interface is implanted into the central nervous system, nervous cells, tissues, and the blood-brain barrier are punctured [15]. The nervous cells and tissue become displaced around the implant, and blood starts to gather around the site. As a result of the insertion of the electrode, this produces an acute inflammatory

foreign body response. The degree of the acute inflammatory response is dependent on several electrode design factors, including size and geometry of the electrode, method of insertion and implantation location within the central nervous system [17]. Proteins from the blood adsorb onto the implant and send out factors signalling molecules, and recruiting other cells [18-20]. This activates the microglia, which responds to the injury site and attack the implant as a foreign body. After a period of time, astrocytes become activated and respond to the area of injury [21-23]. Astrocytes and microglia begin to try and break down the implant. Chronic response occurs when the astrocytes and microglia remain activated over an extended period of time. This also displaces the neurons, which grow away from the site of injury to avoid the activated astrocytes and microglia. Activated astrocytes and microglia form a glial scar around the implant, which isolates the implant. The glial scar also reduces the functionality of the implant. This response remains as long as the implant remains in the body.

The geometric, mechanical, and chemical properties of an electrode all play a role in the foreign body response. In terms of mechanical properties, electrodes must be able to withstand mechanical strains exhibited during daily movement without causing damage to surrounding tissue. If implants are stiffer than the surrounding tissue, this poses a further challenge as movement of the implant can cause further mechanical trauma to the site. Silicon, the material from which most neural implants are fabricated, has a modulus six orders of magnitude higher than tissue

(170 MPa [24]). In contrast, the modulus of human spinal cord without pia matter is 89 kPa [19], and of peripheral nerves is 575 kPa [25]. From these values, a clear mechanical mismatch can be seen between the soft nervous tissue and the implant itself and this mismatch would enhance the inflammation response.

2.3 Invasive Neural Interfaces

Many invasive technologies have been developed to interface with the central nervous system. For some applications, the foreign body response to these devices can limit their utility. The physical, mechanical, and chemical properties of these devices can all affect this foreign body response.

Invasive electrodes are typically fabricated with materials like silicon, platinum, titanium nitride, gold, iridium, carbon and polymers. Electrodes may have a variety of different geometries, suited for a many applications. Among invasive neural interfaces, the different types of electrodes can have different levels of invasiveness. Planar electrodes are patterned on mostly flat, rigid substrates [26]. These electrodes are designed to be placed on the surface of the peripheral nerve for recording [26]. Cuff electrodes typically consist of a flat substrate patterned with multiple electrodes, which can be coiled around a peripheral nerve, for both stimulation and recording [27]. Penetrating electrodes are long needle-like

electrodes that are organised into arrays, implanted into the nerves or the brain *in vivo*, and extend into the tissue, reaching cells beneath the surface [28,29]. Finally, regenerating electrodes are a mesh of surface electrodes that are implanted to promote nerve fibers growth [30]. This is accomplished by implanting the electrodes on the ends of severed peripheral nerves. In the following sections, various types of invasive neural interfaces will be described.

2.3.1 Cuff Electrodes

Cuff electrodes are microelectrode arrays patterned on flexible silicone substrates that are coiled and can be found wrapped around peripheral or central nerves. The electrodes are found on the underside of the cuff and it is mechanically designed to ensure positive contact with nerves in places where nerves are more mechanically active. The main advantage of cuff electrodes is that they do not penetrate the nerve, and therefore do not elicit a foreign body response at or near the neurons of interest [31].

The first cuff microelectrode arrays were fabricated using a reactive ion-etch process [32]. This method provided the ability to preserve underlying gold conductors. Two separate configurations were tested: one with straight conductors and the second with serpentine conductors. The authors determined

that serpentine conductors were able to withstand up to 8% uniaxial strains while maintaining good electrical conduction. The straight patterned conductors lost electrical conduction at 3% [33]. In addition, straight conductors also exhibited a slightly larger modulus compared to serpentine conductors [33]. A key design goal for serpentine shapes was to identify a path which can avoid large strain concentrations and keep the conductor below the material failure limit after cyclic mechanical straining. Serpentine optimization has led to a path comprising many small conductors, which is strainable between 50-100% uniaxially [34,35]. Serpentine connectors are relevant to the work described in this thesis.

A second cuff microelectrode array was developed, and this electrode included thin film gold (30 nm) and PDMS. This electrode array was developed to be wrapped around small nerves where the diameter of the nerve was about 1 mm [36]. After performing mechanical testing for this array at two different strain ranges, the authors were able to determine elastic modulus values at 10% and 40% to be 1.81 MPa and 1.62 MPa, respectively. The main drawback was that 7-9% of the electrical conductance was lost after five cycles of straining to 200%. As the number of cycles reached a range of 1000 to 2000, an increase in the unstrained sample's baseline resistance was observed and the range of strains in which the sample was conductive decreased [36].

The main disadvantage of cuff-electrodes is that the electrodes are positioned on the surface of the tissue. As a result, there is a large gap between the electrodes and the neurons of interest, which makes it hard to intercept signals with high specificity.

2.3.2 Planar Microelectrodes

Planar microelectrodes provide temporal and spatial information about neuronal networks. They are also able to monitor neural electrophysiological activity from cells that undergo physical deformation and injury [37]. In planar microelectrodes, elastically deformable electrodes are fabricated on an elastomeric silicon substrate, mostly medical grade PDMS. These arrays are designed for recording or stimulation of neural tissue and cells *in vivo*. They are usually used in short term studies (maximum of 25 weeks) because they can shift their position in time [38]. The electrodes themselves may be formed using photolithography, or by using laser micromachining to pattern conductive foil. Conductive traces may be insulated using additional layers of silicone elastomer. When electrodes are fabricated using photolithography to pattern layers of evaporated gold, they can accommodate some strain while remaining conductive because the surface of the PDMS itself is usually quite rough, and can be 'unfolded' when stretched. These strainable gold films also formed a network of discontinued cracks in the micrometer scale [39,40]. The researcher found that as

the strain on the PDMS substrate was increased, microcracks were seen to widen and lengthen. Due to Poisson's compression, cracks opened in the straining direction, but closed in the perpendicular direction during uniaxial strain [41] and this allows electrical conduction to take place. Despite a high degree of flexibility, the electrode array exhibited a low signal to noise ratio at high strains, which is a disadvantage of the system. Despite the fact that impressive arrays can be made using microfabricated planar electrodes, these devices still suffer from the drawback. One specific drawback is that they cannot specifically target electrodes beneath the tissue of the surface.

2.3.3 Penetrating Electrodes

Penetrating microelectrode arrays are an array of electrodes that penetrate the tissues to access neurons beneath the surface of the tissue [36]. They are comprised of small needle like electrodes that are fabricated with silicon and/or other metals [36]. Applications of penetrating electrodes include interfacing computers with specific neurons in the brain [41-43] and also to restore certain physiological functions after injuries or trauma. These functions may include the ability to move limbs, walk, see or even hear [44-46]. Penetrating electrodes are used extensively in research because they provide proximity to neurons as well as better spatial resolution and selectivity when compared to surface electrodes [47].

The majority of penetrating electrodes use silicon as a substrate or base material because of the well-established electrical and mechanical properties associated with the material [47]. There are three different penetrating electrode arrays that will be discussed in this section: the Huntington Medical Research Institute (HMRI) array [48], the Michigan array [49] and the Utah array [50]. These arrays are shown in Figure 2.1. These arrays have all demonstrated mechanical and electrical reliability though many experiments.

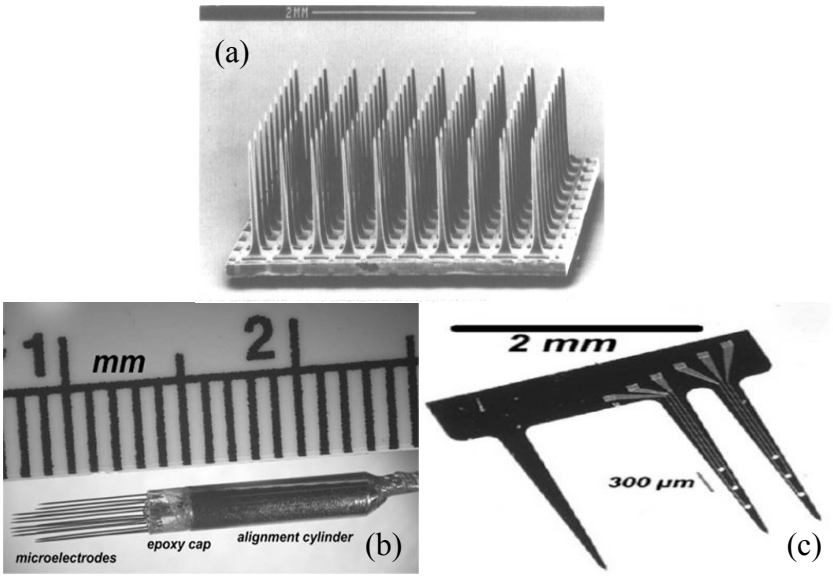

Figure 2.1. Penetrating electrode arrays. (a) Utah array: Reprinted with permission from Elsevier [50] (c) Huntington Medical Research Institute Array [48] © 2006, IEEE (d) section of a Michigan array [49] © 1994, IEEE.

The first electrode array is called the Huntington Medical Research Institute Array (HMRI). This array was developed for long-term implantation to be used for localized stimulation or recording of a neuron [48]. The main application of this array is for deep brain stimulation and recordings [48] to assist in the treatment of movement disorders such as Parkinson's disease, treatment of deafness through direct brain stimulation or to control bladder evacuation in paralyzed patients. The array consists of 16 iridium microelectrodes that are 5-6 mm in length and these electrodes from a cluster or a bundle that are 1.8 mm in diameter [48]. The lead wires are coiled around a silicon tube and covered with a layer of medical grade elastomer [48].

The Michigan array was developed for chronic recordings of neurons in the central nervous system [49]. The array is formed through a micro assembly of planar silicon multisite probes, as seen in Figure 2.1. Multi-site probes or electrodes are electrodes that have multiple points of stimulation or recording on a single electrode. In this array, there are a total of 16 electrodes that are 4 mm long, each with four sites that could be used for stimulation or recording [49]. The probes are connected to the base made of silicon through electroplated nickel lead transfers [49]. The Michigan array has been used for chronic neural recordings in the cerebral cortex of the brain.

Finally, the third penetrating electrode in this group is the Utah array. The Utah array was developed to record signals for a brain-to-computer interface [50]. The Utah array records from a small neuronal population, instead of the single neuron unit that the Michigan array records from [49,50]. The silicon micro-machined array also allows for implant of a large density of electrodes in the cortex of the brain. The array is comprised of 100 electrodes that make up a 16 mm^2 area (4.2 mm x 4.2 mm) [50]. This array is 0.2 mm thick and the 100 electrodes are isolated electrically and arranged in a 10 by 10 manner on the silicon base [50]. The polyimide insulated electrodes are each 1.2 mm long and are etched to include a sharp tip [50]. Gold pads provide the electrical current to each individual electrode [50]. Utah electrodes have been studied for many applications such as restoring mobility and stance, control of prosthetic arms and also restoring bladder control, among others. They are available commercially through companies such as Blackrock Microsystems.

One of the main disadvantages of these electrode arrays includes the imperfect contact between the electrode and the neurons. Also, a second disadvantage is the ability for these arrays to conform to a curved surface. The rigid electrode substrate would also increase the damage to the tissue, which would initiate a foreign body response that was described in the previous section. This is because of the inability of these implants to deform with tissues like the spinal cord. The inability for the implant to deform can be attributed to the mechanical mismatch

between the base and surrounding tissue. These penetrating electrodes have young's modulus in the tens to hundreds of GPa [36] while tissue exhibits modulus many orders of magnitude lower. This mechanical mismatch is particularly problematic when attempting to use these arrays in tissues that undergo large deformation, such as the spinal cord. Because of this reasoning, the development of flexible invasive neural interfaces became prominent.

2.4 New Innovations in Flexible Based Interfaces

Recently, a new type of electrode array was developed for use in intraspinal microstimulation (ISMS). Intraspinal microstimulation is a functional electrical stimulation method of stimulating the motor neuron pools in the spinal cord to produce coordinated movement [51, 52]. This technique is shown to allow for less muscle fatigue than in cases where surface stimulation is applied [51,52]. The motor neuron pools are located in the lumbosacral region of the spinal cord. This region contains the cell bodies for the motor neurons that are linked to the lower limbs and are involved in movement and coordination [52]. For ISMS, it is important to develop a penetrating electrode array that has flexible base, instead of the rigid base in most penetrating arrays. This is important because of the regular strains that the cord exhibit. It has been shown that the spinal cord can elongate by up to 12 percent during daily motion [53]. Rigid arrays would not be

able to deform with the spinal cord and this would cause extensive damage to the surrounding tissue. In order for the implant be viable, the base would need to be flexible and have similar mechanical properties to the spinal cord. This includes modulus values and ability to elongate at a similar rate compared to the spinal cord itself. From literature, a human spinal cord with a pia layer had an elastic modulus of 1.40 MPa and able to elongate up to 12% as a result of day to day movement [53, 54].

Based on these properties, a flexible based electrode array was proposed and developed in my group [55]. The base of this array was made of a medical grade silicon elastomer and electrodes and lead wires were made of a platinum/iridium alloy [55]. The elastomer was used to make the base flexible and able to deform. The base was 300 μm thick, 13 mm long and 7 mm wide [55]. The initial design had six electrodes that were insulated with polyimide and were 30 μm in diameter [55]. Based on literature, this is the only technology that incorporates the penetrating electrode design with the flexible substrate or base.

There were some disadvantages to the early design. While the base could easily and reversible deform to 12 %, it was noted that the leads wires themselves would not return to exactly their original shape after strain. This is due to the fact that the leads were straight wires, which could not themselves extend 12 %. As a result, the base would stretch independently from the leads, trapping additional

length of lead wire in the base upon relaxation. The leads add stiffness to the base and even though the base material is flexible, the microwires are not compliant which adds stiffness to the overall structure. It is, therefore, important to solve this problem to reduce the mechanical mismatch between the spinal cord tissue and this interface.

2.5 Conclusions

Throughout the literature, many attempts have been made to produce electrode arrays that are biocompatible with the body. One obstacle to producing these implants includes the mismatch between the mechanical properties of synthetic materials and the cells inside the body. To prevent further damage, many interfaces try to use materials that have similar mechanical properties compared to the cells they are to be implanted in. As well as mechanical challenges, there are some other challenges which include combating the foreign body response and maintaining electrical conduction after strains is applied.

In order to reduce the mechanical mismatch between the arrays proposed by Khaled *et al* [55] and nervous tissue, we propose to create leads that incorporate a serpentine pattern as a means of strain relief and also to allow the base to strain with spinal cord tissue. The leads in the base will be experimentally tested and

modelled using finite element analysis. With the addition of the strain relief leads, we hope to solve some of the existing problems seen in some arrays mechanically and improve the ability for the neural interface to perform its function fully.

2.6 References

[1] Fact Sheet - Mapping Connections: An Understanding of Neurological Conditions in Canada, Found on: http://www.phac-aspc.gc.ca/cd-mc/nc-mn/mc-fs-ec-fr-eng.php. Accessed on November 26, 2014.

[2] Robinson, C.J. Expanding the scope of IEEE transaction on rehabilitation engineering to explicitly including neural engineering. *IEEE Trans. Rehabil. Eng.* 8:273-275, 2000

[3] Leuthardt, E.C., Roland, J.L., Ray, W.Z., Neuroprosthetics, *The Scientist*, November 1, 2014, Obtained from: http://www.the-scientist.com/?articles.view/articleNo/41324/title/Neuroprosthetics/. Accessed on: November 24, 2014.

[4] Carmena, J.M., Lebedev, M.A., Henriquez, C.S., and Nicolelis, M.A., Stable ensemble performance with single-neuron variability during reaching movements in primates. *J. Neurosci.*, 25:10712-10716, 2005

[5] Cohen, D., and Nicolelis, M.A., Reduction of single-neuron firing uncertainty by cortical ensembles during motor skill learning. *J. Neurosci*., 24:3574-3582, 2004

[6] Mehring , C., Rickert , J., Vaadia , E., Cardosa de Oliveira , S., Aertsen , A., and Rotter , S., Inference of hand movements from local fi eld potentials in monkey motor cortex . *Nat. Neurosci.* , 6:1253 – 1254, 2003

[7] Engel , A.K., Fries , P., and Singer , W. Dynamic predictions: oscillations and synchrony in top - down processing . *Nat. Rev. Neurosci*., 2:704-716, 2001

[8] Harris , K.D., Csicsvari , J., Hirase , H., Dragoi , G., and Buzsaki , G., Organization of cell assemblies in the hippocampus . *Nature* , 424:552 – 556 , 2003

[9] LibersonW.F., Holmquest, H. J., Scott, D., Dow, A. Functional electrotherapy: Stimulation of the peroneal nerve synchronized with the swing phase of the gait in hemiplegic patients. Arch. Phys. Med. Rehab. 42:101–105, 1961.

[10] Brindley, G.S., and Lewin, W.S., The sensations produced by electrical stimulation of the visual cortex. *J. Physiol.*, 196:479-493, 1968

[11] Delgado, J.M.R., Mark, V., Sweet, W., Ervin, F., Weiss, G., Bach-y Rita, G., Hagiwara, R., Intracerebral radio stimulation and recording in completely free patients. *J. Nerv. Ment. Dis.,* 147:329-340, 1968

[12] DiLazzaro, V., Retuccia, D., Olivero, A., Profice, P., Ferrara, L., Insola, A., Mazzone, P., Tonali, P., Rothwell, J.C., Effect of voluntary contraction on descending volleys evoked by transcranial stimulation in conscious humans. *J. Physiol.*, 508:2:625-633, 1998

[13] Jacobs, I., Sunde, K., Deakin, C.D., Hazinski, M.F., Kerber, R.E., Koster, R.W., Morrison, L.J., Nolan, J.P., Sayre, M.R., Part 6: Drfibillation, Electrode Patient Interface: *2010 International Consensus on Cardiopulmonart Resuscitation and Emergency Cardiovascular Care Science with Treatment Recommendations*, Dallas TX.

[14] Coates, T.D., Neural Interfacing: Forging the Human-Machine Connection, *Synthesis Lectures on Biomedical Engineering*, Morgan and Claypool Publishers, 2008

[15] Polikov, V.S., Tresco, P.A., Reichert, W.M., Response of brain tissue to chronically implanted neural electrodes. *J. Neurosci. Methods*, 148:1-18, 2005

[16] Anderson, J.M., Rodriguez, A., Chang, D.T., Foreign Body Reaction to Biomaterials, *Seminar in Immunology*, 20: 86-100, 2008

[17] He, W., and Bellamkonda, R.V., A molecular perspective on understanding and moduluating the performance of chronic central nervous system recording electrodes, in *Indwelling Neural Implants: Strategies for Contending with the In Vivo Environment*, 2008

[18] Bryers, J.D., Giachelli, C.M., Ratner, B.D., Engineering Biomaterials to Integrate and Heal: The Biocompatability Paradigm Shirts. *Biotech. And Bioeng.*, 109(8):1898-1911, 2012

[19] Anderson, J.M., Biological Responses o Materials. *Annual Reviews of Material Research*, 31:81-110, 2001

[20] Bilston, L.E., and Thibault, L.E., The mechanical properties of the human cervical spinal cord in vitro. *Ann. Biomed. Eng.*, 24:67 – 74, 1996

[21] Giordana MT, Attanasio A, Cavalla P, Migheli A, Vigliani MC, Schiffer D., Reactive cell-proliferation and microglia following injury to the rat-brain. *Neuropathol Appl Neurobiol*, 20:163–74, 1994

[22] Fujita T, Yoshimine T, Maruno M, Hayakawa T., Cellular dynamics of macrophages and microglial cells in reaction to stab wounds in rat cerebral cortex. *Acta Neurochir (Wien)* 140:275–279, 1998

[23] Szarowski DH, Andersen MD, Retterer S, Spence AJ, Isaacson M, Craighead HG., et al. Brain responses to micro-machined silicon devices. *Brain Res*;983:23–35, 2003

[24] Hopcroft, M.A., Nix, W.D., Kenny, T.W. What is the Young's modulus of silicon? *J. Microelectromech. Syst.*, 19:229-238, 2010

[25] Borschel, G.H., Kia, K.F., Kuzon, W.M., Jr., Dennis, R.G., Mechanical properties of acellular peripheral nerve. *J. Surg. Res.*, 114:133 – 139, 2003

[26] Yu , Z., and Morrison , B., Experimental mild traumatic brain injury induces functional alteration of the developing hippocampus . *J. Neurophysiol*., 103:499 – 510, 2010

[27] Donaldson , N. , Rieger, R., Schuettler , M., and Taylor , J. Noise and selectivity of velocity - selective multi - electrode nerve cuffs . *Med. Biol. Eng. Comput.*, 46:1005 – 1018, 2008

[28] Cheung , K.C., Implantable microscale neural interfaces . *Biomed. Microdevices* , 9:923 – 938, 2007

[29] Kim , S., Bhandari , R., Klein , M., Negi , S., Rieth , L., Tathireddy , P., Toepper , M., Oppermann , H., and Solzbacher , F., Integrated wireless neural interface based on the Utah electrode array . *Biomed. Microdevices*, 11:453 – 466, 2009

[30] Edell , D.J., A peripheral nerve information transducer for amputees: long - term multichannel recordings from rabbit peripheral nerves . *IEEE Trans. Biomed. Eng*., 33:203 – 214, 1986

[31] Cheung, K.C., Renaud, P., Tanila, H., Djupsund, K., Flexible polyimide microelectrode array for *in vivo* recordings and current source density ananlysis. *Biosens. Bioelectron.*, 22:1783-1790, 2007

[32] Meacham, K.W., Giuly, R.J., Guo, L., Hochman, S., DeWeerth, S.P., A lithographically-patterned, elastic multi-electrode array for surface stimulation of the spinal cord. *Biomed. Microdevice*, 10:259-269, 2008

[33] Heuschkel, M.O, Fejtl, M., Raggenbass, M., Bertrand, D., Renauld, P., A three-dimensional multi-electrode array for multi-site stimulation and recording in acute brain slices. *J. Neurosci. Methods*, 114:135-148, 2002

[34] Sheiko, S.S., Xu, H., Sun, F.C., Shirvanyants, D.G., Rubinstein, M., Shabratov, D., Beers, K.L., Matyjaszewski, K., Molecular pressure sensors. *Adv. Mater.*, 19:2930 – 2934, 2007

[35] Sun, Y.G., and Wang, H.H., High-performance, flexible hydrogen sensors that use carbon nanotubes decorated with palladium nanoparticles. *Adv. Mater.*, 19:2818 – 2823, 2007

[36] McClain, M.A., Clements, I.P., Shafer, R.H., Belleamkinda, R.V., LaPlaca, M.C., Allen, M.G., Highly-compliant microcable neuroelectrodes fabricated from thin-film gold and PDMS. *Biomed Mocrodevices*, 13:361-373, 2011

[37] Yu,Z., Graudejus, O., Tsay, C., Lacour, S.P., Wagner, S., Morrison, B., Monitoring hippocampus electrical activity *in vivo* on an elastically deformable microelectrode array. *J. Neurotruama*, 26:1135-1145, 2009

[38] Henle, C., Raab, M., Cordeiro, J.G., Doostkam, S., Schulze-Bonhage, A., Stieglitz, T., Rickert, J., First long term *in vivo* study on subdurally implanted micro-ECoG electrodes, manufactured with a novel laser technology. *Biomed. Microdevices*, 13:59-68, 2011

[39] Lacour, S.P., Wagner, S., Huang, Z.Y., Suo, Z., Stretchable gold conductotrs on elastomeric substrates. *Appl. Phys. Lett.*, 82:2404-2406, 2003

[40] Gorm, P., Cao, W., Wagner, S., Isotropically stretchable gold conductors on elastomeric substrates. *Soft Matter*, 7:7177-7180, 2011

[41] Cao, W., Gorrn, P., Wagner, S., Modelling the electrical resistance of gold film conductors on uniaxially stretched elastomeric substrates, *Appl. Phys. Lett.*, 98:212112-212113, 2011

[42] Santhanam, G., Ryu, S. I., Byron, M. Y., Afshar, A., and Shenoy, K. V., A high-performance brain–computer interface. *Nature* 442:195–198, 2006

[43] Hochberg. L.R., and Donoghue, J.P., Sensors for brain-computer interfaces. *IEEE Eng. Med. Biol.* 25:32-38, 2006

[44] Moritz, C.T., Perlmutter, S.I., Fetz, E.E., Direct control of paralyzed muscles by cortical neurons. *Nature*, 456:639-642, 2008

[45] Aggarwal, V., Acharya, S., Tenore, F., Shin, H-C., Etienne-Cummings, R., Schieber, M. H. and Thakor, N. V. Asynchronous decoding of dexterous finger movements using M1 neurons. *IEEE Trans. Neural Syst. Rehabil. Eng.* 16:3–14, 2008

[46]Berger, T. W., Hampson, R. E., Song D., Goonawardena A., Marmarelis, V. Z. Deadwyler, S. A., A cortical neural prosthesis for restoring and enhancing memory. *J. Neural Eng.* 8:046017, 2011

[47] Ethier, C., Oby, E. R., Bauman, M. J., Miller, L. E. Restoration of grasp following paralysis through brain-controlled stimulation of muscles. *Nature* 485:368–371, 2013

[48] McCreery, D., Lossinsky, A., Pikov, V., Liu, X., Microelectrode array for chronic deep-brain Microstimulation and recording. *IEEE Transactions on Bio-Medical Engineering*, 53:726-737, 2006

[49] Hoogerwerf, A.C., and Wise, K.D., A three-dimensional microelectrode array for chronic neural recording. *IEEE Transactions on Bio-Medical Engineering*, 41:1136-1146, 1994

[50] Maynard, E.M., Nordhausen C.T., Normann R.A., The Utah intracortical Electrode Array: a recording structure for potential brain-computer interfaces. *Electroencephalogr Clin Neurophysiol* ;102:228-239, 1997

[51] Lau, B., Guevremibt, L., Mushahwar, V.K., Strategies for generating prolonged functional standing using Intraspinal Microstimulation. *IEEE Trans. Neural. Syst. Rehabil. Eng.*, 15:273-285, 2007

[52] Saigal, R., Renzi, C., Mushahwar, V.K., Intraspinal Microstimulation generates functional movement after spinal cord injury. *IEEE Trans. Neural Syst. Rehabil. Eng.,* 12: 430-440, Dec. 2004

[53] Margulies, S.S., Meaney, D.F., Bilston,L.B., Thibault,L.E., Campeau, N.G., Riederer, S.J., "In Vivo Motion of the Human Cervical Spinal Cord in Extension and Flexion," in Proceedings of the 1992 International IRCOBI Conference on the Biomechanics of impacts, VERONA, ITALY, 1992.

[54] E.L. Mazuchowski, and L.E. Thibault, "Biomechanical properties of the human spinal cord and pia matter," *in Summer Bioengineering Conference*, Key Biscayne, Florida, 2003

[55] Khaled, I., Elmallah, S., Cheng, C., Mouusa, W.A., Mushahwar, V.K., Elias, A.L., A flexible based electrode array for Intraspinal Microstimulation. *IEEE Transactions on Biomedical Engineering*, 60:2904-2913, 2013

Chapter 3: Developing Strain Relief Leads

3.1 Introduction

In this chapter, the development of strain relief leads will be discussed. Two different configurations of leads were developed: leads that were embedded in a solid slab of PDMS and lead that were sandwiched between two pieces of PDMS. In both cases, strain relief was implemented by incorporating a sinusoidal wave pattern into the straight leads. The two lead configurations were subjected to 12% strains, which is similar to that of the spinal cord [1] and characterized mechanically. In addition, the properties of the base (PDMS) were investigated when subjected to physiological conditions for up to 3 months and a sterilization protocol. The mechanical properties were then tested and characterized to determine the stress and elastic modulus of the base with strain relief leads. The modulus values were compared to those of the spinal cord (1.40 MPa) [2]. Figure 3.1 shows a schematic of the strain relief leads in a base.

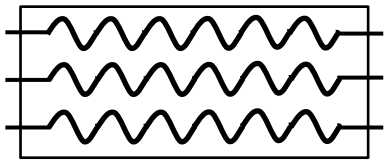

Figure 3.1. Strain relief leads in a PDMS base

3.2 Materials of Construction and Design Parameters

3.2.1 Base

Polydimethyl siloxane (PDMS) is a silicone elastomer that is optically clear, inert, non-toxic and non-flammable that has been commonly used as an elastomer in many devices. MED 6215 (NuSil Technology, Carpinteria, California, USA) was used for all the experimental tests, as determined by Khaled *et al* [3]. A ratio of 10:1 (elastomer:cross-linker by weight) was used, as per manufacturer's instructions to create a medical grade device. The samples were thoroughly mixed and then put into a desiccator in order to get rid of any gas bubbles, which would change the mechanical properties of the sample. The elastomer is then poured into a suitable mold with the desired leads to create the desired lead configuration, which will be described below. The entire sample is put into an oven for 90 minutes at 66°C. The resulting samples are characterized.

3.2.2 Electrodes and Leads

The electrodes and leads are made from Platinum/Iridium (Pt/Ir) which is insulated with polyimide. The two diameter of wire used were 30 µm and 50 µm and these wires had a maximum insulation thickness of 5 µm and 10 µm, respectively. The microwires were obtained from California Fine Wire (Grover

Beach, California, USA). Strain relief was created using plastic racks from SDP/SI (Stock Drive Products/Sterling Instruments, New Hyde Park, New York, USA), as shown in Figure 3.2. Two different plastic racks were used: the first set of plastic racks has a pitch height of 0.203" and the other had a pitch height of 0.281". These two racks created two different amplitude sizes for experiments. In order for strain relief to be created, the wires are placed between two plastic racks and crimped. The result would be a reproducible and regular set of microwires with strain relief incorporated into it. These new patterned microwires would be used for the rest of the experiments.

Figure 3.2. Plastic rack used to create strain relief in leads

3.3 Parameters for Tensile Test

An Instron 4443 Force Tester (Grove City, Pennsylvania, USA) was used to measure stresses and forces as a sample was being strained. The instrument is

shown in Figure 3.3. For each sample, five repetitions were performed to allow for a better picture of the material properties of the base. Before the test started, the width, length and thickness of the sample was measured and inputted to allow for a more accurate calculation of the stress. Before straining, the sample was pre-strained to a stress reading of 0.5 MPa. This was used to straighten the sample to obtain a more accurate measurement once the test started. The samples were strained at a rate of 50 mm/min until a strain of 15% was achieved. The strains, stresses, and forces were outputted onto a spreadsheet file, which could be used for further analysis, such as the calculation of the elastic modulus.

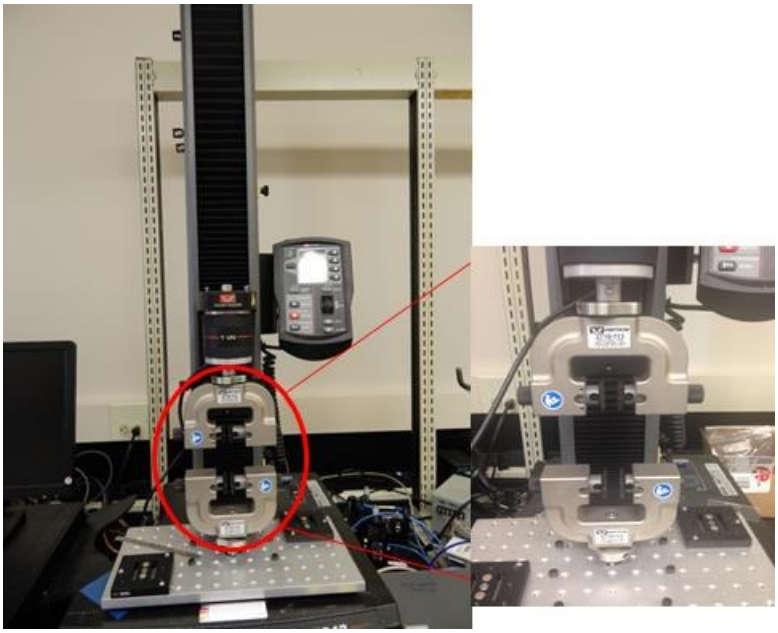

Figure 3.3. Instron mechanical characterization machine and a magnified version of the clamps used during tensile testing

3.4 Embedded Leads

The first configuration for strain relief leads are known as the embedded leads. This set of leads involves PDMS being cured around the wires. This section will describe the fabrication protocol of these leads, the experimental design and results for testing this first configuration. Figure 3.4 shows a side view schematic diagram of three wires embedded in a solid slab of PDMS.

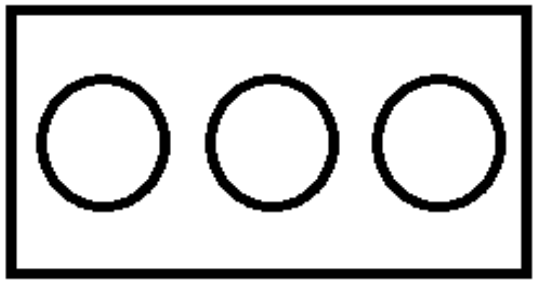

Figure 3.4. Embedded leads in a solid block of PDMS

3.4.1 Fabrication of Embedded Leads

In order to fabricate embedded leads, moulds had to be created for sample creation. The moulds are in a shape of a dog bone and would allow for embedding of microwires so that PDMS can be poured around the sample. The dog bone mould were made of aluminium and had three layers, all attached together using screws. Three layers were chosen in order to allow for the sample

to be easily removed and to allow for easy cleaning of the mould. Aluminium was chosen as the material of construction for the mould because this material would present a less likely chance for the PDMS to bond with, thus allowing for easy sample retrieval. A picture of this mold is shown in Figure 3.5.

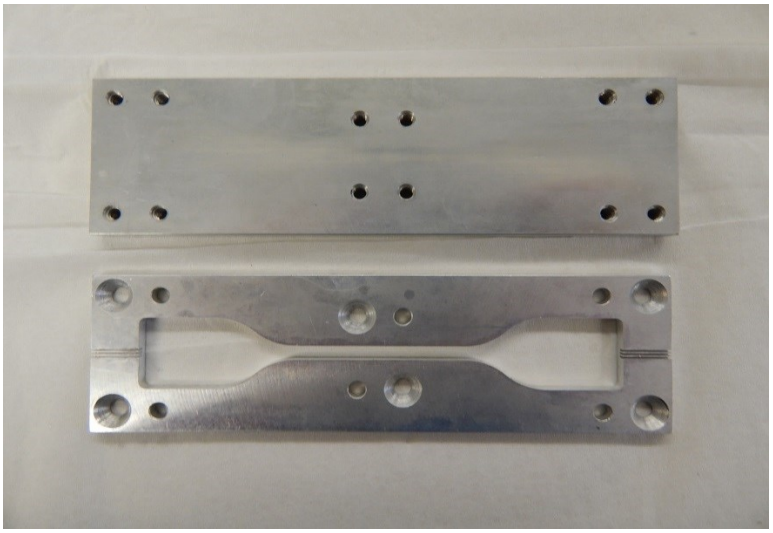

Figure 3.5. Bottom and center plate of mould used for the creation of the embedded leads.

Figure 3.6 shows a schematic of the dog bone with measurements. The dog bones were 10 cm in length and the inside annulus and outside dog bone shapes were 0.3 cm and 1.5 cm, respectively. Two different moulds were made, so the resulting thickness of each sample was either 0.28 mm or 0.3 mm, depending on the mould used. The mould allowed for one to three microwires to be included in the sample. In order to further prevent bonding of the PDMS to the aluminium

surface, low temperature vacuum grease was applied before the PDMS was poured into the mould. In addition, the mould was cleaned with a dilute acetic acid solution after several samples were created.

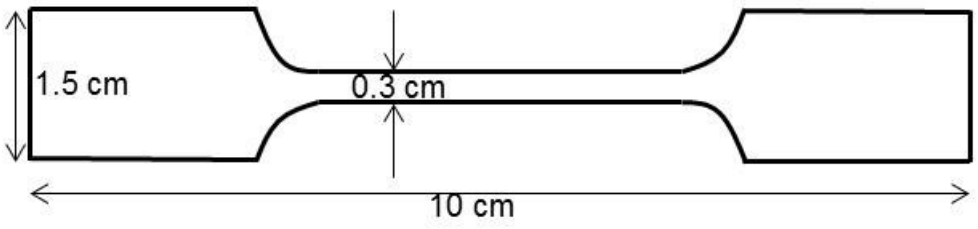

Figure 3.6. Dog bone schematics with measurements

Before pouring PDMS into the mould, microwires would be placed into the mould. In order for the microwires to be fully embedded in the polymer, a bit of tension was applied to make sure the microwires were straight along the middle of the dog bone. The ends of the microwires were taped to the bottom of the mould. PDMS would then be poured and cured in a similar way described in Section 3.2.1.

3.4.2 Experimental Design

The main objective for this section was to determine whether varying microwire diameter (X1: variable 1), strain relief amplitude (X2) and number of embedded microwires (X3) would affect the material properties of the base, specifically, the

elastic modulus of the base. For the embedded leads, a 2^3 experimental design was applied to the system. Each variable had two levels: a high value (assigned a value of 1) and a low value (assigned a value of -1). In this set, microwire diameter was varied between 30 and 50 μm, strain relief pitch height were varied between 0.203" (small) and 0.281" (large) and the number of wires were varied between one and three microwires. Through this experimental design, eight experiments were planned that can give information on which variables or interactions of variables would greatly affect the elastic modulus of the base. The eight experiments with their corresponding variable values are shown below in Table 3.1.

Table 3.1. Experimental Design for Embedded Leads

Experiment Number	Variable		
	Wire Diameter (X1)	**Amplitude Size (X2)**	**Number of Wires (X3)**
1	30 μm (-1)	Small (-1)	1 (-1)
2	50 μm (1)	Small (-1)	1 (-1)
3	30 μm (-1)	Large (1)	1 (-1)
4	50 μm (1)	Large (1)	1 (-1)
5	30 μm (-1)	Small (-1)	3 (1)
6	50 μm (1)	Small (-1)	3 (1)
7	30 μm (-1)	Large (1)	3 (1)
8	50 μm (1)	Large (1)	3 (1)

Based on the experiments, the equation below can be solved:

$$Y = \beta_0 + \beta_1 X_1 + \beta_2 X_2 + \beta_3 X_3 + \beta_{12} X_1 X_2 + \beta_{13} X_1 X_3 + \beta_{23} X_2 X_3 + \beta_{123} X_1 X_2 X_3$$

where Y represents the elastic modulus, X is displayed in the table and β is the coefficients. Large absolute coefficients represent the variables or interactions between variables that are important in determining the modulus. Smaller coefficients will mean that the variable does not significantly affect the modulus of the base. All statistical tests will be based on 95% confidence intervals. In

addition, the sign of the coefficients (+ or -) will indicate whether each variable has a positive or negative effect on the responding variable. The elastic modulus is calculated through linear regression of the linear portion of the stress-strain curve. In order to reduce systematic bias, the runs were performed in random order. In addition to the modulus, the stresses at 15% strain were also analyzed.

3.4.3 Results

The following section will present the stress-strain curves for the embedded wires for both 50 and 30 μm samples. The calculated modulus for each of the 8 experiments will also be described in this section.

Figure 3.7 shows the stress-strain curve for the 50 μm microwire embedded leads samples. Each strain relief point represents 5 samples that have been averaged and the error bars represents standard deviations between the samples. The slope of the curve represents modulus and linear portions of the graph represent elastic straining, which means that samples can return to its initial geometry after the strain is released. When the graph deviates from a linear trend, the deformation becomes plastic, which means that the deformation is permanent and initial geometry cannot be obtained after strain is released. One important observation is that the samples can all strain the required 12% in a repeatable manner. The

samples that have three wires each have a larger stress than their respective sample that had one wire in them. Also, the samples that have small amplitudes tend to have a larger stress than those samples that have larger amplitude strain relief. The straight wire sample broke at approximately 2.5% strain and had a stress that was approximately five times higher than any of the other samples.

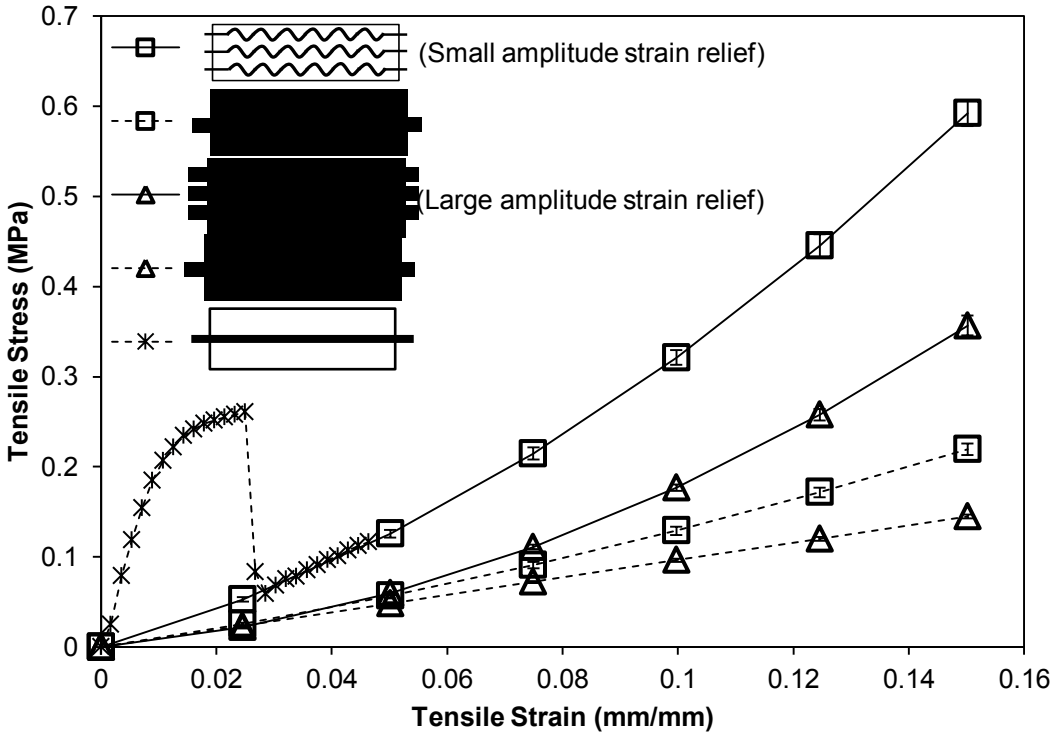

Figure 3.7. Stress-strain curves for 50 μm wire. Solid lines represent samples that have 3 wires while dashed lines represent 1 single wire. Also, square symbols represent small amplitude strain relief while triangles represent large amplitude strain relief. Error bars are derived from standard deviations between five samples.

Figure 3.8 shows a stress-strain curve for 30 μm microwires. As with the previous figure, each data point represents five samples that have been averaged and standard deviations between the samples are represented with error bars. It can be seen that the samples can be deformed in a repeatable manner for the full 15% strain. Also, three samples have a larger stress compared to their single wire counterpart. In addition, the samples that have smaller amplitude strain relief have a larger stress than samples that contain large amplitude strain relief. In addition, the sample with the straight wire breaks at approximately 1.5% strain and at that strain also contains a stress value that is larger than those that has strain relief incorporated.

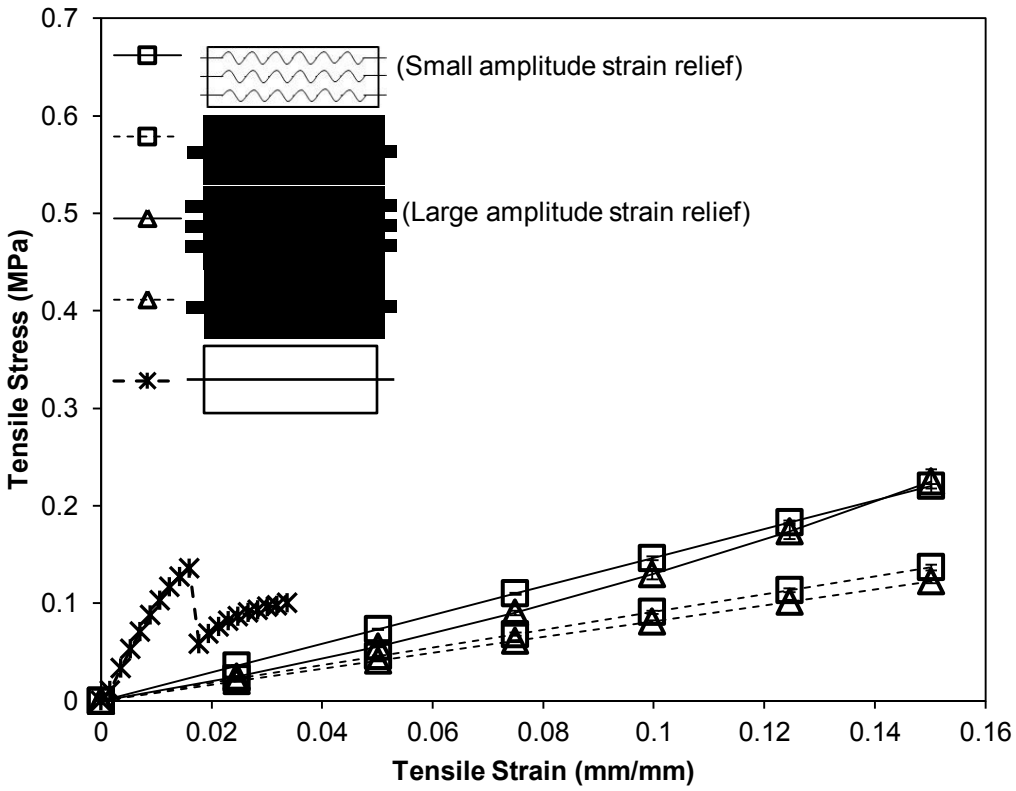

Figure 3.8. Stress-strain curve for 30 μm embedded microwire samples. Solid lines represent 3 microwires while dashed lines represent single microwires. Triangles represent large amplitude strain relief samples while squares represent small strain relief samples. Error bars are derived from standard deviation between five samples.

Table 3.2 shows all the calculated modulus values for each of the experiments described in section 3.4.2 and also the elastic modulus of a single straight wire in PDMS and PDMS only. The elastic modulus was determined from a linear regression of the linear portion of the stress-strain curve. Where the entire curve

is linear, the modulus was calculated from 0% to 15% strain. In cases where the whole stress-strain curve deviates to non-linear, the modulus was calculated based on the linear regression of the linear region before the curve deviates. The point at which the graph deviates from linear to nonlinear was estimated by eye. The values displayed in the table below arethe average of the modulus from each of the individual five samples, and errors are from the standard deviations of all sample repetitions. The r^2 values are also displayed in the table below. Based on the r^2 values, it can be seen that the linear regression fit is a good fit for the data. From the data shown below, the highest modulus can be found from the straight wire while the lowest modulus is the blank sample. All the embedded array modulus fall between this high and low value described.

Table 3.2. Elastic modulus and r^2 values for all embedded array experiments.

Elastic Modulus (MPa) [r^2]		**Embedded Array**		**Straight Wire (PDMS +Wire)**	**Blank Sample (PDMS only)**
		50 µm microwire	**30 µm microwire**		
Large Amplitude	**1 wire**	0.97 ± 0.02 [*0.995*]	0.82 ± 0.01 [*0.992*]	28.9 ± 1.2 [*0.934*]	0.60 ± 0.03 [*0.985*]
	3 wire	1.78 ± 0.04 [*0.954*]	1.31 ± 0.05 [*0.961*]		
Small Amplitude	**1 wire**	1.35 ± 0.04 [*0.994*]	0.91 ± 0.02 [*0.997*]		
	3 wire	2.86 ± 0.04 [*0.966*]	1.47 ± 0.02 [*0.957*]		

3.4.4 Discussion: Stress and Modulus Comparison

In this section, the stress at 12% strain will be compared between embedded samples. In addition, the modulus calculated will also be compared to the controls of the blank PDMS sample and a straight wire embedded in PDMS. In addition, the results of the experimental design equation will be discussed.

3.4.4.1 Stress at 12% Strain Comparison

The first variable investigated to determine the viability of using embedded leads is stress at 12%. When comparing the graphs for the two wire diameters tested, it can be seen that each sample tested for 50 μm exhibits a larger stress compared to its 30 μm counterpart. An example can be seen from three small amplitude strain relief wires. For 50 μm wire, the tensile stress is shown to be approximately 0.4 MPa with the stress for the equivalent 30 μm sample shown to be around 0.15 MPa. In addition, the 50 μm samples, particularly those samples that have three wires embedded in them, exhibit nonlinear stress-strain behaviour. This means that stress increases nonlinearly with increasing strain and this also affect the stiffness of the base. At preliminary glance, based on this data, it can be concluded that 30 μm microwires are a better alternative to 50 μm wires. In addition, the graph shows that for both wire diameters, samples with three

microwires implanted requires larger strains to get to the same stress when compared to samples with one microwire in them. In terms of strain relief amplitude, the graphs do not really show a definitive trend as to what amplitude size is better for the 30 μm; however, for 50 μm, larger amplitudes are better as smaller amplitudes shows a higher stress for the corresponding strains.

3.4.4.2 Elastic Modulus Comparison

The second variable investigated is elastic modulus. One important result was that each of the experimental modulus calculated fell between numbers for the blank polymer and samples with a single microwire embedded in PDMS. This means that the strain relief mechanism was able to do its job in reducing the overall stiffness of the base. Several key trends also appeared from the modulus calculated. The first key trend was that 50 μm wires had a larger modulus or stiffness value compared to the 30 μm embedded samples. This confirms the observation in the section above which states that 30 μm wire should be used. In addition, another key trend is that single wire samples had a smaller modulus compared to three wires. While this seems intuitive, the idea of having a single wire electrode array is impractical.

In addition to comparing the two different lead configurations, the experimental modulus was compared to the modulus obtained from theoretical calculations. The calculation treats the system of embedded leads as resistors in series where the objective is to find the total resistance, or in this case the theoretical modulus. The equation below was used to calculate the theoretical modulus, in order to compare with the experimental values. This equation assumes constant sample geometry and is based on the modulus of a sample with a single lead.

$$E_{theoretical} = E_{PDMS} + nE_{lead}$$

In this equation E_{lead} is calculated by subtracting the modulus of the PDMS from the experimentally-measured modulus of a sample with one embedded wire. For the embedded leads, the range of deviations between theoretical and experimental models is between 0.6% and 8%, which suggests good agreement between experimental and theoretical values.

3.4.4.3 Experimental Design Analysis

The first step in the analysis of the experimental design data is the calculation of the standard error. The standard error (SE) takes into account the standard deviation (SD) of the modulus over five samples and the number of repetitions, n (i.e. 5 samples per experiment) performed for the experiment.

$$SE = \frac{SD_{sample}}{\sqrt{n}}$$

A lower standard error means that the overall experimental results are fairly reproducible. The calculated standard error based on modulus for all eight experiments and a total of 40 degrees of freedom is 0.06, which means that the experiment is fairly repeatable.

Table 3.3 shows the calculated coefficients, which is the solution to the equation listed in section 3.4.2. From the data shown below, it can be concluded that the number of wires, wire diameter and the interaction between these two variables are important in the determination of the modulus or stiffness of the base. These variables all have a positive effect on the responding variable meaning that to achieve a lower stiffness or elastic modulus, the lower limit for each of variable should be taken (i.e. 30 μm and a single wire). This supports the observations seen above.

Table 3.3. Coefficients and their 95% Confidence Interval Value

Coefficients	Coefficient Values	95% CI Value
β0	1.62	0.245
β1	0.48	
β2	-0.09	
β3	0.57	
β12	-0.02	
β13	0.32	
β23	0.06	
β123	0.07	

Based on these experiments, the best three wire configuration involves 30 μm microwires with large amplitude strain relief. The value of 1.31 MPa falls under the target value of 1.40 MPa [1] for spinal cord with pia. However, this sample only has three microwires and further increase in density of leads would largely change the stiffness of the base. The resulting stiffness would then be greater than the target spinal cord stiffness.

One hypothesis as to why the embedded leads exhibit a higher stiffness when lead density increase is that, while the strain relief mechanism works, the ability for the wire to straighten out is hindered because of the polymer surrounding the

sample. The PDMS that was being cured was acting like a resistor and the results are magnified when the number of lead wires is increased. With this in mind, the second lead wire configuration, known as the sandwich arrays were created.

3.5 Sandwich Leads

The sandwich leads are the second lead configuration set tested. The main goal was to develop this lead configuration set that would have a smaller stiffness compared to the embedded arrays and closer to the polymer stiffness of 0.60 MPa. This section will describe the fabrication of the array, as well as experimental design and results. In addition, a comparison would be made between the two configurations at the end.

3.5.1 Fabrication of Sandwich Leads

The main differences between the sandwich leads and the embedded leads are found in the geometry of the sample and the incorporation of PDMS in both samples. While the embedded samples are dog bone shaped, the sandwich arrays have a rectangular shape. The sandwich array is 10 cm long, 1 cm wide and 300 μm thick. In addition, while PDMS is cured around the microwires for the embedded arrays, the sandwich array involves two rectangular pieces of PDMS

acting as an insulator for the microwires with strain relief. This geometry allows the PDMS and the microwires to strain independent of each other.

To create the sandwich arrays, thin pieces of PDMS must be cure on silanized glass. The silanized glass prevents the PDMS from remaining bonded to the glass after curing. A small amount of PDMS is put on the glass slide and spread around using a metal spatula. The sample is cured and then removed from the glass. The resulting PDMS is then cut into strips that are 10 cm long and 1 cm wide. The sandwich is made with either one or three microwires surrounded by the two strips of PDMS. A small amount of PDMS is put on the edges of the rectangular strips and the resulting array is cured once again. The resulting array is then characterized mechanically and the resulting stresses and modulus are compared to embedded results.

3.5.2 Experimental Design

Based on the embedded array results, it was determined that the configuration to develop the sandwich arrays on was based on 30 µm microwires, and three wires with larger strain relief amplitudes. Based on this configuration, three samples were developed. The first sample involved the standard configuration of three 30 µm microwires that were evenly spaced out. In order to compare the effect of

lead density, a second sample involving only a single 30 μm microwire was created. In addition, a third sample was created involving three 30 μm microwires, with strain relief, that were overlapping each other.

3.5.3 Results

Figure 3.9 shows the stress-strain curve for the 30 μm microwire large amplitude sandwich array samples. Each data point represents 5 sandwich array samples that have been averaged and the error bars represents standard deviations of the samples. As with the previous figures, an important observation is that the samples can all be strained comfortably to 15%. The sandwich samples that have three wires in them still show a larger stress than their corresponding single wire sandwich array sample. In addition, the sample that had overlapping wires had a larger stress than the sandwich samples with wires spaced out. As with the embedded sample, the straight wire sample broke at less than 2% strain and had a stress that was still approximately five times higher than any of the other samples being tested.

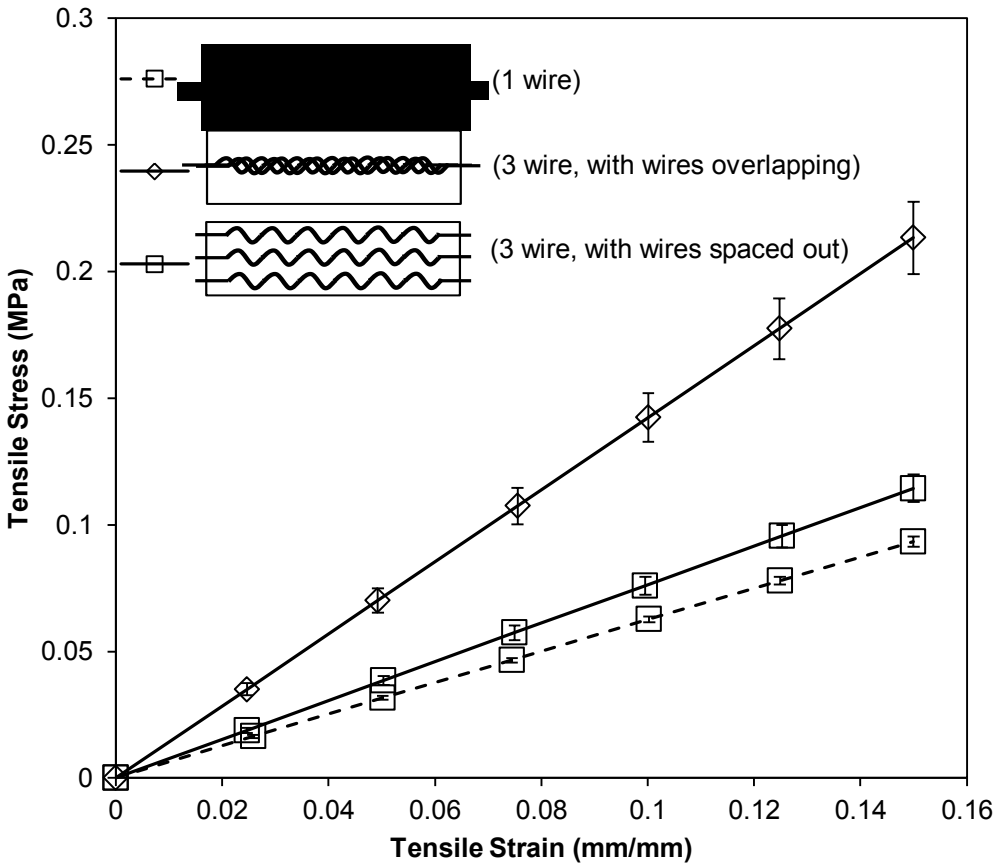

Figure 3.9. Stress-strain curve for sandwich arrays with 30 µm microwires that have large amplitude strain relief. Solid lines represent three wires in sample while dashed line means one wire in sample. Error bars are derived from the standard deviation of the sample

Table 3.4 shows all the calculated modulus values for each of the sandwich array, as well as the corresponding embedded array and also the elastic modulus of a single straight wire in PDMS and PDMS only. As with the embedded array, the

elastic modulus was determined using a linear regression of the linear portion of the stress-strain curve, as described in the embedded array section (Section 3.4). The modulus, displayed in the table below, is taken from the average of the elastic modulus from each of the individual five samples and errors are from the standard deviations of all sample repetitions. Along with the modulus values, the r^2 values are also displayed. Based on the r^2 values, it can be seen that the linear regression is a good fit for the data. From the data below, it can be seen that the modulus for the spaced out wires is smaller than the modulus for the overlapping wires and also closer in value to the modulus of the blank samples.

Table 3.4. Elastic modulus and r^2 values for the sandwich arrays, compared both embedded array counterparts and control samples.

Elastic Modulus (MPa) [r^2]		**Embedded Array**	**Sandwich Array**		**Straight Wire (PDMS+ Wire)**	**Blank Sample (PDMS only)**
Large Amplitude	1 wire	0.82 ± 0.01 [*0.992*]	0.63 ± 0.02 [*0.998*]		28.9 ± 1.2 [*0.934*]	0.60 ± 0.03 [*0.985*]
	3 wire	1.31 ± 0.05 [*0.961*]	1.4±0.1 (overlapping wires) [*0.955*]	0.76 ± 0.04 (spaced wires) [*0.939*]		

3.5.4 Discussion: Stress and Modulus Comparison

Similar trends can be found when comparing the stress at 15% strain and modulus among the sandwich array samples. In the case of stress, the single wire sample had the lowest stress at 15%, while both three wire samples had stresses that were

higher. For the sandwich array with overlapping wires, the stresses appear to nearly double compare to the sandwich array sample with wires that were spaced out. Both single wire sandwich arrays and three wire sandwich arrays have a linear stress-strain curve.

When comparing elastic modulus, it can be seen that the elastic modulus of the single wires is still smaller than three wires that are spaced out. The sandwich array with overlapping wires has a modulus that almost is two times larger than the three wires spaced out samples. These trends agree with the trends found in the stress measurements. When comparing the theoretical elastic modulus values calculated with the experimental values for the spaced-out sandwich arrays, a deviation of 6% was obtained, which suggests good agreement between experimental and theoretical values

A large reason as to why the gap in value for modulus and stress between overlapping wires and spaced out wires is so large is due to the interaction between wires in the overlapping array sample. When straining the overlapping wires sample, the overlapping wires interact with each other. This allows wires to elongate faster than others, causing some wires to be tangled. This internal interaction causes a rise in the stress of the sample with increasing strain. Due to the rise of stress, this influences the elastic modulus of the sample. With the spaced out wires sample, the wires do not interact with each other. Therefore, the

wires are able to strain independently of each other and this causes the stress inside the sample to remain smaller.

3.5.5 Discussion: Embedded and Sandwich Comparison

Figure 3.10 shows the corresponding embedded configuration data overlaid on top of the data from the sandwich array. Comparing the stresses at 15% strain, it can be seen that three wires overlapping has a similar stress output at 15% strain compared to the embedded array. It is also apparent that the 3 spaced out wires and 1 wire sandwich arrays have a much lower stress compared to the embedded array.

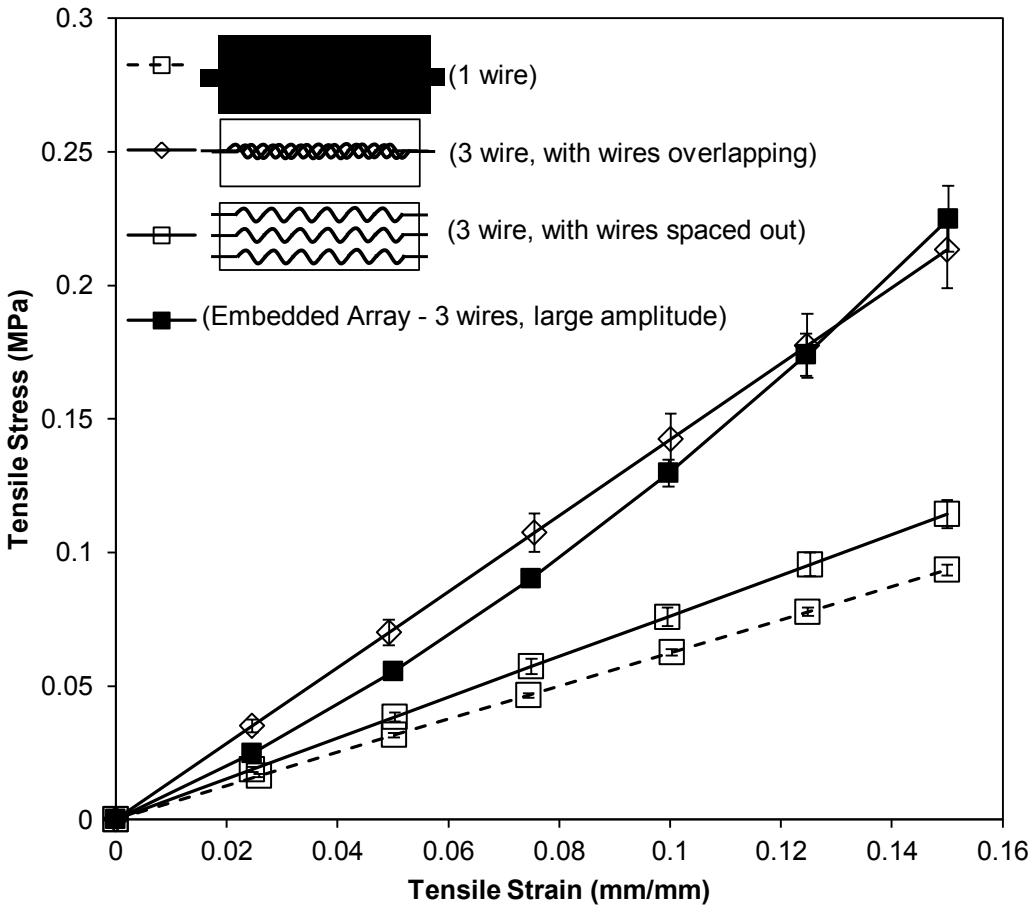

Figure 3.10. Stress-strain curves for sandwich arrays and corresponding embedded configuration. All data points are averaged from five samples. Hollow data points represent sandwich array while shaded data points represent embedded configuration.

Comparing the modulus of the sandwich versus its embedded counterpart, it can be seen that the overlapping sandwich array has a modulus that is higher than the embedded array. The other two sandwich arrays have a modulus that is close to

half of the embedded array's modulus. If we compare the target modulus for the spinal cord stated earlier as 1.40 MPa, it is noted that the three spaced out wires sample has a modulus that is definitely smaller compared to the target modulus. It can also be assumed that increasing the number of leads from one to three does not change the modulus of this array drastically, so therefore a further increase in lead density should not drastically impact the modulus of the base. Based on these findings, it can be concluded that the sandwich leads are better than the embedded leads because it is less stiff and can produce lower stresses.

3.5.5.1 Effect of Geometry Change on Sandwich and Embedded Arrays

One of the key factors in designing the two lead configurations is the geometry of the lead configurations. The embedded leads were tested using dog bone shapes while the sandwich leads were designed in a rectangular shape. The objective of this subsection is to determine whether geometry of the arrays plays an important role in the material properties of the embedded leads. The geometry of the embedded leads was modified to be rectangular, identical to the sandwich leads, and the material properties of the base were characterized.

Figure 3.11 shows the results of the material characterization for a randomly picked configuration of embedded leads and its sandwich array counterpart. It

can be observed on the graph that the geometry does not greatly change the material properties of the base. The stresses and modulus values are all fairly similar between the embedded sample and the sandwich array. This means that the geometry of the samples does not affect the modulus of the sandwich and embedded arrays.

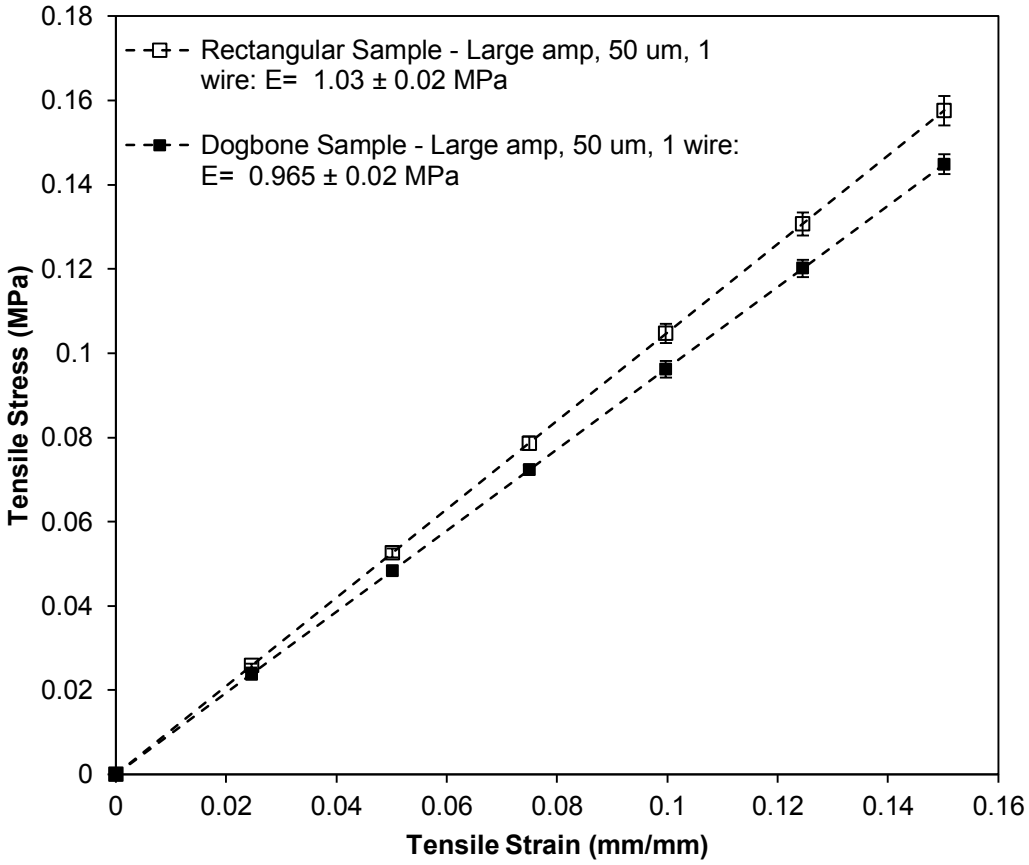

Figure 3.11. Stress-strain curve for the two array configuration with constant geometry. Data points are all averaged from five samples and error bars are taken from the standard deviation of five samples.

3.6 Physiological Test of Base

The goal of this section is to characterize the material properties of the PDMS polymer base after exposure to physiological conditions over an extended period of time. Many studies have looked at the changes in material properties after exposure both in solution and *in vivo*. Silicone rubbers have been implanted in dogs [4-6] and also immersed in pseudo-extracellular fluid [7] for varying lengths of time (between 4 months and 2 years). In both cases, changes in material properties like decrease in tensile strength, and increase in elongation and storage modulus were observed. Another study by Mahomed *et al* [8] studied the short term effects of immersing medical grade silicone elastomers into a saline solution for up to 29 days and noticed no appreciable effect on compressive modulus between 24 hours and 29 days into the study. Other implants, like glass ionomers [9] have also been tested, with no appreciable change in any material properties of the material after immersion in distilled water for 52 weeks. This section will focus on the experimental set-up for the physiological study of the medical grade elastomer used in the development of the flexible based electrode array and investigate the results of the study.

3.6.1 Experimental Set-up

In this study, 15 blank dog bones (i.e. with no microwires) were created. The first set of five dog bone samples were tested before at 0 days to establish a baseline for the properties of the material before subjecting them to physiological conditions. The remaining ten dog bones were immersed in a saline solution and kept in an incubator at 37°C. The pH of the samples was kept at neutral. Five dog bones were removed and their material properties tested after 1 month of incubation, while the other five samples were left in the incubator for three months. After each sample was removed, the material properties were characterized by applying a tensile test using the Instron and steps described in section 3.3. The modulus of the sample was calculated and compared to the baseline material properties taken at the beginning of the test.

3.6.2 Results and Discussion

Figure 3.12 shows the stress-strain curve for the tree groups of tensile tests performed. Each point is an average of five samples. From the graph, there is a small increase in stress over time however; the modulus seems to remain fairly constant. From the graph, it can be concluded that the material properties of the

base are not affected after exposure to a physiological environment over 3 months.

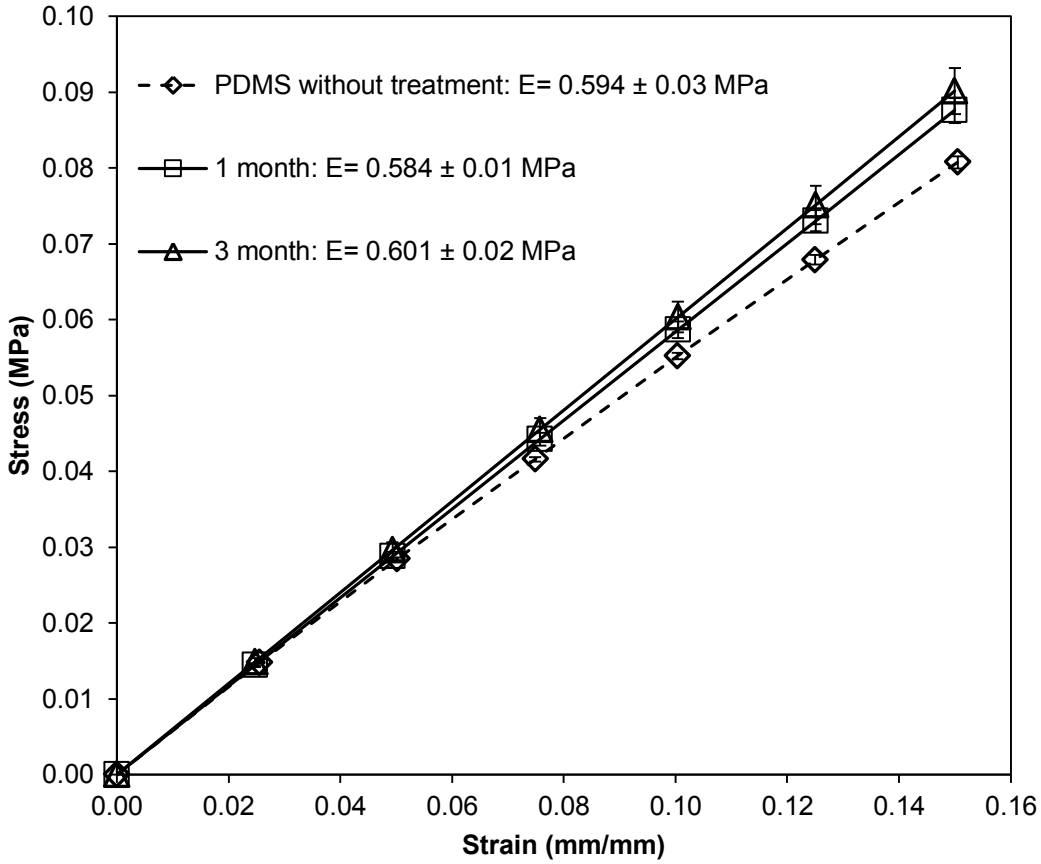

Figure 3.12. Stress-strain curve for physiological tests of the base. All data points are averaged over five samples and the error bars are standard deviation over the samples. Solid lines are physiologically treated samples.

3.7 Sterilization Test of the Base

The main objective of this section is to test the mechanical properties of the base after a sterilization protocol is completed. This section will describe the experimental conditions used and show and compare the experimental results.

3.7.1 Experimental Set-up

For this study, 10 blank dog bones (no microwires, just PDMS) were created. Five dog bones were initially characterized to set-up a baseline for material properties. The remaining five dog bones were put through a sterilization protocol in an autoclave. The samples were wrapped with two towels and then the samples were placed in an autoclave cycle with steam. The samples are sterilized to a temperature of 135°C and then dried. After the sample cooled down, the dog bones were taken to be mechanically characterized. The modulus was calculated and compared to the baseline case to detect changes in material properties.

3.7.2 Results and Discussion

Figure 3.13 shows the stress-strain curve for the sterilized dog bones and the unsterilized dog bones. It can be seen that there is little change in the stress and the modulus after the sterilization procedure.

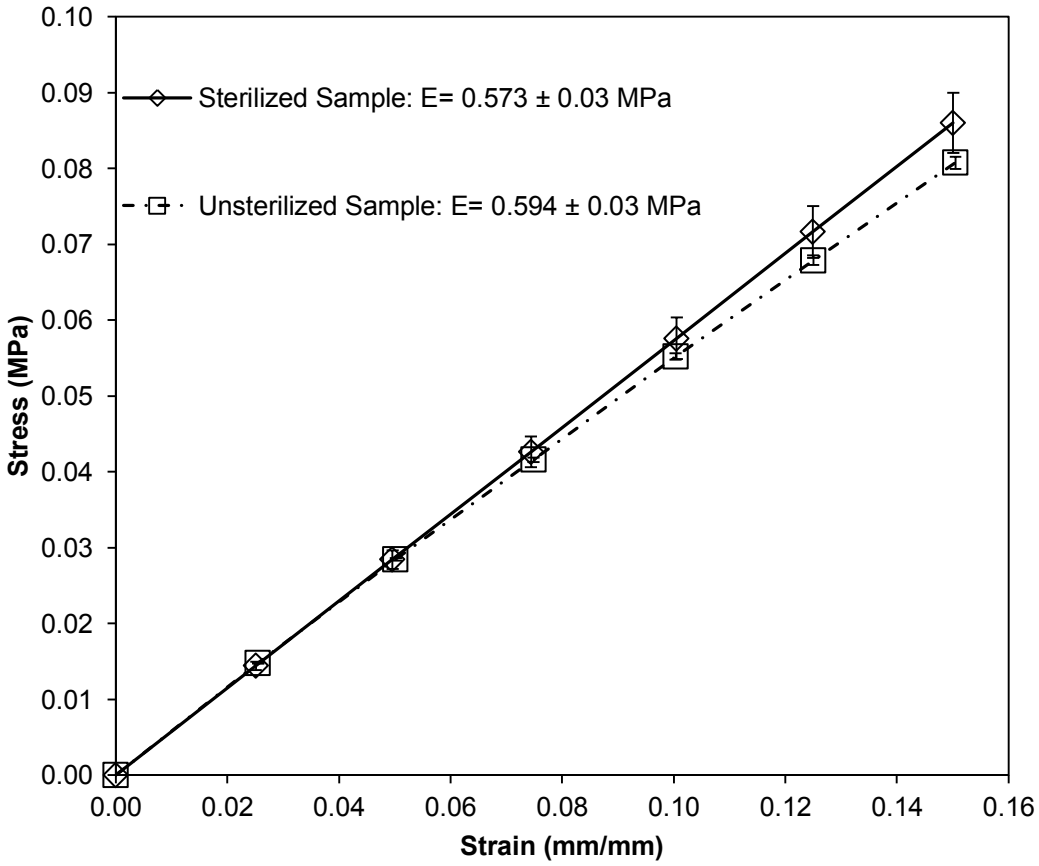

Figure 3.13. Stress-strain curve for sterilization tests. All data points are averaged over 5 samples and error bars are taken from standard deviation of the samples. Sterilized samples are represented by the solid lines

From this graph, it can be concluded that sterilization does not have any effect on the base material properties.

3.8 Conclusion

In this chapter, two different lead configurations were developed and tested: embedded leads and sandwich leads. It was determined that the sandwich leads are a better configuration because they had a lower sample modulus compared to its embedded counterpart. In addition, it was determined that smaller diameter wires were better for decreasing modulus values. It was also seen that the value for the modulus of the sandwich leads were less than the spinal cord modulus value while the embedded leads exceeded the spinal cord values.

In addition, sterilization and physiological studies showed that the polymer base material properties did not change after sterilization procedure or exposure to physiological conditions over three months. With this knowledge, the modelling described in the following chapter was performed in order to aid in the manufacturing of the flexible base electrode array.

3.9 References

[1] S. S. Margulies, D. F. Meaney, L. B. Bilston, L. E. Thibault, N. G. Campeau, and S. J. Riederer, "In Vivo Motion of the Human Cervical Spinal Cord in Extension and Flexion," *in Proceedings of the 1992 International IRCOBI Conference on the Biomechanics of impacts*, VERONA, ITALY, 1992.

[2] E.L. Mazuchowski, and L.E. Thibault, "Biomechanical properties of the human spinal cord and pia matter," *in Summer Bioengineering Conference*, Key Biscayne, Florida, 2003

[3] I. Khaled, S. Elmallah, C. Cheng, W. Moussa, V.K. Mushahwar, and A.L. Elias, "A Flexible Base Electrode Array for Intraspinal Microstimulation" *IEEE Transactions in Biomedical Engineering*, vol. 60, no. 10, pp. 2904-2913, Oct. 2013

[4] J. W. Swanson and J. E. Lebeau, "The Effect of Implantation on the Physical Properties of Silicone Rubbers" *Journal of Biomedical Materials Research*, vol.8, pp. 357-367, 1974

[5] E. Roggendorf, "The Biostability of Silicone Rubbers, a Polyamide, and a Polyester" *Journal of Biomedical Materials Research,* vol. 10, pp.123-143, 1976

[6] R.I. Leininger, V. Mirkovitch, A. Peters, and W.A. Hawks, "Change in properties of plastics during implantation." *Unpublished paper presented at American Society for Artificial Internal Organs*, 1964.

[7] T.C. Ward, and J.T. Perry, "Dynamic mechanical properties of medical grade silicone elastomers stored in simulated body fluids" *Journal of Biomedical Materials Research*, vol. 15, pp. 511-525, 1984

[8] A. Mahomed, N.M. Chidi, D.W.L. Hukins, S.N. Kukureka, D.E.T. Shepherd, "Frequency Dependence of Viscoelastic Properties of Medical Grade Silicones" *Journal of Biomedical Materials Research Part II: Applied Biomaterials*, pp. 210-216, 2008

[9] C.C. Bonifacio, C.J. Kleverlaan, D.P. Raggio, A. Werner, R.C.D de Carvalho, "Physical-mechanical properties of glass ionomers cements indicated fir atraumatic restorative treatment" *Austrailian Dental Journal*, vol. 54, pp. 233-237, 200

Chapter 4: Modelling Strain Relief Leads

4.1 Introduction

In Chapter 3, two different lead configurations (embedded and sandwich leads) were described and characterized to determine which lead configuration provided the greatest strain relief. Based on experimental results, it was shown that sandwich arrays are a better lead configuration due to the lower modulus and stresses associated with the samples. In order to develop a more comprehensive picture, the two lead geometries, sandwich and embedded leads are modelled in this chapter. The main goal of this section is to extend work done in the experimental section to understand how varying different design parameters (including density of leads, base width, wire spacing) affects the average elastic modulus of the sample. A load step study is performed on the embedded arrays to determine the strain at which delamination occurs. All the modulus values obtained will be compared to literature values for spinal cord with pia of 1.40 MPa [1].

4.2 Model Set-up

In order to model the sandwich and embedded lead geometries, a two dimensional numerical finite element model was developed using ANSYS 14.5. The model

set-up, including geometry, element type and boundary conditions will be discussed in this section.

4.2.1 2D Linear Elastic Model Characteristics

The geometry of a typical base is shown in Figure 4.1. The modulus of the PDMS in the base was fixed at 0.55 MPa to match a similar value found in experiments found in Chapter 3 and also to match previous modelling work done [2]. A modulus of 198 GPa was assumed for the modulus of the platinum/iridium microwire leads, which is consistent with tensile tests performed for a single straight microwire and literature value [3]. In our experimental work, polyimide-insulated microwires being tested had diameters of 30 μm to 50 μm, and they were equally spaced apart and running parallel to the long axis of the device. The number of wires was varied throughout the modeling to investigate the effect of increasing wire density on internal stresses, strains and the overall modulus. As in Chapter 3, two different strain relief amplitudes were used. The two amplitudes were picked to match amplitudes that were similar to those used in experiments. Large amplitudes were measured to be 1 mm from the wave midline to the wave crest, while small amplitudes were modelled to be 0.8 mm from midline to crest. In order to utilize the contact elements, which will be discussed

below, there was a gap of 0.01 mm that was built into the model between the wire and the surrounding base.

Figure 4.1. A schematic of lead geometry with dimensions for three microwires in PDMS.

There are two different types of 2-D models. The first type is known as a plane stress model. In this model, the normal and shear stresses perpendicular to the x-y plane are assumed to be zero. The second type of model is known as a plane strain model; in this model the strain normal to the x-y plane and the shear strain are assumed to be zero. Plane stress conditions are typically found in situations where the object is thin compared to the length and the width, and the object is only loaded in the x and y plane. Plane strain conditions are utilized where objects are long (in the z direction) with a cross sectional area that is constant. Loads in a plane strain situation act only in the x-y direction and does not vary a lot in the z-direction. In the model described in this thesis, plane stress conditions

were assumed. This condition was chosen because of the small thickness of the element, in comparison to the length and the width of the model, as well as the strains being applied in the x-direction only.

4.2.2 Element Type

Two different element types are used in the creation of the model. The first element used is a solid element called plane183. This element is a two-dimensional six node triangular structural solid element. All of the solid areas of the model were meshed with this element, which allowed for two-dimensional displacements in both the x and y axis. In addition, this element allowed for outputs of nodal displacement and stress outputs, both crucial in the development of the results of the model. Finally, this element suits the highly suits the irregular shape of the sinusoidal wire that is being modeled.

To model interactions at the interface, a second element group was required: contact elements. The two elements that make up this group are targe169 and contac172. Both these elements assume surface-to-surface contact between two surfaces. In this model, the contact element was between the microwire and the surrounding PDMS. Using these elements, the contact behaviour between the wire and the polymer can be modelled. The target element is the defined as the

element that receives the contact, while the contact element is the element that provides the contact in the pair. In this model, the PDMS surface provides the target region and the microwire was the contact region. The sandwich and embedded arrays are distinguished when defining the contact element. With the sandwich array, the contact element boundary condition is set to include no-separation initially because the there is no physical bonding between PDMS and the surface of the microwire. However the two elements are allowed to split after displacements and strains are applied. This enables the sandwich array to deform like two independent springs. However, for the embedded arrays, the contact elements are set to being bonded, as the PDMS is cast around the microwires. In this situation, the contact is between the PDMS and the polyimide insulator that surrounds the microwire. Literature has shown that bonding between the PDMS and untreated polyimide is really poor [4,5]. For the model, a bonding strength of 30 kPa was chosen [5] based on the literature bonding strength between polyimide and PDMS. This is consistent with weak bonding values between the two materials.

4.2.3 Boundary Conditions

The boundary conditions were implemented to mimic experimental tensile testing. All the nodes have two degrees of freedom, translation or displacement along the

x (horizontal) or y (vertical) axis. This means that the sample will be strained up to 12%, which is the literature value for average spinal cord elongation in day to day activities [1]. Therefore, the boundary conditions must fit within these degrees of freedom. In order to keep the model as closer to a regular tensile test as possible, one short axis boundary was fixed in the x and y direction, meaning that no translational displacement in the horizontal or vertical direction could take place. This is similar to the tensile tests in that one clamp fixes the sample at one end while the second clamp moves linearly to apply strain. A strain of 12% was applied to entire edge of boundary number one in the x direction. In addition, all corners were fixed in the y direction, which means that there was no translation or displacement in the y or vertical direction. This is consistent with the tensile tests as the clamps prevent the corners of the samples from straining in the y direction, while allowing the sample to strain in the x direction. Finally, no boundary conditions were set on long axis boundary, which is consistent with the tensile test as this allowed the deformation of the sample in the x and y direction. An example of a code used to generate a model with six wires in a base is shown in Appendix A.

4.3 Mesh Dependency Test

A mesh dependency test was performed to determine the appropriate mesh size to use within the model. A mesh dependency test investigates whether a variable converges to a certain value when the mesh or element size decreases (i.e. as the total number of degrees of freedom is increased). In this model, the maximum nodal stress is the variable studied. For the study, the element size was varied between 0.25 mm and 0.02 mm. Models that have a mesh size greater than 0.25 mm cannot be solved numerically because of the irregular mesh that forms, while models that are smaller than 0.02 mm produce elements that are too small and the computer used to run the simulation cannot produce an answer because of the lack of processing power to run this model with a fine mesh. For the element used, each node has two degrees of freedom (each node can be mechanically translated only in the x and the y direction). From this, the maximum number of degrees of freedom can be calculated to be two times the total number of nodes, which is given as a value from ANSYS for each mesh size. Figure 4.2 shows the model validation graph for one embedded microwire lead that has 30 μm diameter. From the graph, it can be seen that the maximum nodal stress does converge as the total number of degrees of freedom increases.

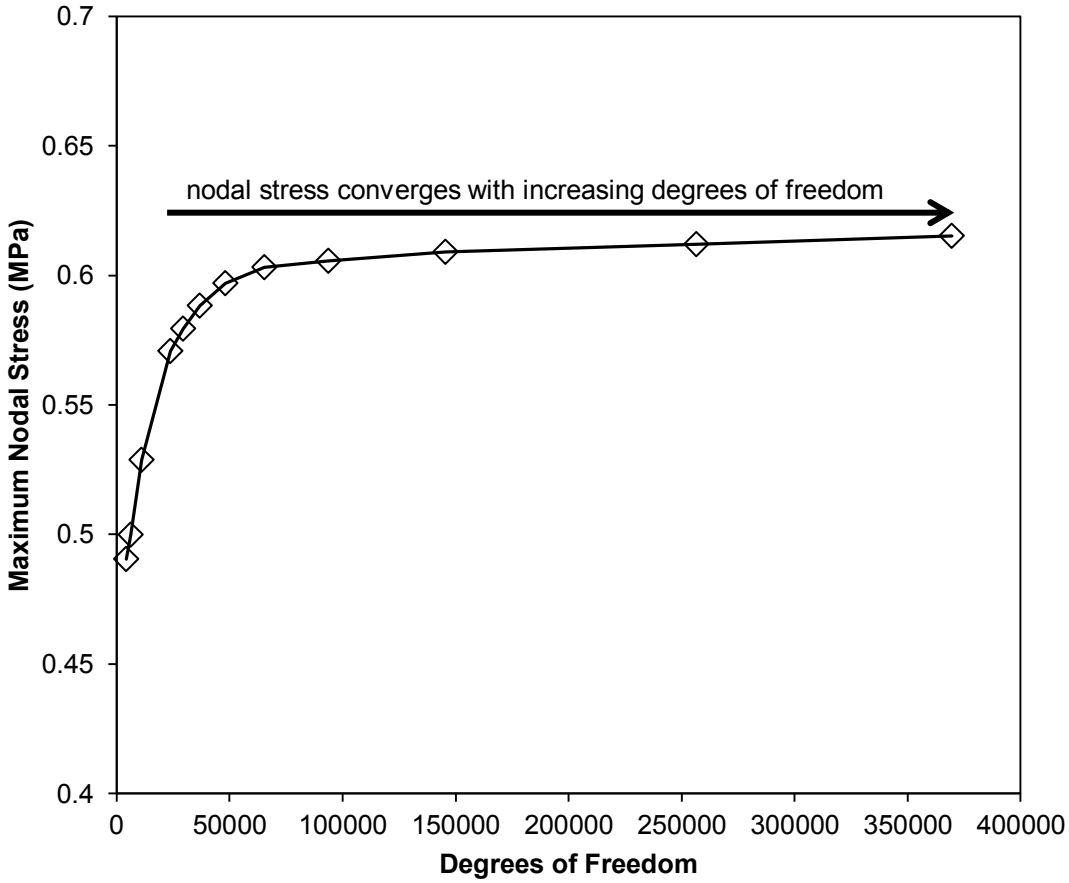

Figure 4.2. Mesh dependency test graph for one 30 µm embedded micro wire lead.

After confirming convergence for maximum nodal stress the time required to achieve a nodal solution was investigated. The optimum mesh size is determined where the maximum nodal stresses converge and a solution can be achieved with a minimal amount of processing time. Figure 4.3 shows the solution times associated with each mesh size.

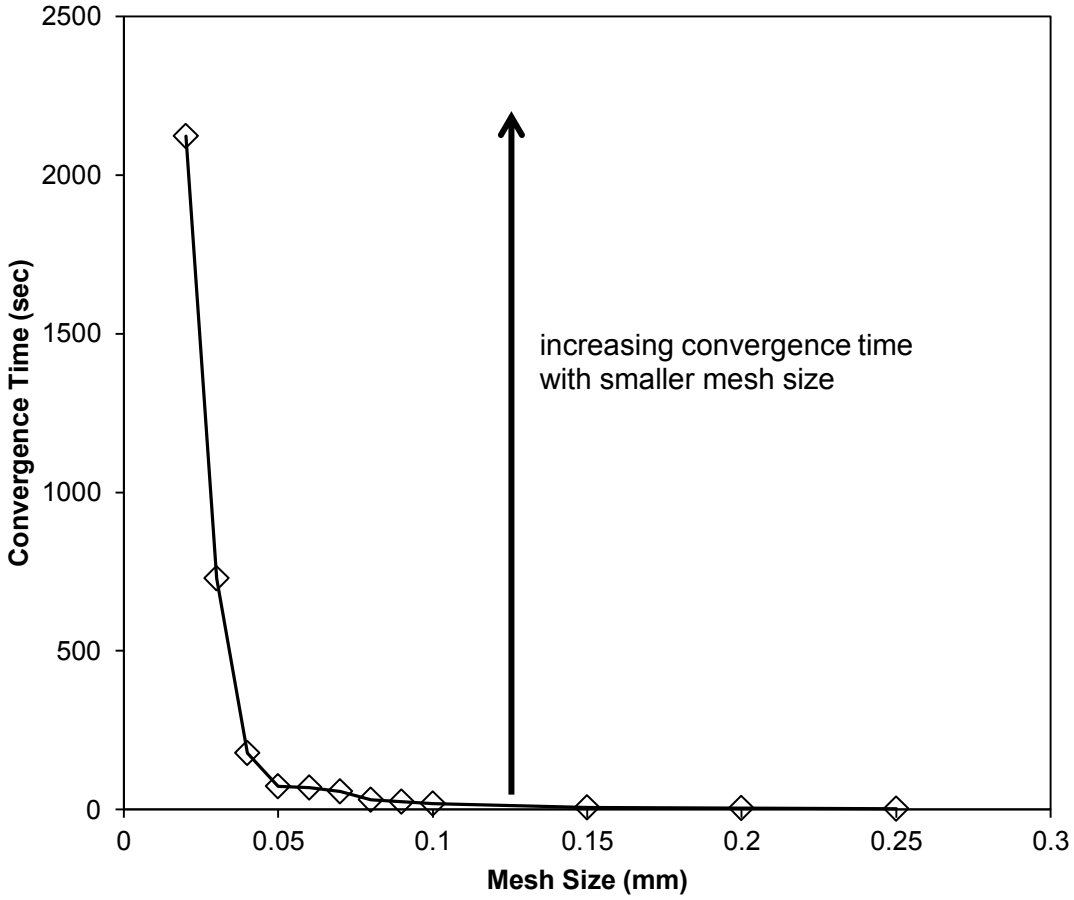

Figure 4.3. Convergence times versus mesh size for model with one 30 μm embedded lead.

From the figure displayed above, it can be seen that there is a large increase in the time required for a model to achieve a solution when the element size is less than 0.05 mm. Based on this table and the graph displayed above, the optimum mesh size was determined to be 0.05 mm. This procedure was carried out for each model to determine the optimum mesh size for each model.

4.4 Results: Comparing Model Modulus with Experimental Results

To determine the modulus of a modeled device at 12% elongation, far field stresses and strains were used. Far field stresses and strains are defined as the stresses and strains that make up the bulk materials in the model. The modulus of the base was determined by taking the far field stress and dividing it by the far field strains. In order to more accurately determine the modulus, each modulus data point displayed in this chapter has an average of five modulus values calculated based on far field stresses and strains. The objective of this section was to see if the modulus outputted by the model is similar to that obtained in experiments. The geometry of the bases was kept the same between the model and the experiments. Figure 4.4 shows a comparison between model and experimental results for the embedded leads, while Figure 4.5 shows comparison with sandwich leads. For the graphs in this chapter, solid data points represent embedded samples while hollow data points represent sandwich samples. The model samples are all joined with a line while experimental samples are shown as discrete data points. The model ran had geometries, element type and boundary conditions similar to those discussed in section 4.2.

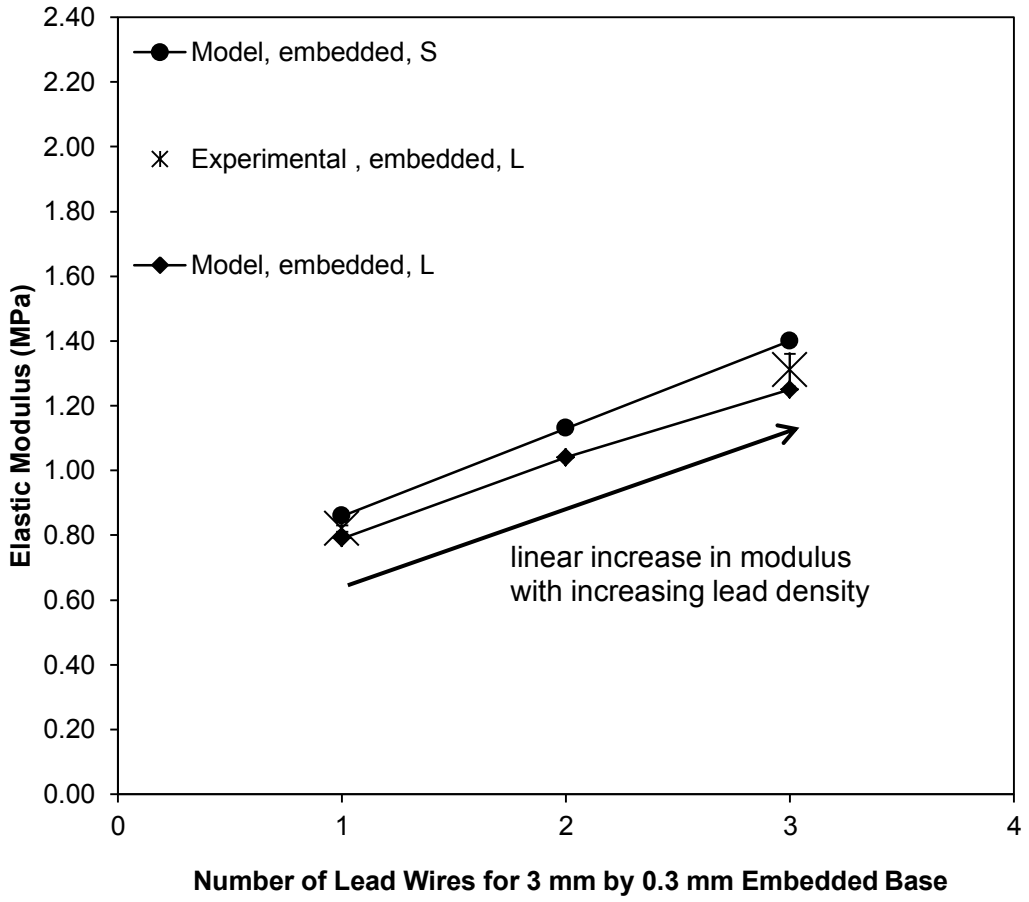

Figure 4.4. Comparison of the elastic modulus obtained experimentally and through modelling of a base with embedded leads that is 3 mm wide by 0.3 mm thick. All model data points are an average of five modulus values from five different far-field elements. Model includes both solid and contact elements. Boundary conditions were set to consistently model a tensile test environment.

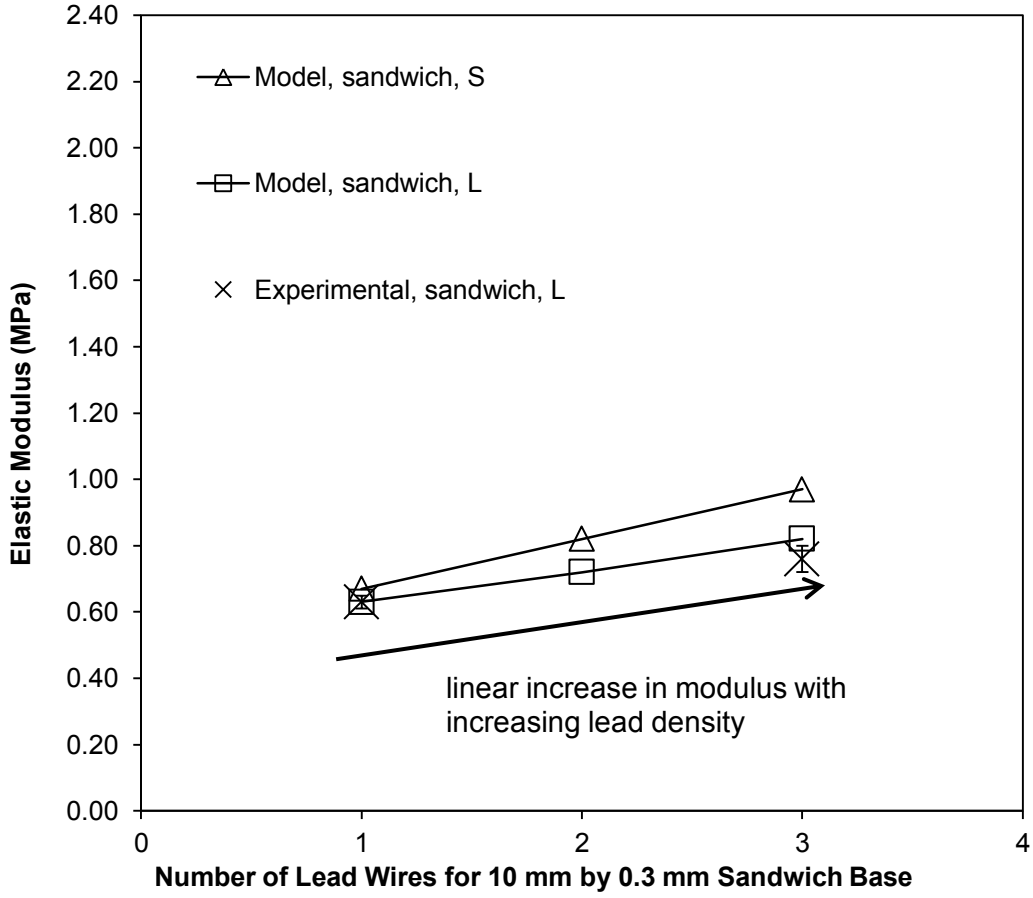

Figure 4.5. Comparison of the elastic modulus obtained experimentally and through modelling of a base with sandwich leads that is 10 mm wide by 0.3 mm thick. All model data points are an average of five modulus values from five different far-field elements. Model includes both solid and contact elements. Boundary conditions were set to consistently model a tensile test environment.

From the graphs, it can be seen that the model data points agree within the error of their corresponding experimental modulus values. Also, it can be observed that the modulus values for the small amplitude strain relief are larger than the corresponding values for the large amplitude strain relief.

In addition to comparing the two different lead configurations, the modulus obtained from the models were compared to the modulus obtained from theoretical calculations performed. The calculation treats the system of embedded and sandwich leads as resistors in series where the objective is to find the total resistance, or in this case the theoretical modulus. The following equation was employed in calculating the theoretical modulus of samples with multiple leads based on the modulus of a sample with similar geometry and a single lead:

$$E_{theoretical} = E_{PDMS} + nE_{lead}$$

In this equation E_{lead} is calculated by subtracting the modulus of the PDMS from the experimentally-measured modulus of a sample with one embedded wire. Table 4.1 shows the model derived modulus for the sandwich and embedded leads and the comparison with the modulus obtained through theoretical calculations.

Table 4.1. Modulus obtained from the model compared to the theoretical calculations for the embedded and sandwich leads and two different amplitude sizes using experimental dimensions.

Configuration	# of Wires	Model Modulus (MPa)	Theoretical Modulus (MPa)	% Discrepancy
Model, embedded, L	1	0.79	-	-
	2	1.04	1.03	-0.97
	3	1.25	1.27	1.57
Model, embedded, S	1	0.86	-	-
	2	1.13	1.17	3.42
	3	1.40	1.48	5.41
Model, sandwich, L	1	0.63	-	-
	2	0.72	0.71	1.41
	3	0.82	0.79	3.80
Model, sandwich, S	1	0.67	-	-
	2	0.82	0.79	3.80
	3	0.97	0.91	6.59

From the table, it can be seen that all the modulus values from the model are all within 7% of calculated theoretical modulus values. This means that the modulus values obtained agree with both experimentally derived values and theoretical calculations.

4.5 Results: Effect of Increasing Lead Density on Elastic Modulus of Bases

In order to adequately expand the model to include six wires, a base width was fixed to 5 mm. This width was picked closer to a midpoint between the sandwich and the embedded samples width and would comfortably fit six wires for the modelling. Figure 4.6 shows a comparison for the modulus obtained from the models for the sandwich and embedded leads with two different amplitudes for strain relief as the number of leads in the base is increased. Boundary conditions and element types are identical to those discussed in section 4.2.

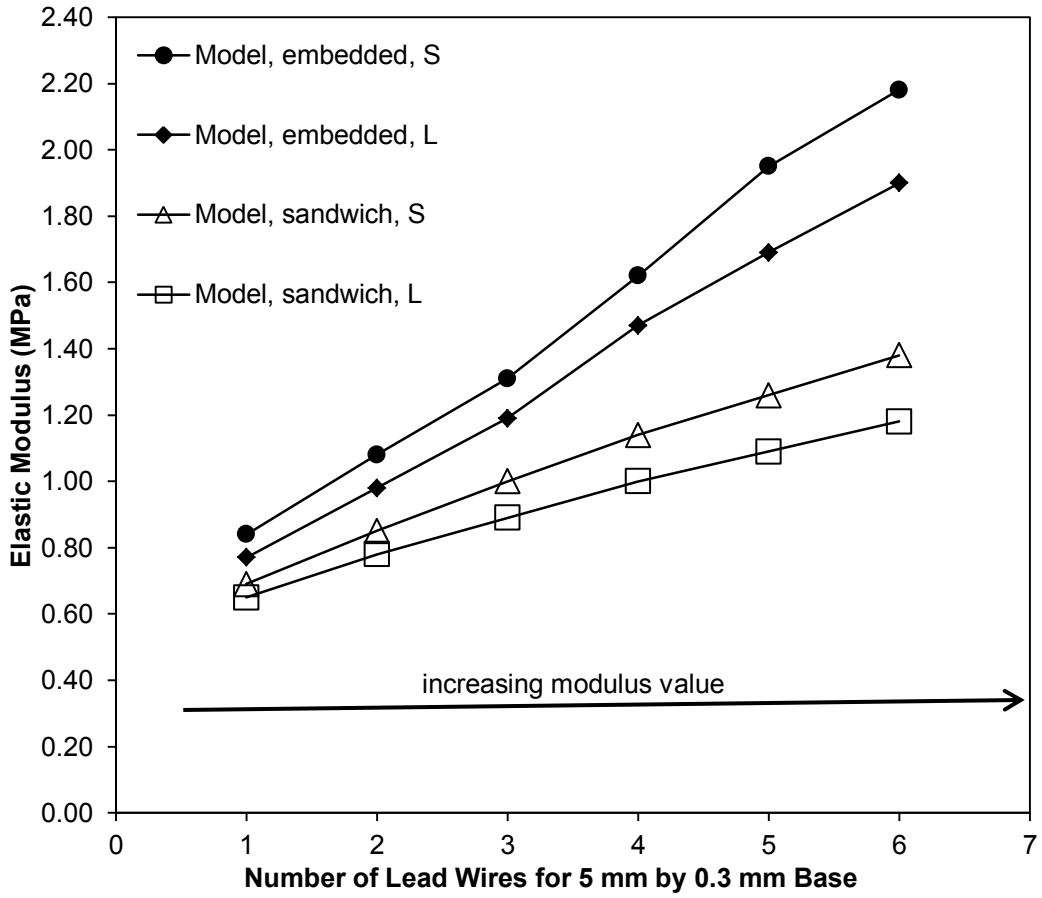

Figure 4.6. Effect of the number of wires, sandwich and embedded arrays and amplitude size (large L, or small S) on the elastic modulus of the base that is 5 mm by 0.3 mm. All model data points are an average of five modulus values from five different far-field elements. Model includes both solid and contact elements. Boundary conditions were set to consistently model a tensile test environment.

When looking at the graph, a few observations can be made. Firstly, the embedded leads have a systematically higher modulus compared to the sandwich array. Also, it can be observed that the modulus of the embedded and sandwich samples that have the small amplitude strain relief are larger than the corresponding samples with the large amplitude in the strain relief wires.

Secondly, as the number of leads in the base increases, it can be seen that the modulus for both the sandwich and the embedded arrays increase. With the embedded arrays, there is an approximately 150% increase in modulus between one and six leads in the base, while the increase in the modulus is approximately 33% for the corresponding sandwich arrays. Furthermore, the sandwich array with six leads in the base and large amplitude strain relief is 73% smaller compared to the its embedded leads counterpart, while the percent difference increases to 89% when comparing the two configurations with small amplitude in the microwire strain relief.

Table 4.2 shows the comparison between modulus obtained from the model and the modulus obtained from the theoretical calculation.

Table 4.2. Modulus obtained from the model compared to the theoretical calculations for the two lead configurations and two different amplitude sizes.

Configuration	# of Wires	Model Modulus (MPa)	Theoretical Modulus (MPa)	% Discrepancy
Model, Sandwich, L	1	0.65	-	-
	2	0.78	0.75	4.00
	3	0.89	0.85	4.71
	4	1.00	0.95	5.26
	5	1.09	1.05	3.81
	6	1.18	1.15	2.61
Model, Embedded, L	1	0.77	-	-
	2	0.98	0.99	1.01
	3	1.19	1.21	1.65
	4	1.47	1.43	2.80
	5	1.69	1.65	2.42
	6	1.90	1.87	1.60
Model, Sandwich, S	1	0.69	-	-
	2	0.85	0.83	2.41
	3	1.00	0.97	3.09
	4	1.14	1.11	2.70
	5	1.26	1.25	0.80
	6	1.38	1.39	0.72
Model, Embedded, S	1	0.84	-	-
	2	1.08	1.13	4.42
	3	1.31	1.42	7.75
	4	1.62	1.71	5.26
	5	1.95	2.00	2.50
	6	2.18	2.29	4.80

From the table, it can be observed that all the modulus obtained from the models are within 7% of the models calculated through the equations, and the theoretical modulus displays similar trends as the graph of modulus values from the model. From this, it can be concluded that the sandwich arrays with large amplitudes are the best configurations when increasing the density of leads in the base because these arrays have the lowest modulus overall with six embedded microwires.

4.6 Results: Effect of Increasing Lead Wire Diameter on Elastic Modulus

Having determined that sandwich arrays with large amplitude strain relief produced the lowest modulus of any configuration when increasing the densities of the leads, the model was subsequently used to determine how much changing the microwire diameters in the leads affects the modulus of the sandwich arrays. All the resulting modulus values will be compared to the value of 1.40 MPa [1] given for the value of human spinal cord with pia. Figure 4.7 shows the graph for the comparison of modulus values generated by the model for three different diameters (30 μm, 50 μm, 70 μm) as well as the experimental results for 30 μm sandwich arrays. The models have a similar geometry, element type, and boundary conditions described in section 4.2.

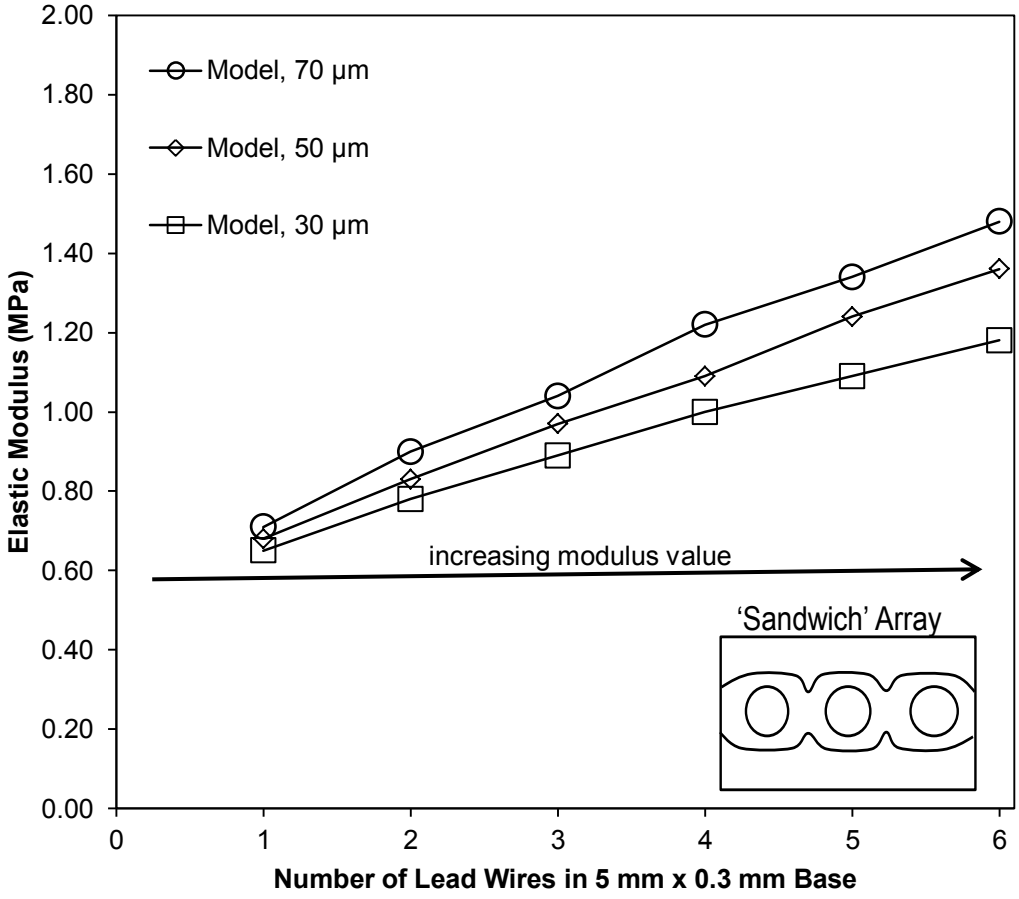

Figure 4.7. Effect of the number of wires, and wire diameter on the elastic modulus of the base that is 5 mm by 0.3 mm with sandwich leads that have large amplitudes. All model data points are an average of five modulus values from five different far-field elements. Model includes both solid and contact elements. Boundary conditions were set to consistently model a tensile test environment.

From the graph, it can be seen that arrays constructed with bases with 70 μm wires have a larger modulus values compared to a base with the other two wire diameters. Also, when the density of leads is increased, it can be observed that the base with 70 μm samples have a modulus increase of 86%, whereas the bases with 30 μm and 50 μm wires exhibit an increase of 59% and 61% respectively. At six leads in the base, it can be seen that a base with 30 μm wire has a modulus that is 27% lower than its respective base with 70 μm leads. Both of these results are due to the increasing stiffness of microwires that have a larger diameter (i.e. microwires with a diameter of 70 μm is stiffer compared to microwires that have a diameter of 30 μm). However, when compared to the 1.40 MPa for the human spinal cord with pia [1], all the modulus values for microwires with increased lead densities is smaller than the values for the human spinal cord with pia.

As with the previous section, the modulus obtained from the model was compared with the theoretical calculated modulus obtained from the equation in section 4.4. The results and the comparison of the theoretical and modulus are displayed in Table 4.3

Table 4.3. Modulus obtained from the model compared to the theoretical calculations for the three different wire diameters tested for the sandwich array configurations.

Wire Diameter	# of Wires	Model Modulus (MPa)	Theoretical Modulus (MPa)	% Discrepancy
Model, 30 µm	1	0.65	-	-
	2	0.78	0.75	4.00
	3	0.89	0.85	4.71
	4	1.00	0.95	5.26
	5	1.09	1.05	3.81
	6	1.18	1.15	2.61
Model, 50 µm	1	0.68	-	-
	2	0.83	0.81	2.47
	3	0.97	0.94	3.19
	4	1.09	1.07	1.87
	5	1.24	1.20	3.33
	6	1.36	1.33	2.26
Model, 70 µm	1	0.71	-	-
	2	0.9	0.87	3.45
	3	1.04	1.03	0.97
	4	1.22	1.19	2.52
	5	1.34	1.35	0.74
	6	1.48	1.51	1.99

From the table, it can be seen that modulus obtained from the model is within 3% of the theoretical modulus. The theoretical modulus also shows that the modulus calculated also does not exceed 1.40 MPa. Based on the table displayed above

and the graphs, all the diameters do exhibit a slight stiffening as lead density in a base increases, however, all three microwire diameters can be used as leads in the sandwich array with six leads in the base, without the base being too stiff, when compared to the modulus of the spinal cord with pia.

4.7 Results: Load Step Study of Embedded Base

The main goal of this study was to determine the strain rate at which the polymer would delaminate from the microwires. Based on the length of the base, set at 6.3 mm, strain rates were determined. The first model was run with a strain rate of 1% and subsequent models were run with strain increments of 1%. Corresponding stress and strain contour plots were outputted. These contour plots show the average stress or elastic strain for the nodes and elements selected. Figure 4.8 shows a contour plot for one wire that is embedded in the base for strain rates up to 5%. From the figures, it can be seen that delamination of the PDMS from the microwires is achieved at 5% strains and the strain plots show a clear strain progression from strain rates of 1% to strain rates of 5%. Section 4.2 describes the other boundary conditions, element type and model geometry for the models in this section.

1% strain

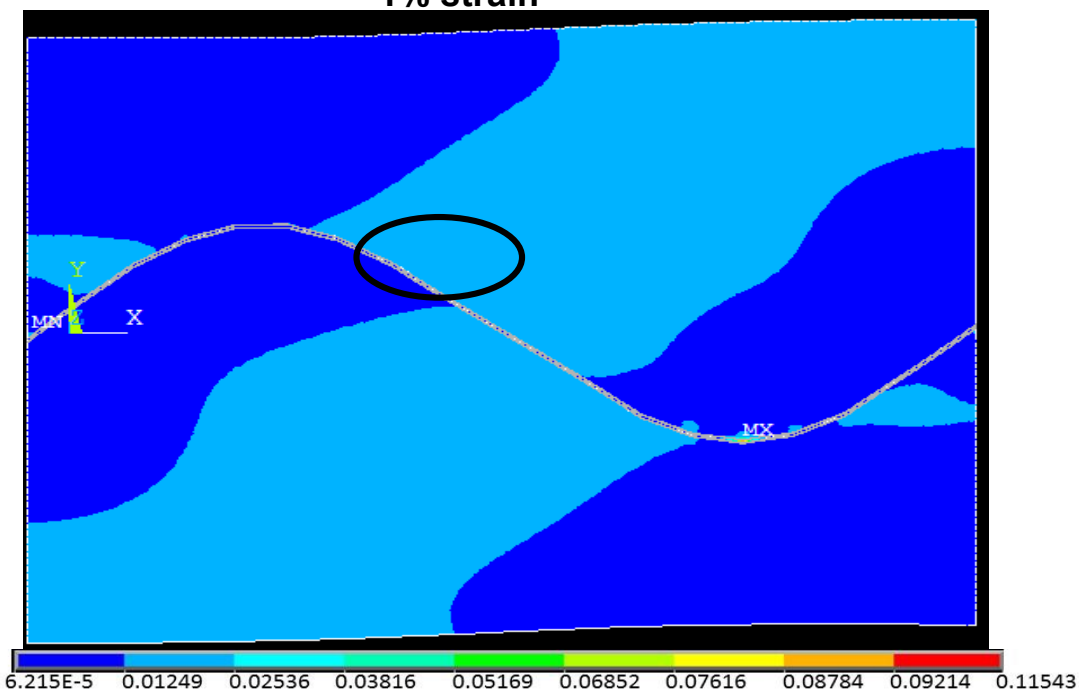

2% strain

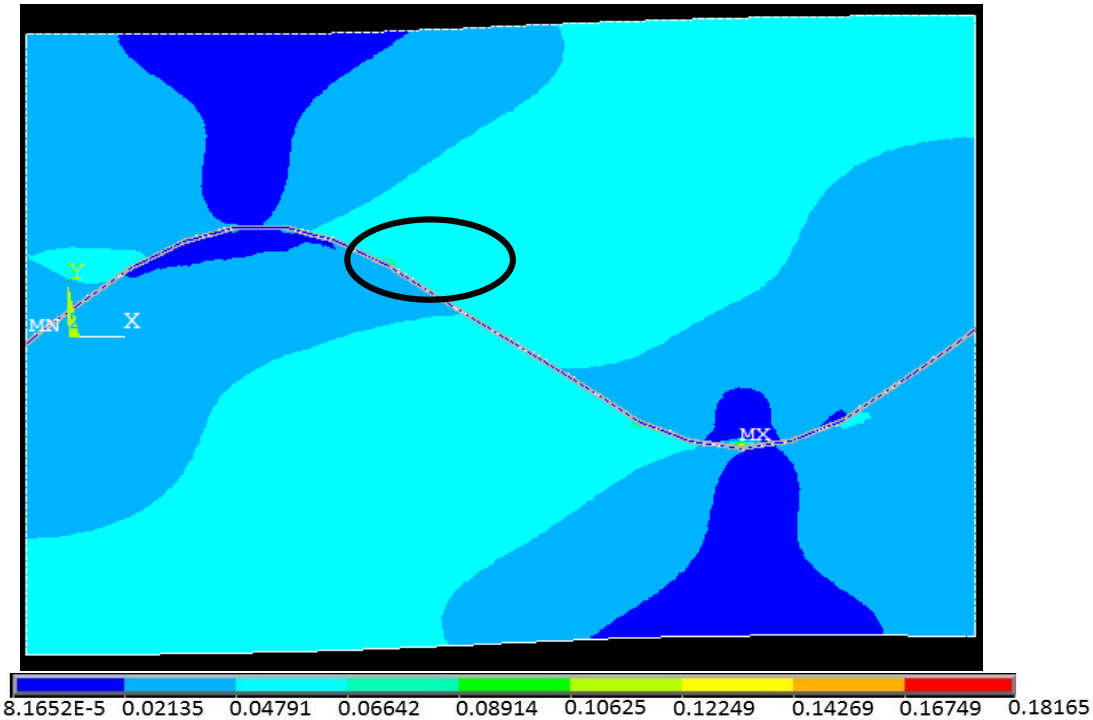

3% strain

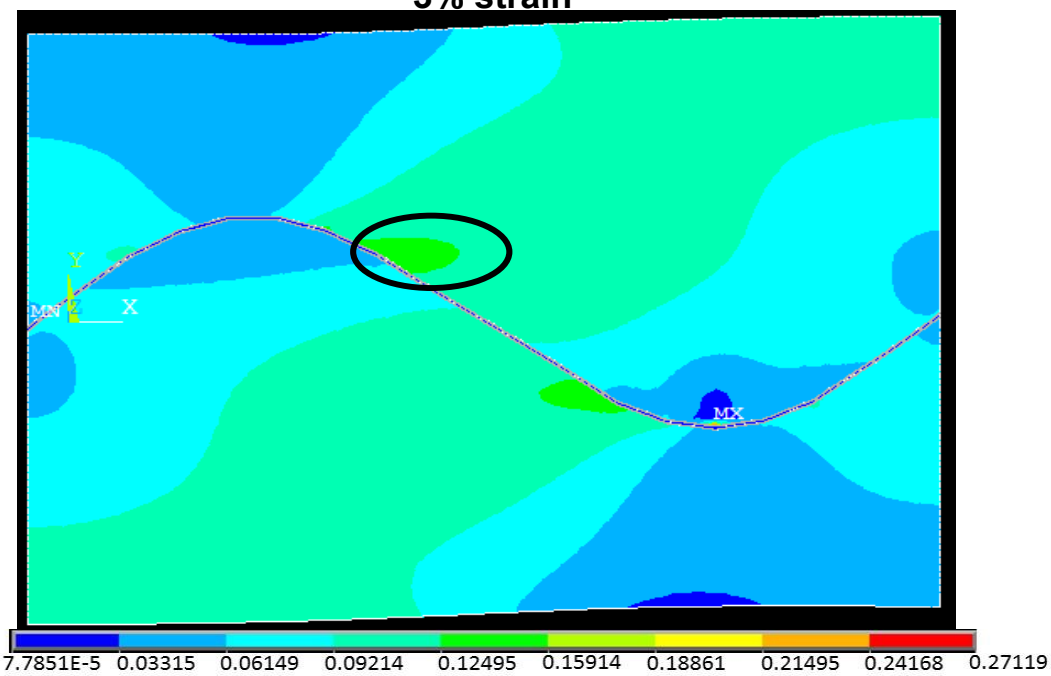

4% strain

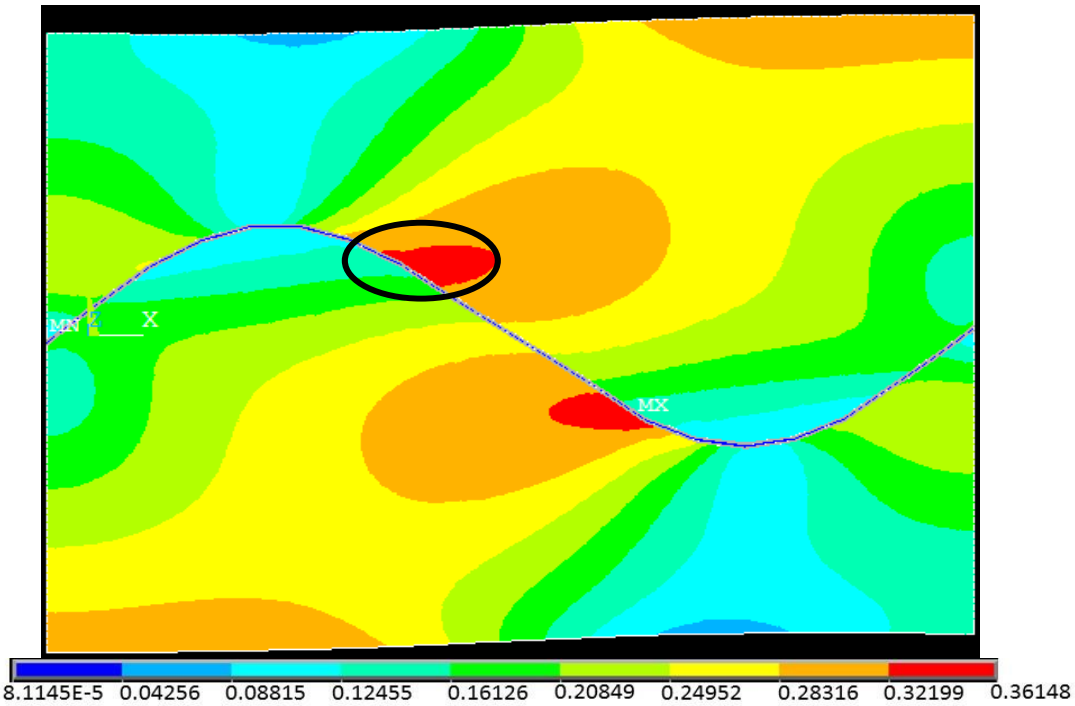

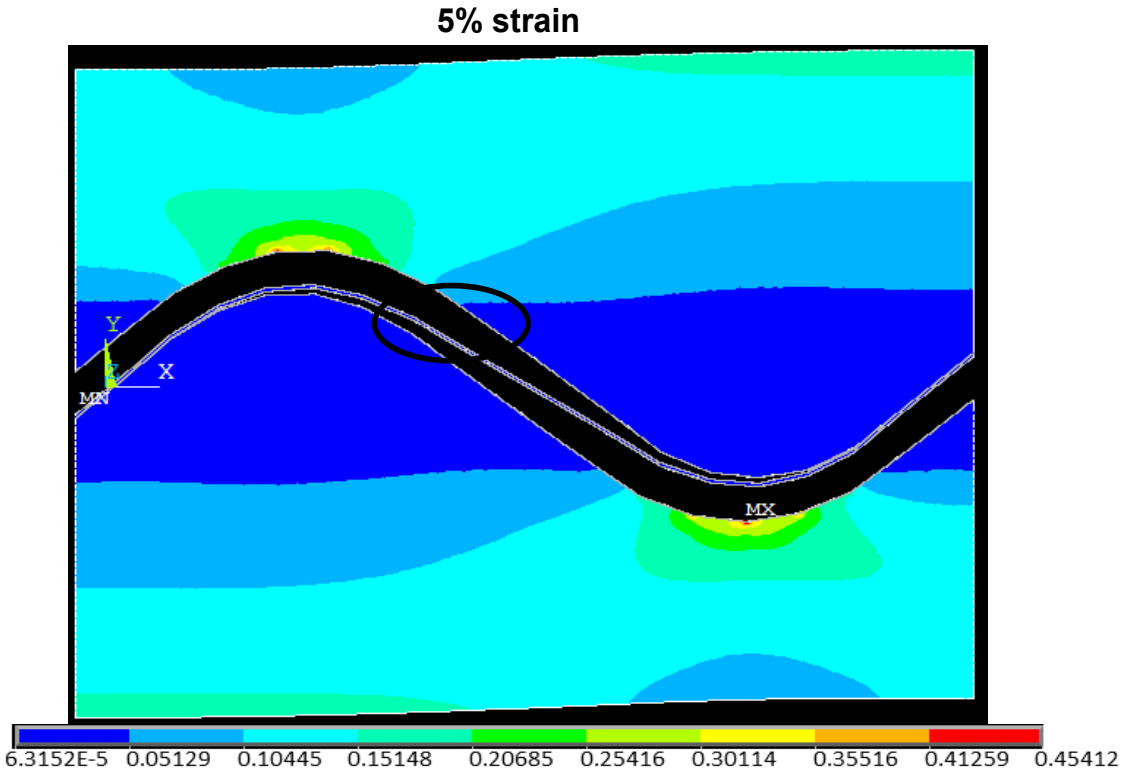

Figure 4.8. Strain contour plots for one wire embedded in PDMS with varied strain rates from 1-5% for each plot. Circle on the plots denotes an area of high strain. Model includes both solid and contact elements. Boundary conditions were set to consistently model a tensile test environment with strained boundary elongated between 1% and 5% strain, where delamination occurs.

To better illustrate the progression in the strain rates, a circle was drawn on each figure seen above. It is clearly seen that at this point, the strain concentration progressively increases until delamination occurs at 5% strain. Looking at the values for the average strain rates, it can be seen that at 1% strain, the values for

elastic strain are about 0.012 while at 4%, the elastic strain average values displayed on the plot is around 0.361, which shows an increase in the internal strains in the sample.

A load step study was also performed for six wires embedded in the PDMS base. As with the previous study for one wire, strain increments of 1% were used. Figure 4.9 shows the strain contour plots for the study. As seen with the previous study, there a clear progression of strains from 1% to 4% strains. At 5% strain, it can be seen that the delamination occurs, which is consistent with the one wire embedded study. As with the previous figure, in order to better demonstrate progression of strain concentration, a circle was drawn at the center of each figure. It can be seen from the circle that there is a clear change in strain concentrations as the figure as the strain rate of the sample is increased. At 5%, when delamination occurs, the strain concentration actually decreases in the middle wires because the entire sample in the middle can act essentially as a spring that is being stretched. This lowers the strain in the middle of the sample and concentrates the strains at the points of delamination. Investigating average strain values, it can be seen that at 1% strain, the area in the circle reaches strain rates of 0.036 while at 4%, the average elastic strain value reaches 0.369, which is consistent but slightly higher average elastic strain values compared to the one wire sample

1% strain

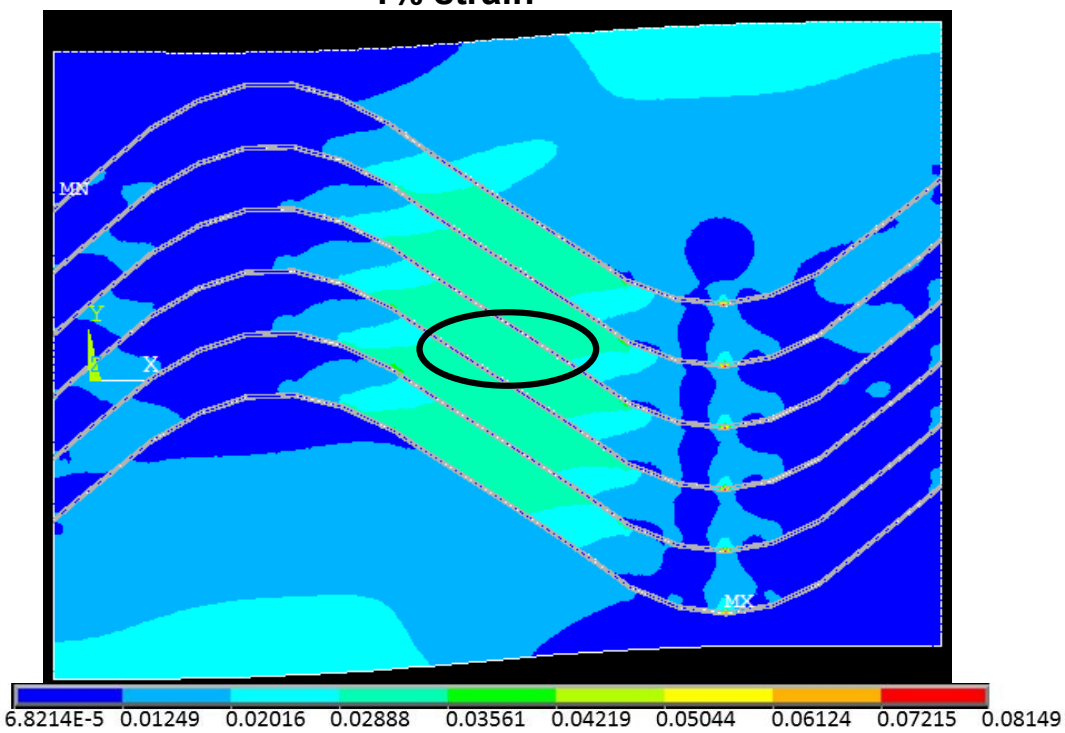

2% strain

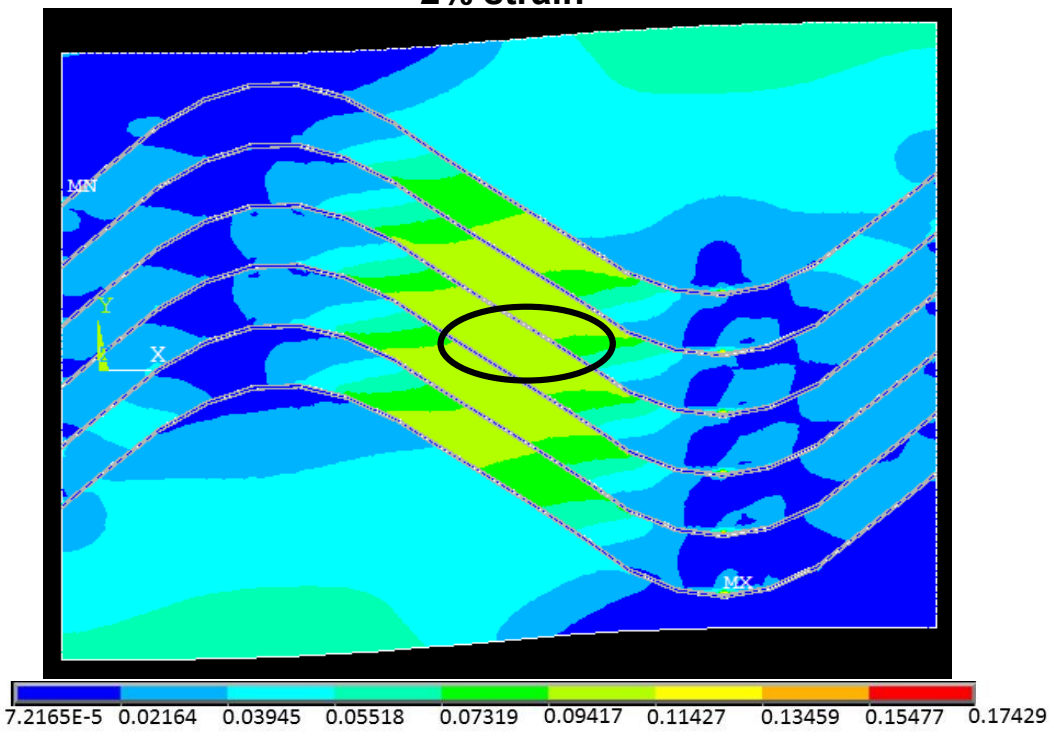

3% strain

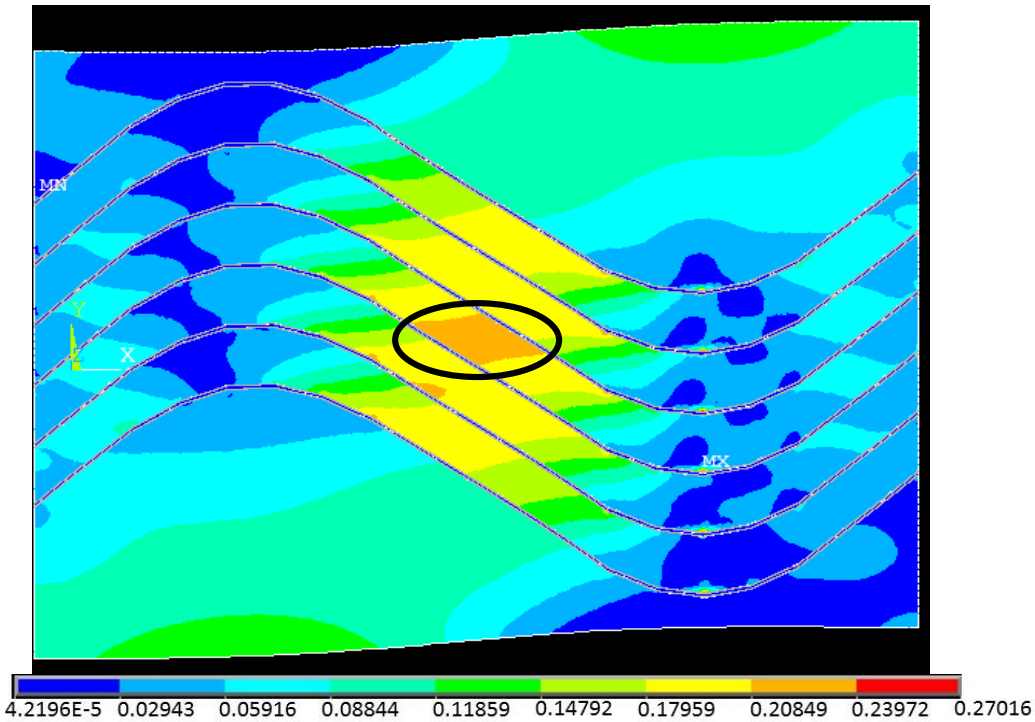

4% strain

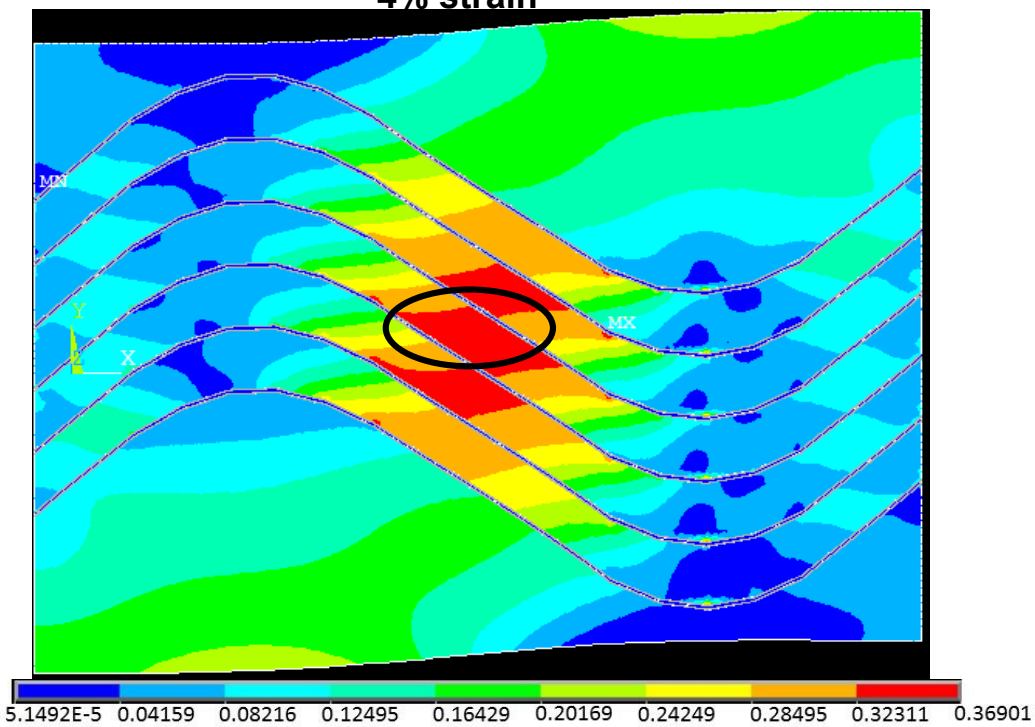

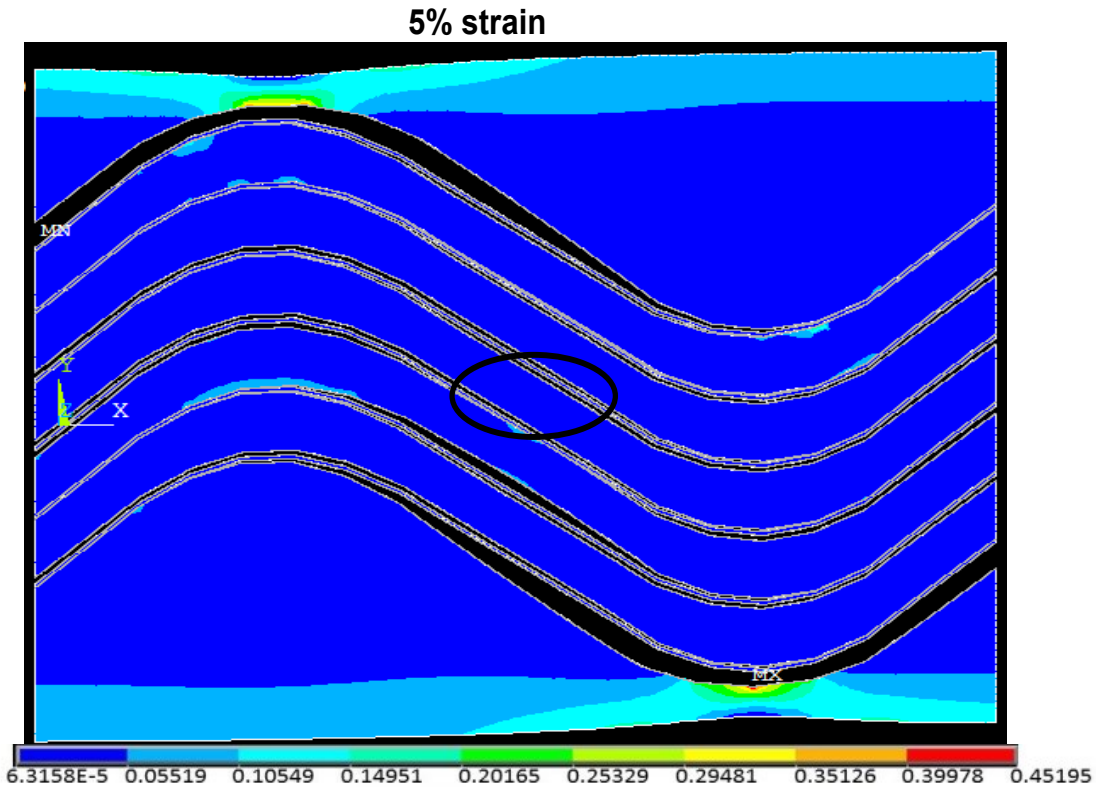

Figure 4.9. Strain contour plots for six wires embedded in PDMS with varied strain rates from 1-5% for each plot. Model includes both solid and contact elements. Boundary conditions were set to consistently model a tensile test environment with strained boundary elongated between 1% and 5% strain, where delamination occurs.

4.8 Results: Effect of Base Width on the Modulus of the Base

The results of the above studies are dependent on the exact geometry of the base employed (5 mm wide x 6.3 mm long). In this section, the overall elastic modulus of the bases with leads was investigated when the width of the base was increased. In this section, the width of the base was increased to 10 mm and then 20 mm, for both embedded and sandwich configurations with one and six wires. Modulus values were calculated from 'far-field' stresses and strains in a similar manner presented in section 4.4. As the width of the bases was increased, the amplitude of the strain relief wires and the spacing between wires were kept constant, and the ratio of these two variables (amplitude/spacing) equaled two. Figure 4.10 shows the graph for increasing base with and corresponding modulus values. All boundary conditions, model geometry and element type are consistent with those described in section 4.2.

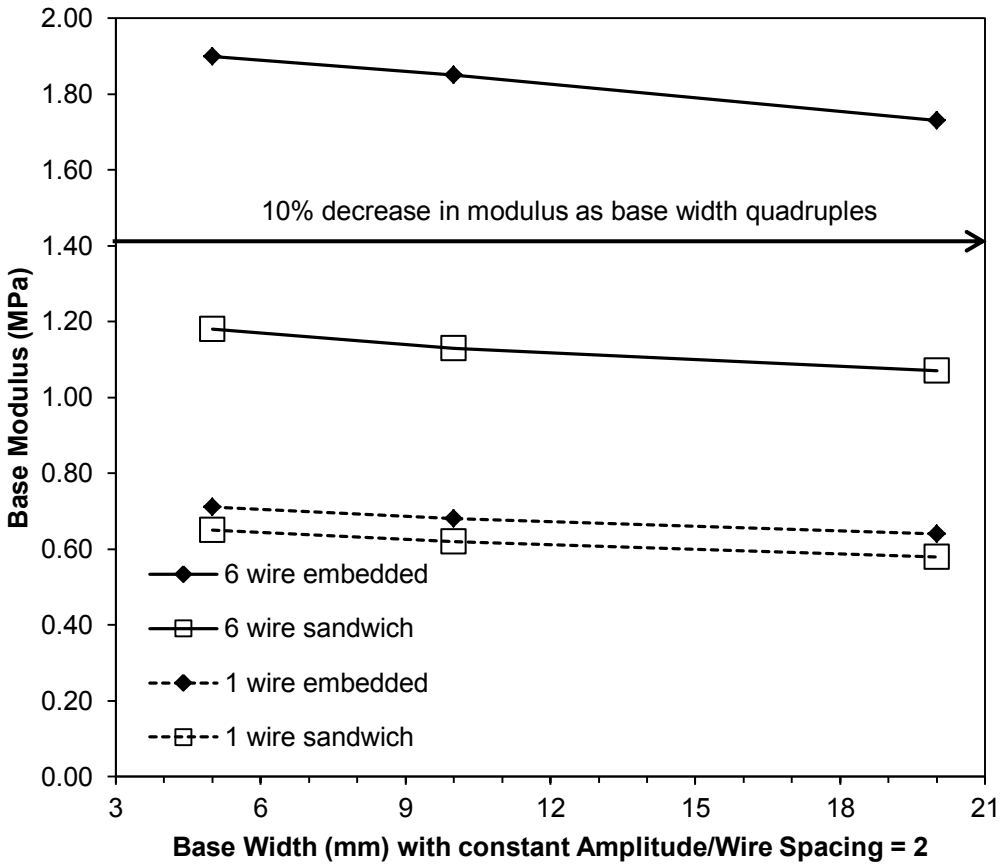

Figure 4.10. Effect of the base width on the elastic modulus of the base that has a constant amplitude/wire spacing ratio equal to two. All model data points are an average of five modulus values from five different far-field elements. Model includes both solid and contact elements. Boundary conditions were set to consistently model a tensile test environment.

From the graph, it can be seen that there is a modest decrease (~10%) in the modulus when the base width quadruples. A few other trends were observed,

which are consistent with previous results. Firstly, bases with 6 wires had higher moduli than equivalent bases with one wire. Second, the embedded arrays have a larger modulus value compared to the sandwich arrays. Also, based on the value of the spinal cord with pia modulus of 1.40 MPa [1], the six wires that are embedded in the PDMS are still too stiff even after the base width is quadrupled. In reality, it may be unrealistic to develop a base that is 20 mm wide but the results of this study show that there is not a large decrease in the modulus even after the base width is changed, indicating that the properties of the base are dominated by the wires.

4.9 Results: Effect of Decreasing Wire Spacing on the Modulus

I also investigated how decreasing spacing between the wires contributes to the modulus of the base. Six sandwich and embedded leads that were 30 μm in diameter were modelled. A second model of one microwire in an embedded and sandwich configuration with a total diameter of 180 μm was also modelled to determine the upper bound for the modulus values. For the purpose of this study, the amplitude of the strain relief in the leads and the dimensions of the base were kept constant at x and y, respectively. Modulus values were determined from 'far-field' stresses and strains and five individual 'far-field' calculations were

used to provide an average for the graph. Figure 4.11 shows the change in the modulus with increasing amplitude and wire spacing ratio (A/S). The boundary conditions, element type and model geometry is described in detail in section 4.2.

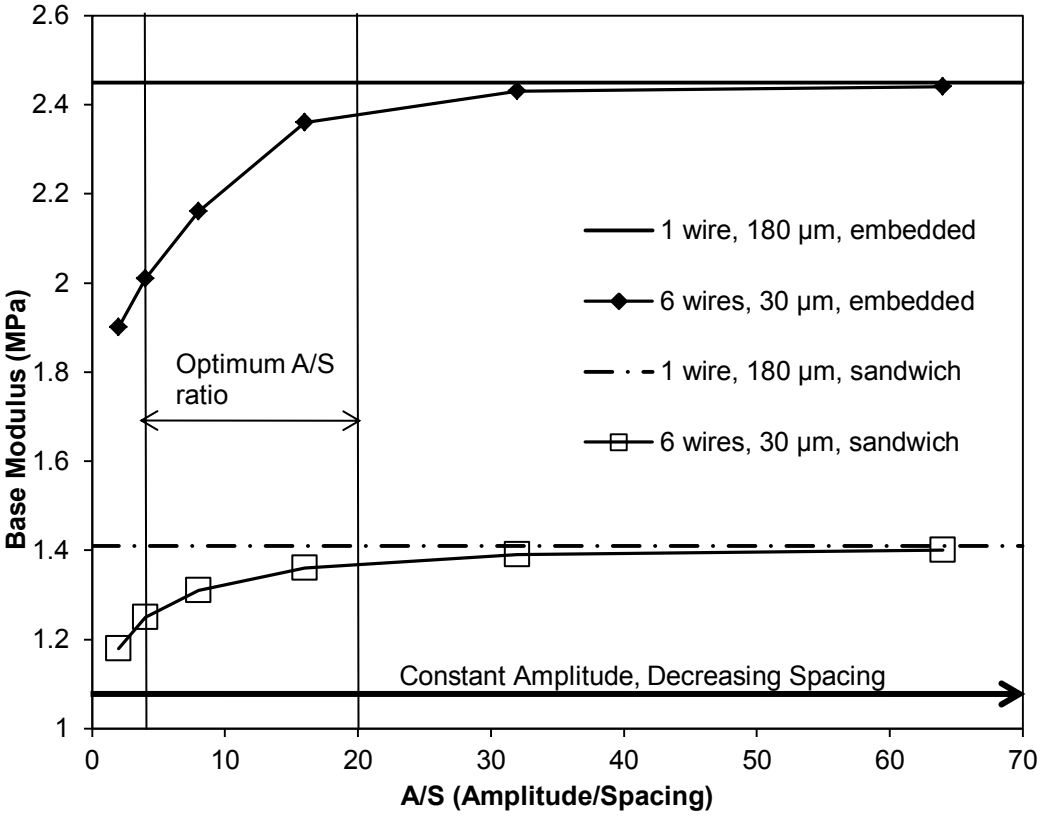

Figure 4.11. Effect of changing the amplitude/wire spacing ratio on the elastic modulus of the base that is set at 5 mm by 6.3 mm. All model data points are an average of five modulus values from five different far-field elements. The optimum A/S ratio is marked between A/S=2 and A/S=16. . Model includes both solid and contact elements. Boundary conditions were set to consistently model a tensile test environment.

As seen in the graph, optimum amplitude over wire spacing ratio range was determined to be between 2 and 16 for both the embedded and the sandwich array. Beyond this range, the moduli of the six wires in the base start to act like a single wire (with a diameter six times as large as a single wire). This is because the spacing between the wires is too small and this causes the amount of force applied to straighten the polymer between the wires to be negligible as compared to the amount of force required to straighten the wire. It can also be observed that the embedded array also has a higher modulus than the sandwich array, which is consistent with the findings and observations in the previous sections. The embedded six wire samples are too stiff for implantation as the modulus exceeds the literature value for the spinal cord with pia [1]. It can also be seen that the past an A/S ratio of 16, the modulus of the sandwich array actually reaches 1.40 MPa, which is the exact literature value of the spinal cord with pia [1]. If the modulus of the implant is greater than what a tissue can tolerate, more damage is caused because it allows for no tolerance in movement between the implant and the tissue. Therefore, it would not be a good idea to manufacture arrays that have an amplitude over spacing between wires ratio larger than 16.

4.10 Model Idealisations and Limitations

Throughout this chapter, the system that was modelled was based on the geometry and conditions tested with a tensile tester. Idealisations of the model were made to keep the strain conditions similar throughout the work. The main focus of this work was a flexible base with embedded wires, whereas in reality these wires would be connected to protruding electrodes which would be inserted into the spinal cord, and also to leads carrying the signal off of the device. When implanted into the spinal cord, the deformations would come from the deformation of the cord itself, and would be translated across the plane of the bottom of the base. Nonetheless, this model is relevant because it helps identify parameters required to achieve a bulk base modulus that is acceptable for implantation, and aid in the manufacturing of these devices. In the future, a model can be developed to account for a more accurate representation of strains applied by the spinal cord can be investigated and a better stress representation within the base can be developed as a result.

4.11 Summary

From the finite element models, it can be determined that the sandwich array is less stiff compared to the corresponding embedded arrays. It can also be concluded that increasing lead density in the base will not make the sandwich

array too stiff for implantation, while the embedded arrays would be too stiff to implant in the spinal cord. Finally, increasing lead diameters for the sandwich array does increase the stiffness of the base, however the increase is still under the threshold for the acceptable stiffness for implantation in the spinal cord.

As a result of the load step study on the embedded arrays, it was determined that delamination between the polyimide insulation of the microwire and the PDMS occurs at 5% strain. It was also determined that the properties of the arrays are dominated by the properties of the wires: if the base width was quadrupled, the modulus of the base would decrease by approximately 10% assuming that the amplitude and spacing of the wires remained constant. Finally, for a base that is 5 mm by 6.3 mm wide, the optimum ratio between the amplitude and the wire spacing ranges from 2 until 16. Larger ratios will cause the elastic modulus of the base to behave like a base with one large wire instead of six smaller wires. Smaller ratios are not possible for the current geometry of the base. Utilizing these findings will help in the manufacturing of the bases and also help to produce arrays that are more compatible with the human tissue.

4.12 References

[1] E.L. Mazuchowski, and L.E. Thibault, "Biomechanical properties of the human spinal cord and pia matter," *in Summer Bioengineering Conference*, Key Biscayne, Florida, 2003

[2] I. Khaled, S. Elmallah, C. Cheng, W. Moussa, V.K. Mushahwar, and A.L. Elias, "A Flexible Base Electrode Array for Intraspinal Microstimulation" *IEEE Transactions in Biomedical Engineering*, vol. 60, no. 10, pp. 2904-2913, Oct. 2013

[3] "Platnium 20% Iridium"| PGM Database, [Online] Accessed at: www.pgmdatabase.com/jmpgm/index.jsp?record=1064, [Accessed: March 22, 2014]

[4] J. Kuncova-Kallio and P.J. Kallio, "PDMS and its Suitability for Analytical Microfluidic Devices" *in Proceedings of the 28th IEEE EMBS Annual International Conference,* NEW YORK CITY, USA, 2006

[5] D.C. Duffy, J.C. McDonald, O. J. A. Schueller and G. M. Whitesides, "Rapid Prototyping of Microfluidic Systems in Poly(dimethylsiloxane)" *Analytical Chemistry*, vol. 70, no. 23, pp. 4974-4984, Dec, 1998

Chapter 5: Conclusion and Future Work

5.1 Conclusion

The main goal of this research was to develop a strain relief technique that would allow the flexible based electrode array (FBEA) to be able to reversibly undergo strains up to 12% [1], which is the literature value for the human spinal cord strains in day-to-day activities. Previous work on the FBEA replaced the stiff bases found in many electrode arrays with a flexible base made of polydimethylsiloxane (PDMS) [2]; however, in that design, the lead wires still contributed significantly to the stiffness of the device, and could even fail under high strain. The goal of my thesis work was to reduce the modulus of the base by introducing strain relief to the lead wires embedded within it, in order to allow the base to deform with the spinal cord.

Strain relief was created by introducing sinusoidal waves to the lead wires in the flexible base, allowing the microwires to straighten when strained. Experimentally, two configurations were created and tested. The first configuration, called the 'array with embedded leads', involves PDMS cured around the microwires with strain relief, forming a solid block of PDMS well-bonded to the surface of the wires. The second configuration developed was called the 'sandwich array', and was formed by sandwiching two pieces of cured PDMS on top of and beneath the microwires with strain relief. The overall modulus of the base for the two configurations was compared to determine which

configuration was better. After comparing the two configurations, it was determined that the sandwich arrays had a lower modulus (0.76 ± 0.04 MPa) compared to the embedded arrays (1.31 ± 0.05 MPa). While the modulus of the embedded arrays was still found to be lower than the modulus of the spinal cord with pia material value from literature (1.40 MPa) [1], further increasing the number of leads would increase the modulus of the base beyond the modulus of the spinal cord, which could potentially result in a stiff base which would cause damage to tissue. The embedded arrays are also stiffer than the sandwich arrays because the PDMS acts as a resistor during straining and this prevents the microwires from straightening out consistently. The sandwich arrays allow the microwires to straighten out without resistance from the PDMS. Based on the experimental work, it can be concluded that the sandwich leads are the better configuration of leads to reduce the modulus of the base and deform with the cord.

In addition to experimental work, a finite element model was created to further extend the experimental results. There were four objectives to the finite element work. The first objective of the finite element model was to determine the effect of increasing the density of leads on the modulus of the base for both sandwich and embedded leads. In addition, a study of increasing the microwire density was performed for the sandwich array and its effect on the stiffness of the base was investigated. Based on the model, it was concluded that increasing lead density in

the embedded arrays, regardless of the amplitude size can lead to stiffness or modulus values that exceed the spinal cord with pia modulus value. It can also be concluded that the sandwich arrays have a modulus that is lower than the embedded arrays but also has a stiffness that is less than the value for the measure human spinal cord stiffness. The sandwich array has modest increase in stiffness as the number of leads in the base is increased. When comparing increasing diameters for sandwich arrays, it can be noted that there is a modest increase in modulus or stiffness for the base with six microwires involved. All the stiffness values do fall under the threshold of the measured human spinal cord stiffness value.

The second objective of the finite element modelling was to determine the strain at which delamination occurs for embedded bases with one and six wires. From the results, it could be concluded that delamination of embedded base occurs at 5% strain. Thirdly, a study of the modulus when width of the base was increased was performed. For this study, the amplitude of the strain relief and the spacing between wires was kept constant. It was determined that as the width of the base quadrupled, the modulus dropped by approximately 10%. Finally, a study of the modulus after changing the spacing between wires was performed. In this study, the effect of modulus was studied as the ratio between amplitude and wire spacing increased. The geometry of the sample and the amplitude of the strain relief were kept constant. Based on the modelling, it was concluded that the optimum ratio

between amplitude and wire spacing was determined to be between 2 and 16. Smaller ratios are not possible due to the current geometry of the base while larger ratios will result in the modulus behaving like a base with one microwire rather than ,a base with six individual microwires.

Overall, both the experimental and finite element model showed that the sandwich leads are the better configuration due to the smaller stiffness observed as compared to embedded arrays with similar number of leads per unit area. As well, the findings in the modelling will help with the manufacturing of devices that are more compatible with human tissue.

5.2 Future Work

The long term goal of this project is to develop a device that can be used in humans to improve the quality of life for individuals who have a spinal cord injury. In order to achieve this goal, there are many things that need to be considered to perfect and advance the design of the FBEA.

One of the critical areas that need to be addressed is how the device will react in biological tissue. To answer this, animal experiments will need to be performed. The animal work will need to incorporate the electrode array with the strain relief capabilities in order to see how the FBEA behaves in the biological system under

the stresses and strains of the spinal cord tissue. A second critical area includes the connection between the leads and the electrode itself. A stable connection that does not impact the modulus of the base and also provides an appropriate electrical connection between the leads and electrodes must be developed.

Expanding the finite element model to include this electrode-lead connection as well as see how the overall array behaves with the electrode is an important study. This can be accomplished by transforming the model into a three dimensional model, where the behaviour of the spinal cord can be tested with the newly designed FBEA. The model can also be further improved by modelling the spinal cord with the actual FBEA implanted, followed by applying several forces and displacements to the cord to monitor and record any deformations with the arrays implanted. This would allow us to visualize the array and also discover whether the array would become deformed after straining.

5.3 References

[1] S. S. Margulies, D. F. Meaney, L. B. Bilston, L. E. Thibault, N. G. Campeau, and S. J. Riederer, "In Vivo Motion of the Human Cervical Spinal Cord in Extension and Flexion," *in Proceedings of the 1992 International IRCOBI Conference on the Biomechanics of impacts*, VERONA, ITALY, 1992.

[2] I. Khaled, S. Elmallah, C. Cheng, W. Moussa, V.K. Mushahwar, and A.L. Elias, "A Flexible Base Electrode Array for Intraspinal Microstimulation" *IEEE Transactions in Biomedical Engineering*, vol. 60, no. 10, pp. 2904-2913, Oct. 2013

Bibliography

W.M. Grill, “Neural Interfaces” American Scientist: the Magazine of Sigma XI, the Scientific Research Society, vol. 98, no. 1, pp.48-57, 2010

“Spinal Cord injuries cost health care $3 billion annually | The Star.” [Online]. Available: http://www.thestar.com/life/health_wellness/2012/01/27/spinal_cord_injuries_cost_health_care_3_billion_annually.html. [Accessed: 28-August-2013]

V.K. Noonan, M. Fingas, A. Farry, D. Baxter, A. Singh, M.G. Fehlings, and M.F. Dvorak, “Incidence and Prevalence of Spinal Cord Injury in Canada: A National Perspective,” Neuro-epidemiology, vol. 38, pp. 219-226, Apr. 2012

V. K. Mushahwar and K. W. Horch, “Proposed specifications for a lumbar spinal cord electrode array for control of lower extremities in paraplegia,” IEEE Transactions on Rehabilitation Engineering: A Publication of the IEEE Engineering in Medicine and Biology Society, vol. 5, no. 3, pp. 237-243, Sep. 1997.

D. McCreery, V. Pikov, A. Lossinsky, L. Bullara, and W. Agnew, “Arrays for chronic functional microstimulation of the lumbosacral spinal cord,” IEEE Transactions on Neural Systems and Rehabilitation Engineering: A Publication of the IEEE Engineering in Medicine and Biology Society, vol. 12, no. 2, pp. 195-207, Jun. 2004.

S.F. Giszter, “Spinal Cord Injury: Present and Future Therapeutic Devices and Prostheses” The American Society for Experimental NeuroTherapeutics. Inc., vol. 5, pp.147-162, Jan. 2008

S. S. Margulies, D. F. Meaney, L. B. Bilston, L. E. Thibault, N. G. Campeau, and S. J. Riederer, “In Vivo Motion of the Human Cervical Spinal Cord in Extension and Flexion,” in Proceedings of the 1992 International IRCOBI Conference on the Biomechanics of impacts, VERONA, ITALY, 1992.

Fact Sheet - Mapping Connections: An Understanding of Neurological Conditions in Canada, Found on: http://www.phac-aspc.gc.ca/cd-mc/nc-mn/mc-fs-ec-fr-eng.php. Accessed on November 26, 2014.

Robinson, C.J. Expanding the scope of IEEE transaction on rehabilitation engineering to explicitly including neural engineering. *IEEE Trans. Rehabil. Eng.* 8:273-275, 2000

Leuthardt, E.C., Roland, J.L., Ray, W.Z., Neuroprosthetics, *The Scientist*, November 1, 2014, Obtained from: http://www.the-scientist.com/?articles.view/articleNo/41324/title/Neuroprosthetics/. Accessed on: November 24, 2014.

Carmena, J.M., Lebedev, M.A., Henriquez, C.S., and Nicolelis, M.A., Stable ensemble performance with single-neuron variability during reaching movements in primates. *J. Neurosci.*, 25:10712-10716, 2005

Cohen, D., and Nicolelis, M.A., Reduction of single-neuron firing uncertainty by cortical ensembles during motor skill learning. *J. Neurosci*., 24:3574-3582, 2004

Mehring , C., Rickert , J., Vaadia , E., Cardosa de Oliveira , S., Aertsen , A., and Rotter , S., Inference of hand movements from local fi eld potentials in monkey motor cortex . *Nat. Neurosci.* , 6:1253 – 1254, 2003

Engel , A.K., Fries , P., and Singer , W. Dynamic predictions: oscillations and synchrony in top - down processing . *Nat. Rev. Neurosci*., 2:704-716, 2001

Harris , K.D., Csicsvari , J., Hirase , H., Dragoi , G., and Buzsaki , G., Organization of cell assemblies in the hippocampus . *Nature* , 424:552 – 556 , 2003

LibersonW.F., Holmquest, H. J., Scott, D., Dow, A. Functional electrotherapy: Stimulation of the peroneal nerve synchronized with the swing phase of the gait in hemiplegic patients. Arch. Phys. Med. Rehab. 42:101–105, 1961.

Brindley, G.S., and Lewin, W.S., The sensations produced by electrical stimulation of the visual cortex. *J. Physiol.*, 196:479-493, 1968

Delgado, J.M.R., Mark, V., Sweet, W., Ervin, F., Weiss, G., Bach-y Rita, G., Hagiwara, R., Intracerebral radio stimulation and recording in completely free patients. *J. Nerv. Ment. Dis.,* 147:329-340, 1968

DiLazzaro, V., Retuccia, D., Olivero, A., Profice, P., Ferrara, L., Insola, A., Mazzone, P., Tonali, P., Rothwell, J.C., Effect of voluntary contraction on descending volleys evoked by transcranial stimulation in conscious humans. *J. Physiol.*, 508:2:625-633, 1998

Jacobs, I., Sunde, K., Deakin, C.D., Hazinski, M.F., Kerber, R.E., Koster, R.W., Morrison, L.J., Nolan, J.P., Sayre, M.R., Part 6: Drfibillation, Electrode Patient Interface: *2010 International Consensus on Cardiopulmonart Resuscitation and Emergency Cardiovascular Care Science with Treatment Recommendations*, Dallas TX.

Coates, T.D., Neural Interfacing: Forging the Human-Machine Connection, *Synthesis Lectures on Biomedical Engineering*, Morgan and Claypool Publishers, 2008

Polikov, V.S., Tresco, P.A., Reichert, W.M., Response of brain tissue to chronically implanted neural electrodes. *J. Neurosci. Methods*, 148:1-18, 2005

Anderson, J.M., Rodriguez, A., Chang, D.T., Foreign Body Reaction to Biomaterials, *Seminar in Immunology*, 20: 86-100, 2008

He, W., and Bellamkonda, R.V., A molecular perspective on understanding and moduluating the performance of chronic central nervous system recording electrodes, in *Indwelling Neural Implants: Strategies for Contending with the In Vivo Environment*, 2008

Bryers, J.D., Giachelli, C.M., Ratner, B.D., Engineering Biomaterials to Integrate and Heal: The Biocompatability Paradigm Shirts. *Biotech. And Bioeng.*, 109(8):1898-1911, 2012

Anderson, J.M., Biological Responses o Materials. *Annual Reviews of Material Research*, 31:81-110, 2001

Bilston, L.E., and Thibault, L.E., The mechanical properties of the human cervical spinal cord in vitro. *Ann. Biomed. Eng.*, 24:67 – 74, 1996

Giordana MT, Attanasio A, Cavalla P, Migheli A, Vigliani MC, Schiffer D., Reactive cell-proliferation and microglia following injury to the rat-brain. *Neuropathol Appl Neurobiol*, 20:163–74, 1994

Fujita T, Yoshimine T, Maruno M, Hayakawa T., Cellular dynamics of macrophages and microglial cells in reaction to stab wounds in rat cerebral cortex. *Acta Neurochir (Wien)* 140:275–279, 1998

Szarowski DH, Andersen MD, Retterer S, Spence AJ, Isaacson M, Craighead HG., et al. Brain responses to micro-machined silicon devices. *Brain Res*;983:23–35, 2003

Hopcroft, M.A., Nix, W.D., Kenny, T.W. What is the Young's modulus of silicon? *J. Microelectromech. Syst.*, 19:229-238, 2010

Borschel, G.H., Kia, K.F., Kuzon, W.M., Jr., Dennis, R.G., Mechanical properties of acellular peripheral nerve. *J. Surg. Res.*, 114:133 – 139, 2003

Yu , Z., and Morrison , B., Experimental mild traumatic brain injury induces functional alteration of the developing hippocampus . *J. Neurophysiol.*, 103:499 – 510, 2010

Donaldson , N. , Rieger, R., Schuettler , M., and Taylor , J. Noise and selectivity of velocity - selective multi - electrode nerve cuffs . *Med. Biol. Eng. Comput.*, 46:1005 – 1018, 2008

Cheung , K.C., Implantable microscale neural interfaces . *Biomed. Microdevices* , 9:923 – 938, 2007

Kim , S., Bhandari , R., Klein , M., Negi , S., Rieth , L., Tathireddy , P., Toepper , M., Oppermann , H., and Solzbacher , F., Integrated wireless neural interface based on the Utah electrode array . *Biomed. Microdevices*, 11:453 – 466, 2009

Edell , D.J., A peripheral nerve information transducer for amputees: long - term multichannel recordings from rabbit peripheral nerves . *IEEE Trans. Biomed. Eng*., 33:203 – 214, 1986

Cheung, K.C., Renaud, P., Tanila, H., Djupsund, K., Flexible polyimide microelectrode array for *in vivo* recordings and current source density ananlysis. *Biosens. Bioelectron.*, 22:1783-1790, 2007

Meacham, K.W., Giuly, R.J., Guo, L., Hochman, S., DeWeerth, S.P., A lithographically-patterned, elastic multi-electrode array for surface stimulation of the spinal cord. *Biomed. Microdevice*, 10:259-269, 2008

Heuschkel, M.O, Fejtl, M., Raggenbass, M., Bertrand, D., Renauld, P., A three-dimensional multi-electrode array for multi-site stimulation and recording in acute brain slices. *J. Neurosci. Methods*, 114:135-148, 2002

Sheiko, S.S., Xu, H., Sun, F.C., Shirvanyants, D.G., Rubinstein, M., Shabratov, D., Beers, K.L., Matyjaszewski, K., Molecular pressure sensors. *Adv. Mater.*, 19:2930 – 2934, 2007

Sun, Y.G., and Wang, H.H., High-performance, flexible hydrogen sensors that use carbon nanotubes decorated with palladium nanoparticles. *Adv. Mater.*, 19:2818 – 2823, 2007

McClain, M.A., Clements, I.P., Shafer, R.H., Belleamkinda, R.V., LaPlaca, M.C., Allen, M.G., Highly-compliant microcable neuroelectrodes fabricated from thin-film gold and PDMS. *Biomed Mocrodevices*, 13:361-373, 2011

Yu,Z., Graudejus, O., Tsay, C., Lacour, S.P., Wagner, S., Morrison, B., Monitoring hippocampus electrical activity *in vivo* on an elastically deformable microelectrode array. *J. Neurotruama*, 26:1135-1145, 2009

Henle, C., Raab, M., Cordeiro, J.G., Doostkam, S., Schulze-Bonhage, A., Stieglitz, T., Rickert, J., First long term *in vivo* study on subdurally implanted micro-ECoG electrodes, manufactured with a novel laser technology. *Biomed. Microdevices*, 13:59-68, 2011

Lacour, S.P., Wagner, S., Huang, Z.Y., Suo, Z., Stretchable gold conductotrs on elastomeric substrates. *Appl. Phys. Lett.*, 82:2404-2406, 2003

Gorm, P., Cao, W., Wagner, S., Isotropically stretchable gold conductors on elastomeric substrates. *Soft Matter*, 7:7177-7180, 2011

Cao, W., Gorrn, P., Wagner, S., Modelling the electrical resistance of gold film conductors on uniaxially stretched elastomeric substrates, *Appl. Phys. Lett.*, 98:212112-212113, 2011

Santhanam, G., Ryu, S. I., Byron, M. Y., Afshar, A., and Shenoy, K. V., A high-performance brain–computer interface. *Nature* 442:195–198, 2006

Hochberg. L.R., and Donoghue, J.P., Sensors for brain-computer interfaces. *IEEE Eng. Med. Biol.* 25:32-38, 2006

Moritz, C.T., Perlmutter, S.I., Fetz, E.E., Direct control of paralyzed muscles by cortical neurons. *Nature*, 456:639-642, 2008

Aggarwal, V., Acharya, S., Tenore, F., Shin, H-C., Etienne-Cummings, R., Schieber, M. H. and Thakor, N. V. Asynchronous decoding of dexterous finger movements using M1 neurons. *IEEE Trans. Neural Syst. Rehabil. Eng.* 16:3–14, 2008

Berger, T. W., Hampson, R. E., Song D., Goonawardena A., Marmarelis, V. Z. Deadwyler, S. A., A cortical neural prosthesis for restoring and enhancing memory. *J. Neural Eng.* 8:046017, 2011

Ethier, C., Oby, E. R., Bauman, M. J., Miller, L. E. Restoration of grasp following paralysis through brain-controlled stimulation of muscles. *Nature* 485:368–371, 2013

McCreery, D., Lossinsky, A., Pikov, V., Liu, X., Microelectrode array for chronic deep-brain Microstimulation and recording. *IEEE Transactions on Bio-Medical Engineering*, 53:726-737, 2006

Hoogerwerf, A.C., and Wise, K.D., A three-dimensional microelectrode array for chronic neural recording. *IEEE Transactions on Bio-Medical Engineering*, 41:1136-1146, 1994

Maynard, E.M., Nordhausen C.T., Normann R.A., The Utah intracortical Electrode Array: a recording structure for potential brain-computer interfaces. *Electroencephalogr Clin Neurophysiol* ;102:228-239, 1997

Lau, B., Guevremibt, L., Mushahwar, V.K., Strategies for generating prolonged functional standing using Intraspinal Microstimulation. *IEEE Trans. Neural. Syst. Rehabil. Eng.*, 15:273-285, 2007

Saigal, R., Renzi, C., Mushahwar, V.K., Intraspinal Microstimulation generates functional movement after spinal cord injury. *IEEE Trans. Neural Syst. Rehabil. Eng.,* 12: 430-440, Dec. 2004

E.L. Mazuchowski, and L.E. Thibault, "Biomechanical properties of the human spinal cord and pia matter," *in Summer Bioengineering Conference*, Key Biscayne, Florida, 2003

Khaled, I., Elmallah, S., Cheng, C., Mouusa, W.A., Mushahwar, V.K., Elias, A.L., A flexible based electrode array for Intraspinal Microstimulation. *IEEE Transactions on Biomedical Engineering*, 60:2904-2913, 2013

W. Swanson and J. E. Lebeau, "The Effect of Implantation on the Physical Properties of Silicone Rubbers" *Journal of Biomedical Materials Research*, vol.8, pp. 357-367, 1974

E. Roggendorf, "The Biostability of Silicone Rubbers, a Polyamide, and a Polyester" *Journal of Biomedical Materials Research,* vol. 10, pp.123-143, 1976

R.I. Leininger, V. Mirkovitch, A. Peters, and W.A. Hawks, "Change in properties of plastics during implantation." *Unpublished paper presented at American Society for Artificial Internal Organs*, 1964.

T.C. Ward, and J.T. Perry, "Dynamic mechanical properties of medical grade silicone elastomers stored in simulated body fluids" *Journal of Biomedical Materials Research*, vol. 15, pp. 511-525, 1984

A. Mahomed, N.M. Chidi, D.W.L. Hukins, S.N. Kukureka, D.E.T. Shepherd, "Frequency Dependence of Viscoelastic Properties of Medical Grade Silicones" *Journal of Biomedical Materials Research Part II: Applied Biomaterials*, pp. 210-216, 2008

C.C. Bonifacio, C.J. Kleverlaan, D.P. Raggio, A. Werner, R.C.D de Carvalho, "Physical-mechanical properties of glass ionomers cements indicated fir atraumatic restorative treatment" *Austrailian Dental Journal*, vol. 54, pp. 233-237, 200

"Platnium 20% Iridium"| PGM Database, [Online] Accessed at: www.pgmdatabase.com/jmpgm/index.jsp?record=1064, [Accessed: March 22, 2014]

J. Kuncova-Kallio and P.J. Kallio, "PDMS and its Suitability for Analytical Microfluidic Devices" *in Proceedings of the 28th IEEE EMBS Annual International Conference,* NEW YORK CITY, USA, 2006

D.C. Duffy, J.C. McDonald, O. J. A. Schueller and G. M. Whitesides, "Rapid Prototyping of Microfluidic Systems in Poly(dimethylsiloxane)" *Analytical Chemistry*, vol. 70, no. 23, pp. 4974-4984, Dec, 1998

Appendix A: Finite Element Annotated Sample Code

In this appendix, a sample finite element code is displayed for analysis of six wires in a base with large amplitude strain relief.

```
! clear out old stuff and start afresh
finish
/clear, start

/prep7

! set up some parameters, mesh size
eSizeLeads = 0.05
eSizeBase = 0.05

! Set up material properties

! base
mp, ex, 1, 550
mp, prxy, 1, 0.45

! electrodes
mp, ex, 2, 193e6
mp, prxy, 2, 0.45

! Set up plot numbering display
/pnum, kp, 1
/pnum, line, 1
/pnum, area, 0

!Electrode Lead

! Plot Key points

!Wire 1

!Upper Section
K,1,0,0
K,2,0.698,0.643
K,3,1.047,0.866
K,4,1.396,0.9848
K,5,1.745,0.985
```

```
K,6,2.094,0.8660
K,7,2.443,0.643
K,8,4.014,-0.7660
K,9,4.363,-0.940
K,10,4.712,-1
K,11,5.061,-0.9397
K,12,5.4105,-0.766
K,13,6.283,0
!Lower Section
K,14,0,-0.03
K,15,0.698,0.613
K,16,1.047,0.836
K,17,1.396,0.9548
K,18,1.745,0.955
K,19,2.094,0.8360
K,20,2.443,0.613
K,21,4.014,-0.7960
K,22,4.363,-0.970
K,23,4.712,-1.03
K,24,5.061,-0.9697
K,25,5.4105,-0.796
K,26,6.283,-0.03

!Spaces
!Upper Section
K,27,0,0.001
K,28,0.698,0.644
K,29,1.047,0.867
K,30,1.396,0.9858
K,31,1.745,0.986
K,32,2.094,0.8670
K,33,2.443,0.644
K,34,4.014,-0.7650
K,35,4.363,-0.939
K,36,4.712,-0.99
K,37,5.061,-0.9387
K,38,5.4105,-0.765
K,39,6.283,0.001
!Lower Section
K,40,0,-0.031
K,41,0.698,0.612
K,42,1.047,0.835
```

```
K,43,1.396,0.9538
K,44,1.745,0.954
K,45,2.094,0.8350
K,46,2.443,0.612
K,47,4.014,-0.7970
K,48,4.363,-0.971
K,49,4.712,-1.031
K,50,5.061,-0.9707
K,51,5.4105,-0.797
K,52,6.283,-0.031

!Wire 2
!Upper Section
K,53,0,0.5
K,54,0.698,1.143
K,55,1.047,1.366
K,56,1.396,1.4848
K,57,1.745,1.485
K,58,2.094,1.3660
K,59,2.443,1.143
K,60,4.014,-0.266
K,61,4.363,-0.44
K,62,4.712,-0.5
K,63,5.061,-0.4397
K,64,5.4105,-0.266
K,65,6.283,0.5
!Lower Section
K,66,0,0.47
K,67,0.698,1.113
K,68,1.047,1.336
K,69,1.396,1.4548
K,70,1.745,1.455
K,71,2.094,1.3360
K,72,2.443,1.113
K,73,4.014,-0.296
K,74,4.363,-0.47
K,75,4.712,-0.53
K,76,5.061,-0.4697
K,77,5.4105,-0.296
K,78,6.283,0.47

!Spaces
```

```
!Upper Section
K,79,0,0.501
K,80,0.698,1.144
K,81,1.047,1.367
K,82,1.396,1.4858
K,83,1.745,1.486
K,84,2.094,1.3670
K,85,2.443,1.144
K,86,4.014,-0.265
K,87,4.363,-0.439
K,88,4.712,-0.49
K,89,5.061,-0.4387
K,90,5.4105,-0.265
K,91,6.283,0.501
!Lower Section
K,92,0,0.469
K,93,0.698,1.112
K,94,1.047,1.335
K,95,1.396,1.4538
K,96,1.745,1.454
K,97,2.094,1.3350
K,98,2.443,1.112
K,99,4.014,-0.297
K,100,4.363,-0.471
K,101,4.712,-0.531
K,102,5.061,-0.4707
K,103,5.4105,-0.297
K,104,6.283,0.469
```

!Wire 3

```
!Upper Section
K,105,0,-0.5
K,106,0.698,0.143
K,107,1.047,0.366
K,108,1.396,0.4848
K,109,1.745,0.485
K,110,2.094,0.366
K,111,2.443,0.143
K,112,4.014,-1.2660
K,113,4.363,-1.440
K,114,4.712,-1.5
K,115,5.061,-1.4397
```

```
K,116,5.4105,-1.266
K,117,6.283,-0.5
!Lower Section
K,118,0,-.53
K,119,0.698,0.113
K,120,1.047,0.336
K,121,1.396,0.4548
K,122,1.745,0.455
K,123,2.094,0.336
K,124,2.443,0.113
K,125,4.014,-1.2960
K,126,4.363,-1.470
K,127,4.712,-1.53
K,128,5.061,-1.4697
K,129,5.4105,-1.296
K,130,6.283,-0.53

!Spaces
!Upper Section
K,131,0,-0.499
K,132,0.698,0.144
K,133,1.047,0.367
K,134,1.396,0.4858
K,135,1.745,0.486
K,136,2.094,0.367
K,137,2.443,0.144
K,138,4.014,-1.2650
K,139,4.363,-1.439
K,140,4.712,-1.49
K,141,5.061,-1.4387
K,142,5.4105,-1.265
K,143,6.283,-0.499
!Lower Section
K,144,0,-0.531
K,145,0.698,0.112
K,146,1.047,0.335
K,147,1.396,0.4538
K,148,1.745,0.454
K,149,2.094,0.335
K,150,2.443,0.112
K,151,4.014,-1.2970
K,152,4.363,-1.471
```

```
K,153,4.712,-1.531
K,154,5.061,-1.4707
K,155,5.4105,-1.297
K,156,6.283,-0.531

!Wire 4
!Upper Section
K,157,0,1
K,158,0.698,1.643
K,159,1.047,1.866
K,160,1.396,1.9848
K,161,1.745,1.985
K,162,2.094,1.8660
K,163,2.443,1.643
K,164,4.014,0.234
K,165,4.363,0.06
K,166,4.712,0
K,167,5.061,0.0603
K,168,5.4105,0.234
K,169,6.283,1
!Lower Section
K,170,0,0.97
K,171,0.698,1.613
K,172,1.047,1.836
K,173,1.396,1.9548
K,174,1.745,1.955
K,175,2.094,1.8360
K,176,2.443,1.613
K,177,4.014,0.204
K,178,4.363,0.03
K,179,4.712,-0.03
K,180,5.061,0.0303
K,181,5.4105,0.204
K,182,6.283,0.97
!Spaces
!Upper Section
K,183,0,1.001
K,184,0.698,1.644
K,185,1.047,1.867
K,186,1.396,1.9858
K,187,1.745,1.986
K,188,2.094,1.8670
```

```
K,189,2.443,1.644
K,190,4.014,0.235
K,191,4.363,0.061
K,192,4.712,0.01
K,193,5.061,0.0613
K,194,5.4105,0.235
K,195,6.283,1.001
!Lower Section
K,196,0,0.969
K,197,0.698,1.612
K,198,1.047,1.835
K,199,1.396,1.9538
K,200,1.745,1.954
K,201,2.094,1.8350
K,202,2.443,1.612
K,203,4.014,0.203
K,204,4.363,0.029
K,205,4.712,-0.031
K,206,5.061,0.0293
K,207,5.4105,0.203
K,208,6.283,0.969
```

!Wire 5

```
!Upper Section
K,209,0,-1
K,210,0.698,-0.357
K,211,1.047,-0.134
K,212,1.396,-0.0152
K,213,1.745,-0.015
K,214,2.094,-0.134
K,215,2.443,-0.357
K,216,4.014,-1.7660
K,217,4.363,-1.940
K,218,4.712,-2
K,219,5.061,-1.9397
K,220,5.4105,-1.766
K,221,6.283,-1
!Lower Section
K,222,0,-1.03
K,223,0.698,-0.387
K,224,1.047,-0.164
K,225,1.396,-0.0452
```

```
K,226,1.745,-0.045
K,227,2.094,-0.164
K,228,2.443,-0.387
K,229,4.014,-1.7960
K,230,4.363,-1.970
K,231,4.712,-2.03
K,232,5.061,-1.9697
K,233,5.4105,-1.796
K,234,6.283,-1.03

!Spaces
!Upper Section
K,235,0,-0.999
K,236,0.698,-0.356
K,237,1.047,-0.133
K,238,1.396,-0.0142
K,239,1.745,-0.014
K,240,2.094,-0.133
K,241,2.443,-0.356
K,242,4.014,-1.7650
K,243,4.363,-1.939
K,244,4.712,-1.99
K,245,5.061,-1.9387
K,246,5.4105,-1.765
K,247,6.283,-0.999
!Lower Section
K,248,0,-1.031
K,249,0.698,-0.388
K,250,1.047,-0.165
K,251,1.396,-0.0462
K,252,1.745,-0.046
K,253,2.094,-0.165
K,254,2.443,-0.388
K,255,4.014,-1.7970
K,256,4.363,-1.971
K,257,4.712,-2.031
K,258,5.061,-1.9707
K,259,5.4105,-1.797
K,260,6.283,-1.031

!Wire 6
!Upper Section
```

```
K,261,0,1.5
K,262,0.698,2.143
K,263,1.047,2.366
K,264,1.396,2.4848
K,265,1.745,2.485
K,266,2.094,2.366
K,267,2.443,2.143
K,268,4.014,0.734
K,269,4.363,0.56
K,270,4.712,0.5
K,271,5.061,0.5603
K,272,5.4105,0.734
K,273,6.283,1.5
!Lower Section
K,274,0,1.47
K,275,0.698,2.113
K,276,1.047,2.336
K,277,1.396,2.4548
K,278,1.745,2.455
K,279,2.094,2.336
K,280,2.443,2.113
K,281,4.014,0.704
K,282,4.363,0.53
K,283,4.712,0.47
K,284,5.061,0.5303
K,285,5.4105,0.704
K,286,6.283,1.47

!Spaces
!Upper Section
K,287,0,1.501
K,288,0.698,2.144
K,289,1.047,2.367
K,290,1.396,2.4858
K,291,1.745,2.486
K,292,2.094,2.367
K,293,2.443,2.144
K,294,4.014,0.735
K,295,4.363,0.561
K,296,4.712,0.51
K,297,5.061,0.5613
K,298,5.4105,0.735
```

```
K,299,6.283,1.501
!Lower Section
K,300,0,1.469
K,301,0.698,2.112
K,302,1.047,2.335
K,303,1.396,2.4538
K,304,1.745,2.454
K,305,2.094,2.335
K,306,2.443,2.112
K,307,4.014,0.703
K,308,4.363,0.529
K,309,4.712,0.469
K,310,5.061,0.5293
K,311,5.4105,0.703
K,312,6.283,1.469


!Base
K,313,0,-2.2725
K,314,0,2.7275
K,315,6.283,2.7275
K,316,6.283,-2.2725

!Join Key points together

L,314,315
L,314,287
L,315,299

!Wire 6
L,261,262
L,262,263
L,263,264
L,264,265
L,265,266
L,266,267
L,267,268  !10
L,268,269
L,269,270
L,270,271
L,271,272
L,272,273
```

```
L,261,274
L,273,286

L,274,275
L,275,276
L,276,277  !20
L,277,278
L,278,279
L,279,280
L,280,281
L,281,282
L,282,283
L,283,284
L,284,285
L,285,286
```

!Upper Space Section 6

```
L,287,261  !30
L,287,288
L,288,289
L,289,290
L,290,291
L,291,292
L,292,293
L,293,294
L,294,295
L,295,296
L,296,297  !40
L,297,298
L,298,299
L,299,273
```

!Lower Space Section 6

```
L,274,300
L,300,301
L,301,302
L,302,303
L,303,304
L,304,305
L,305,306  !50
```

```
L,306,307
L,307,308
L,308,309
L,309,310
L,310,311
L,311,312
L,312,286

L,300,183
L,312,195
```

!Wire 4

```
L,157,158  !60
L,158,159
L,159,160
L,160,161
L,161,162
L,162,163
L,163,164
L,164,165
L,165,166
L,166,167
L,167,168  !70
L,168,169
L,157,170
L,169,182

L,170,171
L,171,172
L,172,173
L,173,174
L,174,175
L,175,176
L,176,177  !80
L,177,178
L,178,179
L,179,180
L,180,181
L,181,182
```

!Upper Space Section 4

```
L,183,157
L,183,184
L,184,185
L,185,186
L,186,187  !90
L,187,188
L,188,189
L,189,190
L,190,191
L,191,192
L,192,193
L,193,194
L,194,195
L,169,195
```

!Lower Space Section 4

```
L,170,196  !100
L,196,197
L,197,198
L,198,199
L,199,200
L,200,201
L,201,202
L,202,203
L,203,204
L,204,205
L,205,206  !110
L,206,207
L,207,208
L,182,208

L,196,79
L,208,91
```

!Wire 2

```
L,53,54
L,54,55
L,55,56
L,56,57
L,57,58  !120
```

```
L,58,59
L,59,60
L,60,61
L,61,62
L,62,63
L,63,64
L,64,65
L,53,66
L,65,78

L,66,67  !130
L,67,68
L,68,69
L,69,70
L,70,71
L,71,72
L,72,73
L,73,74
L,74,75
L,75,76
L,76,77  !140
L,77,78

! Upper Space Section 2
L,53,79
L,79,80
L,80,81
L,81,82
L,82,83
L,83,84
L,84,85
L,85,86
L,86,87  !150
L,87,88
L,88,89
L,89,90
L,90,91
L,78,91

! Lower Space Section 2
L,66,92
L,92,93
```

```
L,93,94
L,94,95
L,95,96  !160
L,96,97
L,97,98
L,98,99
L,99,100
L,100,101
L,101,102
L,102,103
L,103,104
L,78,104

L,27,92  !170
L,39,104


!Wire 1
L,1,2
L,2,3
L,3,4
L,4,5
L,5,6
L,6,7
L,7,8
L,8,9
L,9,10                                                    !180
L,10,11
L,11,12
L,12,13
L,13,26
L,14,1

L,14,15
L,15,16
L,16,17
L,17,18
L,18,19                                                   !190
L,19,20
L,20,21
L,21,22
L,22,23
```

```
L,23,24
L,24,25
L,25,26

! Upper Space Section 1
L,1,27
L,27,28
L,28,29  !200
L,29,30
L,30,31
L,31,32
L,32,33
L,33,34
L,34,35
L,35,36
L,36,37
L,37,38
L,38,39  !210
L,39,13

! Lower Space Section 1
L,14,40
L,40,41
L,41,42
L,42,43
L,43,44
L,44,45
L,45,46
L,46,47
L,47,48  !220
L,48,49
L,49,50
L,50,51
L,51,52
L,52,26

L,40,131
L,52,143

! Wire 3

L,105,106
```

```
L,106,107
L,107,108  !230
L,108,109
L,109,110
L,110,111
L,111,112
L,112,113
L,113,114
L,114,115
L,115,116
L,116,117
L,105,118  !240
L,117,130

L,118,119
L,119,120
L,120,121
L,121,122
L,122,123
L,123,124
L,124,125
L,125,126
L,126,127  !250
L,127,128
L,128,129
L,129,130

! Upper Space Section 3
L,105,131
L,131,132
L,132,133
L,133,134
L,134,135
L,135,136
L,136,137  !260
L,137,138
L,138,139
L,139,140
L,140,141
L,141,142
L,142,143
L,117,143
```

```
! Lower Space Section 3
L,118,144
L,144,145
L,145,146  !270
L,146,147
L,147,148
L,148,149
L,149,150
L,150,151
L,151,152
L,152,153
L,153,154
L,154,155
L,155,156  !280
L,130,156

L,144,235
L,156,247

!Wire 5

L,209,210
L,210,211
L,211,212
L,212,213
L,213,214
L,214,215
L,215,216  !290
L,216,217
L,217,218
L,218,219
L,219,220
L,220,221
L,221,234
L,209,222


L,222,223
L,223,224
L,224,225  !300
L,225,226
```

```
L,226,227
L,227,228
L,228,229
L,229,230
L,230,231
L,231,232
L,232,233
L,233,234
```

! Upper Space Section 5

```
L,235,209  !310
L,235,236
L,236,237
L,237,238
L,238,239
L,239,240
L,240,241
L,241,242
L,242,243
L,243,244
L,244,245  !320
L,245,246
L,246,247
L,221,247
```

! Lower Space Section 3

```
L,248,222
L,248,249
L,249,250
L,250,251
L,251,252
L,252,253
L,253,254  !330
L,254,255
L,255,256
L,256,257
L,257,258
L,258,259
L,259,260
L,260,234
```

```
L,248,313
L,260,316
L,313,316  !340

!Create solid areas between lines
LSEL, NONE
LSEL, A, LINE, , 1, 3, 1
LSEL, A, LINE, , 31, 42, 1
AL, ALL  !Area 1

LSEL, NONE
LSEL, A, LINE, , 4, 29, 1
AL, ALL  !Area 2



LSEL, NONE
LSEL, A, LINE, , 45, 56, 1
LSEL, A, LINE, , 58, 59, 1
LSEL, A, LINE, , 87, 98, 1
AL, ALL  !Area 3

LSEL, NONE
LSEL, A, LINE, , 60, 85, 1
AL, ALL  !Area 4

LSEL, NONE
LSEL, A, LINE, , 101, 112, 1
LSEL, A, LINE, , 114, 115, 1
LSEL, A, LINE, , 143, 154, 1
AL, ALL  !Area 5

LSEL, NONE
LSEL, A, LINE, , 116, 141, 1
AL, ALL  !Area 6

LSEL, NONE
LSEL, A, LINE, , 157, 168, 1
LSEL, A, LINE, , 170, 171, 1
LSEL, A, LINE, , 199, 210, 1
AL, ALL  !Area 7
```

```
LSEL, NONE
LSEL, A, LINE, , 172, 197, 1
AL, ALL  !Area 8

LSEL, NONE
LSEL, A, LINE, , 213, 224, 1
LSEL, A, LINE, , 226, 227, 1
LSEL, A, LINE, , 255, 266, 1
AL, ALL  !Area 9

LSEL, NONE
LSEL, A, LINE, , 228, 253, 1
AL, ALL  !Area 10

LSEL, NONE
LSEL, A, LINE, , 269, 280, 1
LSEL, A, LINE, , 282, 283, 1
LSEL, A, LINE, , 311, 322, 1
AL, ALL  !Area 11

LSEL, NONE
LSEL, A, LINE, , 284, 309, 1
AL, ALL  !Area 12


LSEL, NONE
LSEL, A, LINE, , 325, 336, 1
LSEL, A, LINE, , 338, 340, 1
AL, ALL  !Area 13


! using triangular plane183 elements
et, 1, plane183
keyopt, 1, 1, 1
! select our electrodes
asel, s, area, , 2,12,2

! set the material parameters
! (use material 2)
aatt, 2, , 1, 0,
```

```
! set the element size/thickness
aesize, all, eSizeLeads

! and mesh it
amesh, all

asel,none

! select our base
asel, s, area, ,1,13,2

! set the material parameters
! (use material 1)
aatt, 1, , 1, 0,

! set the element size
aesize, all, eSizeBase

! and mesh it
amesh, all

Lsel, none
Lsel, all

Asel, all

! Manually Input the contact element conditions. Under
Preprocessor, click modeling then create then click
contact pair.  Create a contact pair. Using all lines
associated with the wire as the target and all lines
associated with the spaces to be the contact pair.
Assign bonding value between base and insulated wire.
Create contact pair


! make sure everything is selected
allsel, all

!! now go on to solution phase
finish
/solution
```

```
! do a static analysis
antype, 0

! now stretch one end of the cord by 12%
dl, 2, , ux, -0.75396
dl, 16, , ux, -0.75396
dl, 30, , ux, -0.75396
dl, 44, , ux, -0.75396
dl, 58, , ux, -0.75396
dl, 72, , ux, -0.75396
dl, 86, , ux, -0.75396
dl, 100, , ux, -0.75396
dl, 114, , ux, -0.75396
dl, 128, , ux, -0.75396
dl, 142, , ux, -0.75396
dl, 156, , ux, -0.75396
dl, 170, , ux, -0.75396
dl, 185, , ux, -0.75396
dl, 198, , ux, -0.75396
dl, 212, , ux, -0.75396
dl, 226, , ux, -0.75396
dl, 240, , ux, -0.75396
dl, 254, , ux, -0.75396
dl, 268, , ux, -0.75396
dl, 282, , ux, -0.75396
dl, 297, , ux, -0.75396
dl, 310, , ux, -0.75396
dl, 324, , ux, -0.75396
dl, 338, , ux, -0.75396

! Keep the other end of the cord stationary

dl, 3, , ux, 0
dl, 17, , ux, 0
dl, 43, , ux, 0
dl, 57, , ux, 0
dl, 59, , ux, 0
dl, 73, , ux, 0
dl, 99, , ux, 0
dl, 113, , ux, 0
dl, 115, , ux, 0
```

```
dl, 129, , ux, 0
dl, 155, , ux, 0
dl, 169, , ux, 0
dl, 171, , ux, 0
dl, 184, , ux, 0
dl, 211, , ux, 0
dl, 225, , ux, 0
dl, 227, , ux, 0
dl, 241, , ux, 0
dl, 267, , ux, 0
dl, 281, , ux, 0
dl, 283, , ux, 0
dl, 296, , ux, 0
dl, 323, , ux, 0
dl, 337, , ux, 0
dl, 339, , ux, 0


! and solve!
solve

! move to post-processing to display results
/post1

! plot a contour plot of the nodal von mises stress
plnsol, s, eqv, 0, 1

! shows a table of all equivalent nodal stresses and
strains

Etable,,s,eqv  !nodal equivalent stress
Etable,,epel,eqv  ! nodal equivalent strain

Pretab  ! prints a list of nodal values for equivalent
stress and strains
```